

Natalia Sánchez Romero

Development and validation of a
new nephrotoxicity model
mimicking cell physiology
microenvironment

Departamento
Farmacología y Fisiología

Director/es
Giménez López, Ignacio

<http://zaguan.unizar.es/collection/Tesis>



Reconocimiento – NoComercial – SinObraDerivada (by-nc-nd): No se permite un uso comercial de la obra original ni la generación de obras

© Universidad de Zaragoza
Servicio de Publicaciones



Universidad
Zaragoza

Tesis Doctoral

**DEVELOPMENT AND VALIDATION OF
A NEW NEPHROTOXICITY MODEL
MIMICKING CELL PHYSIOLOGY
MICROENVIRONMENT**

Autor

Natalia Sánchez Romero

Director/es

Giménez López, Ignacio

UNIVERSIDAD DE ZARAGOZA

Farmacología y Fisiología

2017

**DEVELOPMENT AND VALIDATION OF
A NEW NEPHROTOXICITY MODEL
MIMICKING CELL PHYSIOLOGY
MICROENVIRONMENT**



Natalia Sánchez-Romero

DEVELOPMENT AND VALIDATION OF A NEW NEPHROTOXICITY
MODEL MIMICKING CELL PHYSIOLOGY MICROENVIRONMENT

Thesis
2017

Natalia Sánchez-Romero

**DEVELOPMENT AND VALIDATION OF A
NEW NEPHROTOXICITY MODEL
MIMICKING CELL PHYSIOLOGY
MICROENVIRONMENT**

Natalia Sánchez-Romero



UNIVERSIDAD DE ZARAGOZA

PROGRAMA DE DOCTORADO EN BIOMEDICINA Y BIOTECNOLOGÍA

DEPARTAMENTO DE FISIOLÓGIA Y FARMACOLOGÍA

DEVELOPMENT AND VALIDATION OF A NEW NEPHROTOXICITY MODEL MIMICKING CELL PHYSIOLOGY MICROENVIRONMENT

Memoria presentada por Natalia Sánchez-Romero

Licenciada en Biotecnología

Para optar al grado de Doctor por la Universidad de Zaragoza

Director: Ignacio Giménez López

El Profesor de la Universidad de Zaragoza abajo firmante,

HACE CONSTAR:

Que la memoria de Tesis presentada por D^a Natalia Sánchez Romero con el Título "*Development and validation of a new nephrotoxicity model mimicking cell physiology microenvironment*" para optar al grado de Doctor por la Universidad de Zaragoza, ha sido realizada bajo mi dirección, cumple los requisitos necesarios por la legislación vigente, se enmarca dentro de las líneas de investigación seguidas por la candidata durante sus estudios de Postgrado, coincide con el Proyecto de Tesis presentado originalmente, y posee la calidad científica necesaria para la obtención de dicho título.

Por lo tanto, emite el siguiente INFORME FAVORABLE.

Zaragoza, a 29 de marzo de 2017

Fdo.: Ignacio Giménez

Profesor Titular Fisiología

Dpto. Farmacología y Fisiología

El desarrollo y ejecución de esta Tesis Doctoral se han enmarcado dentro del proyecto: “Estudio experimental de la regeneración y regulación en epitelios renales para la validación de un dispositivo microfabricado para cultivo tisular” financiado por el Ministerio de Ciencia e Innovación (DPI2011-28262-C04-02) y la ayuda predoctoral FPI concedida a D^a Natalia Sánchez Romero, financiada por el Ministerio de Economía, industria y competitividad (BES-2012-059562).



A mis padres, por todo.
ESTA TESIS ES VUESTRA.

A mis hermanos y sobrinos,

A Pedro,

Gracias por el apoyo incondicional que me habéis dado
siempre. Sin vosotros, no habría llegado hasta aquí.

“Ever tried. Ever failed. No matter. Try again. Fail again. Fail better” Samuel Beckett



AGRADECIMIENTOS

Me gustaría comenzar este apartado agradeciendo a todas las personas que integráis el grupo FISIOPREN:

A mi director de Tesis, el **Dr. Ignacio Giménez**. Al final, lo hemos conseguido. Muchas gracias; a **Laura**, por compartir las alegrías y frustraciones científicas a lo largo de estos 4 años; a **Pilar, Carmen** y a todos los **estudiantes** que habéis pasado por el laboratorio, gracias por formar parte de esta aventura; a **Natacha**, porque durante los 3 últimos meses de mi Tesis, siempre me recibió con una gran sonrisa.

Todos, sin excepción alguna, me habéis aportado algo y habéis conseguido que hoy sea la persona que soy. Gracias.

I want to express a special acknowledgment to **Dr. Roos**, my mentor during my internships in Utrecht. It was a pleasure and a privilege to work with you. I will be eternally thankful to you for all the scientific support and publications during my internship there.

I also cannot forget all the Roos group members: **Michele**, thank you for being a great labmate and also a good friend; to **Pedro**, for making my visit very easy and for all the knowledge about transporter assays; to **Milôs**, for your support and patience, you are a fantastic labmate; to **Manoe**, for transmitting me your love for Science; to **Jitske**, for your help and ideas during my second visit; to **Muhammed**, for your incredible capacity to work (¡qué tío!).

Thank you everyone! You made my internships the best time of my Thesis.

Quiero agradecer el apoyo y ayuda de todas las personas que forman los servicios técnicos del IACS. Especialmente, me gustaría dedicar unas palabras a **David**, porque en cultivos desempeña un trabajo impecable y a nivel personal, siempre ha tenido una palabra de ánimo para mí; a **César** porque siempre que he necesitado su ayuda, ha estado ahí con una paciencia infinita; a **Mark y a Irene**, porque son simplemente geniales, a nivel profesional y personal.

No podía olvidarme en la planta A de todas las personas que forman predocs. Con todos vosotros, el “sufrimiento” ha sido más llevadero. Muchas gracias a todos y ¡¡¡ánimo!!!. De esta sala, no solo me llevo buenos compañeros, también amigos: **Iris, Pilar y Sofía**. A vosotras estaré eternamente agradecida, por saber escucharme, por saber animarme, por ayudarme cuando lo necesitaba, por sacarme una sonrisa dentro y fuera del laboratorio ¡sois increíblemente geniales!

Un párrafo solo para él se merece en estos agradecimientos **Edu**. Te lo he dicho mil veces, pero te lo repito una vez más: sin ti, el primer mes hubiera regresado de cabeza a Jerez. Gracias por ser un compañero y una persona ejemplar. Gracias por todo Edu.

Quería agradecer también a **Elena y Asun**. Vuestra amabilidad y simpatía me han hecho estos 4 años mucho más fáciles.

A **Pilar** y a **Eva** de recepción, porque es un gusto trabajar con gente como vosotras.

A **Montse** y **Carmen**, porque después de 4 años, formabais parte de cada una de mis tardes en el CIBA.

¡Quién me iba a decir a mí que iba a terminar echando de menos el CIBA! En general, gracias a todas las personas que lo formáis.

Para lo último, quería dejar los agradecimientos a mis amigos y familia.

Gracias a mis amigas **Carmen** y **Jenn**, porque no solo me han acompañado durante la Tesis, llevan casi un tercio de mi vida haciéndolo y espero sean muchos años más. ¡Muchas gracias chicas! Dicho esto, id pensando fecha para una buena fiesta... (hay cosas que no cambian).

Gracias a ti **Leti** (Wilmaaa), por hacer mi vida holandesa muy fácil y divertida. Espero que pronto nos veamos por el de beurs, por ejemplo.

A mis hermanos, **Patricia** y **Juan**, porque son los mejores hermanos que alguien podría tener. Muchas gracias por apoyarme siempre, llamarme, escucharme, soportarme, hacerme reír, hacerme llorar. Sois los mejores y siempre estáis cuando más os necesito. Gracias por formar parte de esta Tesis y de mi vida

A mis sobrinos, **Mª Luisa** y **Carlos**, porque son los niños de mis ojos y a pesar de la distancia, sigo siendo su tatita favorita, cosa que me hace la persona más feliz del mundo. Gracias por cada llamada que me hacéis, solo con eso me alegráis la vida continuamente.

A **Pedro**, meu amigo, meu 50%, my soulmate, meu companheiro de vida e meu grande amor. Obrigada pela paciência infinita e por ser alguém "significativamente" essencial e indispensável na minha vida. Obrigada por todo vermejo. Amo-te.

Por último y porque son las personas más importantes de mi vida, quería dedicar unas líneas de agradecimiento a mis padres, **Juan** y **Mª Luisa**. Esta tesis debería llevar vuestro nombre, porque si he llegado hasta aquí es gracias a ustedes. Sois unos padres increíblemente generosos y buenos y estaré eternamente agradecida por el cuidado, cariño y amor que siempre me habéis dado a mí y a mis hermanos. Podría escribir otra Tesis entera agradeciándoos cosas, así que simplemente, gracias por todo. Os quiero.

INDEX OF CONTENT

RESUMEN.....	6
SUMMARY.....	13
LIST OF ABBREVIATIONS.....	19
1 GENERAL INTRODUCTION.....	22
1.1 INTRODUCTION	25
1.1.1 Anatomy of the kidneys	25
1.1.2 Function of the kidneys.....	27
1.1.3 The nephron.....	30
1.1.4 Basic processes performed by the nephrons.....	36
1.1.5 The evolution of nephro pharmacology	40
1.1.6 Engineered renal models for reducing animal studies	42
1.1.7 Experimental models using renal cell cultures	48
1.1.8 Other nephro pharmacological models.....	51
1.2 HYPOTHESIS AND RESEARCH AIMS	57
1.2.1 Objectives.....	57
1.3 BIBLIOGRAPHY.....	59
2 ISOLATION AND CHARACTERIZATION OF HUMAN PROXIMAL TUBULAR PRIMARY CELLS IN CULTURE	68
2.1 INTRODUCTION	71
2.2 OBJECTIVES.....	78
2.3 MATERIAL AND METHODS	79
2.3.1 Source of renal tissue.....	79
2.3.2 Cell culture medium.....	79
2.3.3 Collagen coating of culture vessel surface.....	79
2.3.4 Protocol used in human renal cell isolation.....	80

2.3.5 Cell culture	83
2.3.6 Analysis of phenotypic markers expression by Reverse transcriptase- polymerase chain reaction (RT-PCR).....	84
2.3.7 Analysis of phenotypic markers by Immunofluorescence	87
2.3.8 Analysis of phenotypic markers by Immunocytochemistry	88
2.3.9 Cytochemical demonstration of GGT1 activity	89
2.3.10 Analysis of phenotypic markers by flow cytometry.....	90
2.3.11 Determination of Enzyme activity in live cultured cells.....	91
2.3.12 Transporter assays	93
2.3.13 Statistics	96
2.4 RESULTS	97
2.4.1 Protocol of hPTPC isolation.....	97
2.4.2 Evolution of hPTPC morphology and doubling time through subcultivation.....	98
2.4.3 Transcriptional expression of phenotypic markers in hPTPC	101
2.4.4 Immunofluorescence analysis by using epithelial markers	103
2.4.5 Immunocytochemistry characterization	104
2.4.6 Flow cytometry analysis.....	108
2.4.7 Determination of Enzyme activity in live cultured cells.....	111
2.4.8 Transporter assays	113
2.5 DISCUSSION	118
2.6 BIBLIOGRAPHY	123
3 GENERATION AND VALIDATION OF A NEW NEPHROTOXICITY MODEL BASED IN THE USE OF CISPLATIN IN HUMAN PRIMARY PROXIMAL TUBULE CELLS.....	134
3.1 INTRODUCTION	137
3.2 OBJECTIVES	141

3.3 MATERIAL AND METHODS	142
3.3.1 Cell culture	142
3.3.2 Experimental design.....	142
3.3.3 Cisplatin exposure.....	142
3.3.4 Small molecules treatment.....	143
3.3.5 Assays to evaluate the effects of cisplatin in hPTPC.....	144
3.4 RESULTS	150
3.4.1 96 wells plate nephrotoxicity model.....	150
3.4.2 Heterogeneous increase in GGT1 activity in cisplatin treated hPTPC cells.	155
3.4.3 The effects of cisplatin in hPTPC are irreversible.....	156
3.4.4 Model validation: testing for small molecules with potential anti- cisplatin effects	157
3.5 DISCUSSION.....	161
3.6 BIBLIOGRAPHY.....	168
4 TRANSFER OF THE GENERATED NEPHROTOXICITY MODEL TO FLUIDIC DEVICES THAT MIMIC THE CELLULAR PHYSIOLOGICAL MICROENVIRONMENT.	176
4.1 INTRODUCTION	179
4.2 OBJECTIVES.....	182
4.3 MATERIAL AND METHODS	183
4.3.1 Cell culture	183
4.3.2 Coating protocol	183
4.3.3 Fluidic devices	184
4.3.4 Fluidic perfusion system	185
4.3.5 Phenotyping of cells cultured in microfluidic devices by Multiplex PCR and GGT1 cytochemical staining	186

4.3.6 Modifications of Cisplatin cytotoxicity assay for use in microfluidic devices.....	192
4.3.7 Statistic.....	196
4.4 RESULTS	197
4.4.1 Culture of hPTPC cells in custom-made Fluidic devices.....	197
4.4.2 Culture of hPTPC cells in Ibidi μ -Slide VI 0.4.....	209
4.4.3 Nephrotoxicity model based in cisplatin employed in hPTPC growing in Ibidi μ Slides	214
4.5 DISCUSSION	226
4.6 BIBLIOGRAPHY	230
4.7 ANNEX	235
5 Conclusions	238
5 Conclusiones.....	239

RESUMEN

Los riñones son órganos muy eficientes que llevan a cabo múltiples funciones en el organismo. Una de las principales funciones que realizan es la eliminación de productos de desecho y exceso de fluido del cuerpo a través de la orina. La regulación de las sales y el contenido de ácido, son funciones desempeñados por estos órganos. En el riñón también tiene lugar la producción de diferentes hormonas. El riñón está constituido por las nefronas, que son las unidades estructurales y funcionales de estos órganos. Dentro de las nefronas podemos diferenciar las siguientes estructuras: El glomérulo, que es la primera parte de la nefrona donde el plasma es filtrado desde la sangre. Inmediatamente después, encontramos el túbulo, cuya estructura es semejante a un tubo largo y estrecho, donde el fluido filtrado desde la sangre es procesado y convertido en orina. A lo largo del túbulo, encontramos los siguientes segmentos: túbulo proximal, asa de Henle, túbulo distal y tubo colector.

En esta Tesis Doctoral, nos centraremos en el estudio del segmento formado por el túbulo proximal (TP) [1]. La principal función desempeñada por el TP es la reabsorción y secreción de metabolitos y para realizar estas funciones las células del TP cuentan con un gran contenido de diferentes transportadores de membrana [2-5]. El túbulo proximal está formado por células epiteliales, las cuales están polarizadas, característica que nos permite distinguir entre dos zonas bien diferenciadas, la zona apical y la zona basolateral. Las células del TP contienen una estructura denominada borde en cepillo que aumenta el área de superficie de las células y este incremento es útil durante los procesos de reabsorción [6]. Conviene destacar que las células renales están continuamente expuestas al ultra filtrado del plasma y que el flujo luminal genera una fuerza de cizallamiento (*shear stress*, SS) sobre la superficie apical de las células. Las células del TP pueden detectar estas SS a través del cilio primario o de las

microvellosidades del borde en cepillo. La señalización intracelular desencadenada por la SS luminal es un estímulo fisiológico clave para las células tubulares renales [7]. A pesar de la relevancia del flujo luminal en la nefrona, así como en el desarrollo de enfermedades, hay relativamente pocos estudios *in vitro* que incluyan este estímulo. El flujo luminal debería ser un requisito imprescindible para la generación de un modelo de función tubular *in vitro*, fisiológicamente más similar al que encontramos *in vivo*.

Las células del TP *in vivo* presentan unas características dinámicas diferentes en ambos compartimentos. Cuando se trabaja *in vitro*, se alteran esas características dinámicas ya que las células son expuestas a la inmovilización de su compartimento basolateral, en contacto con la superficie donde las células crecen y en el lado apical se renueva el medio cada 2-4 días, eliminando el efecto que el SS ejerce en ambos compartimentos. La ausencia del flujo luminal, así como la alteración de las características dinámicas de las células en ambos compartimentos, son dos de los problemas que encontramos en las condiciones de cultivo convencional 2D, eliminando la posibilidad de reproducir la función tubular renal, la cual consiste en concentrar o diluir los solutos en el fluido luminal. Por tanto, es evidente que las técnicas de cultivo convencionales 2D, a pesar del gran conocimiento que nos han aportado sobre la función celular y molecular, no son capaces de reproducir el ambiente fisiológico de las células del TP. Esto a la vez, podría explicar la dificultad en la traslación de los resultados *in vitro* a aplicaciones *in vivo* [8].

En los últimos años y con el objetivo de aproximarse a la creación *in vitro* de microambientes fisiológicamente más similares a los encontrados *in vivo*, han surgido colaboraciones entre las áreas de Ingeniería y las áreas de Biología [9] interesadas en el desarrollo de dispositivos microfluídicos [10] para su uso en estudios de epitelio renal. Los dispositivos mencionados anteriormente, son

estructuras situadas en la escala micro y nano, que han posibilitado el desarrollo de los microchips, dispositivos miniaturizados capaces de imitar sistemas naturales de forma precisa si se acoplan a sistemas continuos de perfusión en los canales que componen estos dispositivos, los cuales son habitados por las células sembradas en ellos. Estos dispositivos ofrecen ventajas como la reproducción de la arquitectura multicelular o de la interfaz tejido-tejido, la recreación del microambiente físico-químico y la perfusión vascular, originando niveles de tejidos funcionales, que no pueden obtenerse con los métodos de cultivo 2D o 3D. Otra ventaja, es que al trabajar en escala micro-nanométrica, el ahorro de las soluciones necesarias para el mantenimiento de las células, o para la ejecución de experimentos, se ve drásticamente reducido. A nivel experimental, este tipo de dispositivos presentan gran potencial en el área de la organogénesis y la fisiología y, en el contexto del descubrimiento y desarrollo de nuevos fármacos, tiene especial valor en el estudio de los mecanismos de acción, toxicidad e identificación de biomarcadores.

A partir de la información expuesta anteriormente, se detectó un problema y se propuso una hipótesis: las herramientas de cultivo convencionales no recrean con precisión el ambiente fisiológico donde crecen las células y por tanto, esto puede originar la pérdida de reproducibilidad de la respuesta celular contra agentes tóxicos y mecanismos de reparación unidos a daño renal. Con el objetivo de aceptar o rechazar la hipótesis propuesta se propone la creación de un modelo de nefrotoxicidad, usando dispositivos de cultivo biomiméticos que tendrán acoplados las herramientas necesarias para poder usar flujo, y de esta manera reproducirán mejor el microambiente de las células del TP.

La elección del TP para desarrollar esta Tesis, se basa en que en este segmento de la nefrona se procesa la mayoría de tóxicos y fármacos y tiene lugar el daño agudo y crónico renal. Por tanto, desde el punto de vista clínico y con el

objetivo de estudiar nefrotoxicidad, el TP representa un segmento cuyos estudios pueden aportar mucho conocimiento. Con el objetivo de crear un modelo de nefrotoxicidad, el uso de cultivos primarios de células del TP humanas (hPTPC), daría lugar a una fácil traslación de los resultados a la clínica.

La molécula elegida para la creación del modelo de nefrotoxicidad es el cisplatino, un compuesto antitumoral usado en el tratamiento contra diversos tipos de cánceres, entre los que destacan pulmón, testículo y cérvix. Uno de los principales efectos secundarios de este compuesto es la nefrotoxicidad [11] en el TP. Los mecanismos de acción del cisplatino incluyen su paso al interior de las células del TP mediante los transportadores basolaterales OCT2 y CTR-1, así como la enzima GGT1, encargada de la conversión del cisplatino en una molécula mucho más reactiva tras entrar en contacto con esta enzima [12].

A partir de las hPTPC y del modelo de nefrotoxicidad que se desarrolló, se estudió el efecto de la estimulación mecánica proporcionado por el flujo, sobre la sensibilidad al cisplatino, permitiendo recrear un ambiente más semejante al que encontramos *in vivo*.

Los resultados obtenidos a lo largo de esta tesis nos sugieren que:

1. El protocolo de aislamiento empleado para la obtención de células primarias de TP procedentes de nefrectomías humanas, hPTPC, y la posterior caracterización de las células, nos permitió obtener un cultivo formado mayoritariamente por células de TP que expresaban los principales marcadores de este segmento de la nefrona.
2. El uso combinado del ensayo de actividad enzimática de GGT1 y el ensayo de viabilidad, nos permitió distinguir los efectos del cisplatino. La combinación de estos ensayos se validó como una herramienta útil a la hora de monitorizar la función celular y viabilidad celular.

3. El modelo de nefrotoxicidad empleando cisplatino fue consistente para su uso en células creciendo en dispositivos fluídicos.
4. El cultivo de hPTPC aislado y caracterizado durante esta tesis, no mostró diferencia en la sensibilidad al modelo de cisplatino en dispositivos fluídicos en presencia de la estimulación mecánica proporcionada por el flujo y comparado con células en condiciones estáticas.

BIBLIOGRAFÍA

- [1] C. Lute, Principles of Renal Physiology, 2012.
- [2] H. Koepsell, The SLC22 family with transporters of organic cations, anions and zwitterions, *Mol Aspects Med* 34(2-3) (2013) 413-35.
- [3] R. Masereeuw, F.G. Russel, Therapeutic implications of renal anionic drug transporters, *Pharmacol Ther* 126(2) (2010) 200-16.
- [4] S.K. Nigam, W. Wu, K.T. Bush, M.P. Hoenig, R.C. Blantz, V. Bhatnagar, Handling of Drugs, Metabolites, and Uremic Toxins by Kidney Proximal Tubule Drug Transporters, *Clin J Am Soc Nephrol* 10(11) (2015) 2039-49.
- [5] L. Wang, D.H. Sweet, Renal organic anion transporters (SLC22 family): expression, regulation, roles in toxicity, and impact on injury and disease, *AAPS J* 15(1) (2013) 53-69.
- [6] M.J. Wilmer, M.A. Saleem, R. Masereeuw, L. Ni, T.J. van der Velden, F.G. Russel, P.W. Mathieson, L.A. Monnens, L.P. van den Heuvel, E.N. Levtchenko, Novel conditionally immortalized human proximal tubule cell line expressing functional influx and efflux transporters, *Cell Tissue Res* 339(2) (2010) 449-57.
- [7] V. Raghavan, O.A. Weisz, Discerning the role of mechanosensors in regulating proximal tubule function, *Am J Physiol Renal Physiol* 310(1) (2016) F1-5.
- [8] T.C. Fuchs, P. Hewitt, Biomarkers for drug-induced renal damage and nephrotoxicity-an overview for applied toxicology, *AAPS J* 13(4) (2011) 615-31.
- [9] A.D. van der Meer, A. van den Berg, Organs-on-chips: breaking the in vitro impasse, *Integr Biol (Camb)* 4(5) (2012) 461-70.
- [10] E.K. Sackmann, A.L. Fulton, D.J. Beebe, The present and future role of microfluidics in biomedical research, *Nature* 507(7491) (2014) 181-9.
- [11] A. Wilmes, C. Bielow, C. Ranninger, P. Bellwon, L. Aschauer, A. Limonciel, H. Chassaing, T. Kristl, S. Aiche, C.G. Huber, C. Guillou, P. Hewitt, M.O. Leonard, W. Dekant, F. Bois, P. Jennings, Mechanism of cisplatin proximal tubule toxicity revealed by integrating transcriptomics, proteomics, metabolomics and biokinetics, *Toxicol In Vitro* 30(1 Pt A) (2015) 117-27.

[12] L. Fliedl, M. Wieser, G. Manhart, M.P. Gerstl, A. Khan, J. Grillari, R. Grillari-Voglauer, Controversial role of gamma-glutamyl transferase activity in cisplatin nephrotoxicity, *ALTEX* 31(3) (2014) 269-78.

SUMMARY

The kidneys are very efficient organs that perform multiple functions in the body. One of the main functions performed by the kidneys is the elimination of waste products and excess fluid from the body through the urine. The regulation of body salts and acid content are functions played by these organs. In the kidney also takes place the production of different hormones. The kidney is made up of nephrons, which are the structural and functional units of these organs. The nephrons are composed by the following structures: The glomerulus, which is the first part of the nephron, where the plasma is filtered from the blood. Immediately afterward, we find the tubule, which structure is like a long narrow tube, where the filtered fluid from the blood is processed into the urine. The tubule is divided into different segments: proximal tubule, loop of Henle, distal tubule and collecting tube.

In this Thesis, we focused on the study of the segment formed by the proximal tubule (PT) [1]. The main role played by the PT is the reabsorption and secretion of metabolites and to perform these functions, PT cells have a high content of different membrane transporters [2-5]. The PT is formed by epithelial cells, which are polarized, a feature that allows us to distinguish between two distinct areas, the apical zone, and the basolateral zone. PT cells contain a structure called brush border that increases the surface area of the cells, and this increase is useful during the reabsorption processes [6]. It should be noted that renal cells are continually exposed to ultrafiltration of the plasma and that the luminal flux generates a shear stress (SS) on the apical surface of the cells. PT cells can detect this SS through the primary cilium or the brush border. The intracellular signaling triggered by the luminal SS is a physiological stimulus essential for renal tubular cells [7]. Despite the relevance of luminal flow in the nephron, as well as in the development of diseases, there are relatively few *in*

vitro studies including this stimulus. Luminal flow should be a prerequisite for the generation of an *in vitro* physiological model to study tubular function, similar to what is found in *in vivo* environment.

PT cells *in vivo* exhibit different dynamic characteristics in both compartments. When we are working with these cells *in vitro*, these dynamic characteristics are altered since the cells are exposed to the immobilization of their basolateral compartment, in contact with the surface where the cells grow, and on the apical side, the medium is renewed every 2-4 days, eliminating the effect that the SS exerts on both compartments. The absence of luminal flow, as well as the alteration of the dynamic characteristics of the cells in both compartments, are two of the problems found in conventional 2D culture conditions, eliminating the possibility of reproducing renal tubular function, which consists of concentrating or diluting the solutes present in the luminal fluid. Therefore, it is evident that conventional 2D culture techniques, despite the high knowledge that they have provided us on the cellular and molecular function, are not able to reproduce the physiological environment of the PT cells. This could explain the difficulty we have in translating *in vitro* results into *in vivo* applications [8].

In the last years, with the aim of creating *in vitro* microenvironments physiologically similar to those found *in vivo*, we observe an increase in the number of collaborations between the areas of Engineering and Biology [9] interested in the development of microfluidic devices [10] for use in renal epithelial studies. The devices mentioned above are structures in the micro and nano scale, which have enabled the development of microchips, miniaturized devices capable of accurately mimicking natural systems since they contain continuous infusion systems in the channels that make up these devices, covered by the cells seeded in them. These devices offer advantages such as

reproduction of the multicellular architecture or the tissue-tissue interface, the recreation of the physicochemical microenvironment and the vascular perfusion, resulting in levels of functional tissues, which cannot be obtained with 2D or 3D culture methods. Another advantage is the size of these devices, in the micro-nanometric scale. This supposes to save solutions for the maintenance of the cells, or for the execution of experiments because their volume is drastically reduced. At the experimental level, this type of device has great potential in the area of organogenesis and physiology and, in the context of discovery and development of new drugs, it has a special value in the study of the mechanisms of action, toxicity, and identification of biomarkers.

From the above information, a problem was detected and a hypothesis was proposed: the conventional culture tools do not accurately recreate the physiological environment where the cells grow and therefore, this can cause the lack of reproducibility of cellular response to toxic agents and repair mechanisms linked to renal damage. With the objective of accepting or rejecting the proposed hypothesis, it was proposed to create a model of nephrotoxicity using biomimetic culture devices that will have the necessary tools coupled to be able to use flow. This will help to reproduce the microenvironment of PT cells more accurately.

The choice of PT to develop this Thesis is based on the fact that in this segment of the nephron the majority of toxins and drugs are processed and here is where acute and chronic renal damage take places. Therefore, from the clinical point of view and with the aim of studying nephrotoxicity, PT represents the segment of choice. In order to create a model of nephrotoxicity, the use of human primary cultures of PT cells (hPTPC), would lead to an easy translation of the results to the clinic.

The molecule chosen to create the nephrotoxicity model is cisplatin, an antitumor compound used in the treatment of various types of cancers, including lung, testis and cervix. However, one of the major side effects of this compound is nephrotoxicity [11] in PT. The mechanism of action of cisplatin includes the entrance of the molecule to the hPTPC through the basolateral transporters OCT2 and CTR-1, as well as the enzyme GGT1, responsible for the conversion of cisplatin into a much more reactive molecule after entering in contact with this enzyme [12].

From the hPTPC and the nephrotoxicity model developed, we proposed to study the effect of mechanical stimulation on cisplatin sensitivity produced under flow. This allowed us to recreate a more physiological environment, closer to what we find in vivo.

The results obtained along this Doctoral Thesis suggest:

1. The isolation protocol employed to obtain primary PT cells from human nephrectomies, hPTPC, and the posterior cell characterization, allowed us to obtain a highly enriched culture of PT cells, expressing the main PT markers.
2. Combined use of GGT1 activity and cell viability assays allowed us to distinguish different cisplatin effects and were validated as useful assays to monitor cell function and cellular status.
3. The cisplatin nephrotoxicity model was consistent and amenable for its use on cells grown in microfluidic devices.
4. The hPTPC isolated and characterized along this Thesis did not present any difference in the sensitivity to cisplatin model in fluidic devices in the presence of the mechanical stimulation created by flow and compared with cells growing in static condition.

BIBLIOGRAPHY

- [1] C. Lute, Principles of Renal Physiology, 2012.
- [2] H. Koepsell, The SLC22 family with transporters of organic cations, anions and zwitterions, *Mol Aspects Med* 34(2-3) (2013) 413-35.
- [3] R. Masereeuw, F.G. Russel, Therapeutic implications of renal anionic drug transporters, *Pharmacol Ther* 126(2) (2010) 200-16.
- [4] S.K. Nigam, W. Wu, K.T. Bush, M.P. Hoenig, R.C. Blantz, V. Bhatnagar, Handling of Drugs, Metabolites, and Uremic Toxins by Kidney Proximal Tubule Drug Transporters, *Clin J Am Soc Nephrol* 10(11) (2015) 2039-49.
- [5] L. Wang, D.H. Sweet, Renal organic anion transporters (SLC22 family): expression, regulation, roles in toxicity, and impact on injury and disease, *AAPS J* 15(1) (2013) 53-69.
- [6] M.J. Wilmer, M.A. Saleem, R. Masereeuw, L. Ni, T.J. van der Velden, F.G. Russel, P.W. Mathieson, L.A. Monnens, L.P. van den Heuvel, E.N. Levtchenko, Novel conditionally immortalized human proximal tubule cell line expressing functional influx and efflux transporters, *Cell Tissue Res* 339(2) (2010) 449-57.
- [7] V. Raghavan, O.A. Weisz, Discerning the role of mechanosensors in regulating proximal tubule function, *Am J Physiol Renal Physiol* 310(1) (2016) F1-5.
- [8] T.C. Fuchs, P. Hewitt, Biomarkers for drug-induced renal damage and nephrotoxicity-an overview for applied toxicology, *AAPS J* 13(4) (2011) 615-31.
- [9] A.D. van der Meer, A. van den Berg, Organs-on-chips: breaking the in vitro impasse, *Integr Biol (Camb)* 4(5) (2012) 461-70.
- [10] E.K. Sackmann, A.L. Fulton, D.J. Beebe, The present and future role of microfluidics in biomedical research, *Nature* 507(7491) (2014) 181-9.

[11] A. Wilmes, C. Bielow, C. Ranninger, P. Bellwon, L. Aschauer, A. Limonciel, H. Chassaingne, T. Kristl, S. Aiche, C.G. Huber, C. Guillou, P. Hewitt, M.O. Leonard, W. Dekant, F. Bois, P. Jennings, Mechanism of cisplatin proximal tubule toxicity revealed by integrating transcriptomics, proteomics, metabolomics and biokinetics, *Toxicol In Vitro* 30(1 Pt A) (2015) 117-27.

[12] L. Fliedl, M. Wieser, G. Manhart, M.P. Gerstl, A. Khan, J. Grillari, R. Grillari-Voglauer, Controversial role of gamma-glutamyl transferase activity in cisplatin nephrotoxicity, *ALTEX* 31(3) (2014) 269-78.

LIST OF ABBREVIATIONS

a.s.	After Seeding
αSMA	alpha Smooth Muscle Actin
APM	Aminopeptidase M
AQP1	Aquaporin-1
ATL	Ascending Thin Limb
ABC	ATP-binding cassette transporter family
ASP+	4-4 dimethylamino styryl-N-methylpyridinium iodide
BM	Basement Membrane
BCA	Bicinchoninic Acid
BEC	Biliary Epithelial Cells
BMC	Bone Marrow stromal Cells
BSA	Bovine Serum Albumin
BCRP	Breast Cancer Resistance Protein
CB28	Calbindin-28
CDDP	Cisplatin
CKD	Chronic Kidney Disease
CD	Collecting Ducts
CTR1	Copper Transporter 1
CV	Crystal Violet
COP	Cyclic Olefin Copolymer
CD13⁺	Aminopeptidase N
CD10⁺	Acute lymphocytic leukemia antigen
DTL	Descending Thin Limb
DPPIV	Dipeptidyl Peptidase IV
DT	Distal Tubule
EMT	Epithelial-Mesenchymal Transition

ECM	Extracellular Matrix
GMNA	γ -glutamyl-4-methoxy-2-naphthylamide
GGpN	Gamma Glutamyl-p-nitroanilide
GGT1	Gamma Glutamyl Transferase
GPpN	Glycine Proline-p-nitroanilide
GFR	Glomerular Filtration Rate
GSH	platinum-glutathione conjugates
HK2	Human Kidney-2
hPTPC	human primary proximal tubular cells
HPg	Hydrostatic Pressure in the glomerulus
MCR	Medio de Células Renales
MATEs	Multidrug and Toxin Extrusion proteins
MRP2/4	Multidrug Resistance Proteins 2 and 4
NFP	Net Filtration Pressure
NaPi	Sodium-Phosphate transporter
OAT	Organic Anion Transporter
OATP4C1	Organic Anion Transporting Peptide 4C1
OCT	Organic Cation Transporters
P-gp	P-glycoprotein
PC	Polycarbonate
PDMS	Polydimethylsiloxane
PMNA	Polymethylmethacrylate
PS	Polystyrene
PCT	Proximal Convoluted Tubule
PST	Proximal Straight Tubule
PT	Proximal Tubule
PB	PrestoBlue
RT-PCR	Reverse Transcriptase-Polymerase Chain Reaction

List of abbreviations

SS	Shear Stress
SGLT-2	Sodium-Glucose Linked Transporter-2
SM	Stromal Matrix
TAL	Thick Ascending Limb
ZO-1	Zonula Occludens 1 protein



CHAPTER

1

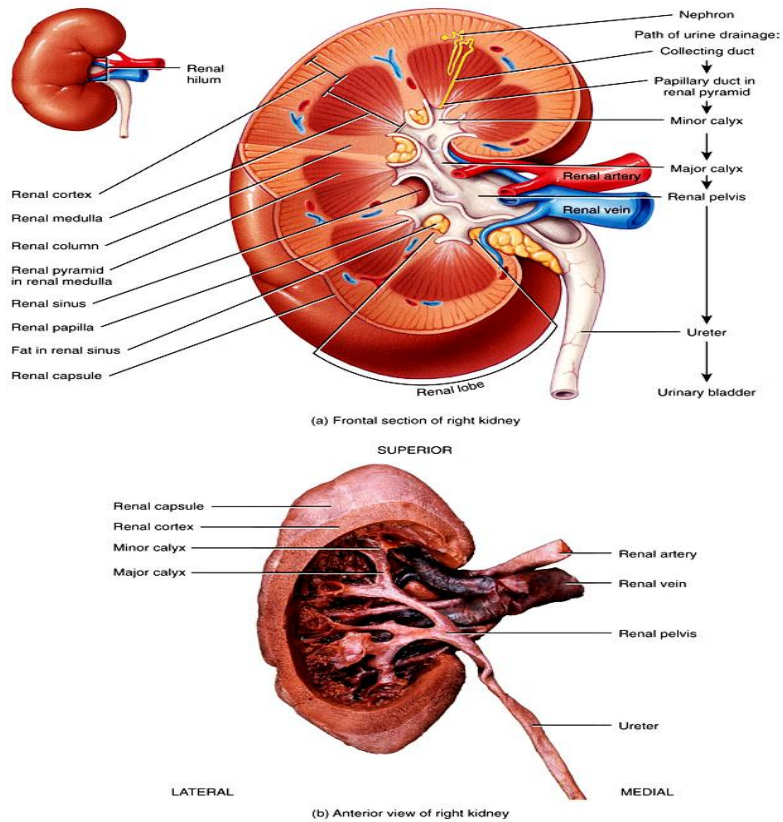
General
introduction

1.1 INTRODUCTION

1.1.1 Anatomy of the Kidneys

The kidneys are located outside the peritoneal cavity and on each side of the spine, we can find one. The shape of the kidneys is quite similar to a bean. The kidney size is dependent on body weight, so in an adult human, each kidney measures around 12-14 cm of length, 6-8 cm largeness and 4 cm of thickness. The kidney can be divided into two regions: the cortical and the medullar region. The cortex is the granular outer layer surrounding the medullar region. The medulla is the darker inner region of the kidney that can be subdivided into the outer and inner medulla. The cortex and medulla have properties structurally and functionally different: the cortex has a granular appearance, absent in the medulla, and each medullary pyramid is divisible into a zone adjacent to the cortex and a zone that includes the papilla. All these distinctions reflect the arrangement of the various tubules and blood vessels. The rounded, outer convex surface of each kidney faces the side of the body, and the indented surface, called the hilum, is medial. Each hilum is made up by a renal artery, renal vein, nerves, and a ureter. The ureter is a tube that carries urine from the kidney to the urinary bladder. There are two ureters, one attached to each kidney. The ureter can be divided in two parts: the upper half of the ureter is located in the abdomen, and the lower half of the ureter is located in the pelvic area. The renal pelvis is the dilated proximal part of the ureter in the kidney. In humans, the renal pelvis is the point of convergence of two or three funnel-like structures called major calyces. Every major calyce is formed from minor calyces, and this last structure fits over the renal tissue called pyramids. The tip of each pyramid is called a papilla and it projects into a minor calyx. The

calyces act as collecting cups for the urine formed by the renal tissue in the pyramids. The pyramids constitute the medulla of the kidney. Overlying the medullary tissue is found the cortex, and covering the cortical tissue on the very external surface of the kidney is found a thin connective tissue capsule (Figure 1.1). The cortex and the medulla are constructed almost entirely of functional structures like tubules and blood vessels. Between the tubules and blood vessels lies an interstitium, which comprises less than 10% of the renal volume. The interstitium contains the specific cells that synthesize an extracellular matrix of collagen, proteoglycans, and glycoproteins. The kidney is an organ highly vascularized receiving 20% of cardiac output and the renal vascular system comprises a renal artery and vein, respectively routes of entry and exit of blood to the kidney [1, 2].



Anatomic representation of a human kidney. a) Frontal section of right kidney. b) Anterior view of right kidney. The kidney can be divided in two different portions: the outer portion is formed by the cortex, and it contains all the glomeruli. The inner portion is known as medulla, and it is constituted by pyramids able to drain into the renal pelvis calyces, that in turn, it is formed by minor calyces. Source: Gerard J. Tortora and Bryan Derrickson, *Principios de Anatomía y Fisiología*, 2013 [3].

1.1.2 Function of the kidneys

The kidneys are essential organs in the homeostatic regulation of the human body, able to handle 180 L of plasma filtrate every day, to finally excrete about 1.5 L per day in the form of urine containing waste products or foreign substances.

The kidneys perform different functions for the body, most of which are essential for life. Below, the main functions are listed:

Function 1: Regulation of Water and Electrolyte Balance. The kidneys match renal excretion to the intake of water and electrolytes to regulate the osmolality and volume of body fluids. Differences between input and output are regulated by the kidney. So, a deficit of water or electrolytes can be compensated by increasing the intake and the retention, whereas excesses are compensated by varying the output of water in the urine. Electrolytes like Na^+ , K^+ , and Mg^{2+} amongst others, form part of our diet and they are present in our body [4].

Function 2: Regulation of Arterial Blood Pressure. The kidneys play a central role in the regulation of arterial blood pressure. Blood pressure depends on blood volume, and the kidneys' maintenance of sodium and water balance achieves regulation of blood volume. Renal artery perfusion pressure regulates the blood pressure through the sodium excretion and influences the activity of various vasoactive systems such as the renin-angiotensin-aldosterone system that regulate smooth muscle in the peripheral vasculature [5].

Function 3: Excretion of Metabolic Waste. The kidneys work as filters, removing metabolic wastes and toxins from the blood and excreting them through the urine. Some of these metabolic wastes are the urea, uric acid, creatinine, the end products of hemoglobin breakdown, among others. Usually, these waste products of metabolism are toxic and should be removed from the body [6].

Function 4: Excretion of Bioactive Substances. The excretion of bioactive substances includes hormones and drugs that affect the body function. In the organism, there are different forms of excretion of these

types of bioactive substances performed by different organs like the liver, the lungs and the kidneys amongst others, and it is worth to mention the role of the specific drug transporters played in these organs [7].

Function 5: Regulation of Red Blood Cell Production. The erythrocytes production takes place in the bone marrow under the control of a peptide hormone called erythropoietin [8], which major source of secretion is the kidney. EPO is secreted in the kidney by the juxtaglomerular cells, and its secretion is produced in response to decreased O₂ delivery and increased levels of androgens. EPO stimulates the bone marrow to increase its production of erythrocytes [9].

Function 6: Regulation of Vitamin D Production. Vitamin D synthesis involves a series of biochemical transformations. The last biochemical transformation takes place in the kidneys. The active form of vitamin D (1,25-dihydroxyvitamin D₃) plays a critical role in calcium and phosphorus metabolism, bone growth, and tissue differentiation [10].

Function 7: Gluconeogenesis. Although the liver has the critical role of maintaining blood glucose homeostasis and therefore, is the major site of gluconeogenesis, a substantial fraction occurs in the kidneys, particularly during physiological conditions such as a prolonged fast and pathological conditions, as liver failure. The kidney can provide glucose to the blood via renal gluconeogenesis. In the renal cortex, glutamine is the preferred substance for gluconeogenesis [11].

Function 8: Regulation of acid-base balance. The correct maintaining of a normal body pH is essential to the efficient functioning of many physiological processes. In the kidneys take place the excretion of the acids and also, the acid-base regulation, through the reabsorption of the

filtered bicarbonate. In the acid-base balance, the kidney is responsible for the reabsorption of filtered bicarbonate and the excretion of acids. Both processes involve secretion of H^+ into the lumen by the renal tubule cells, but only the second leads to excretion of H^+ from the body [12].

1.1.3 The nephron

The nephron is the structural and functional unit of the kidney. The human kidney contains approximately 1 million nephrons. Every nephron is constituted by the renal corpuscle, a spherical structure that works as a filtering component and the renal tubule, that is a long narrow tube where the filtered fluid is processed and converted into urine, and it is constituted by different segments: Proximal Tubule, Loop of Henle, Distal Tubule, Collecting Duct. (Figure 1.2) [13].

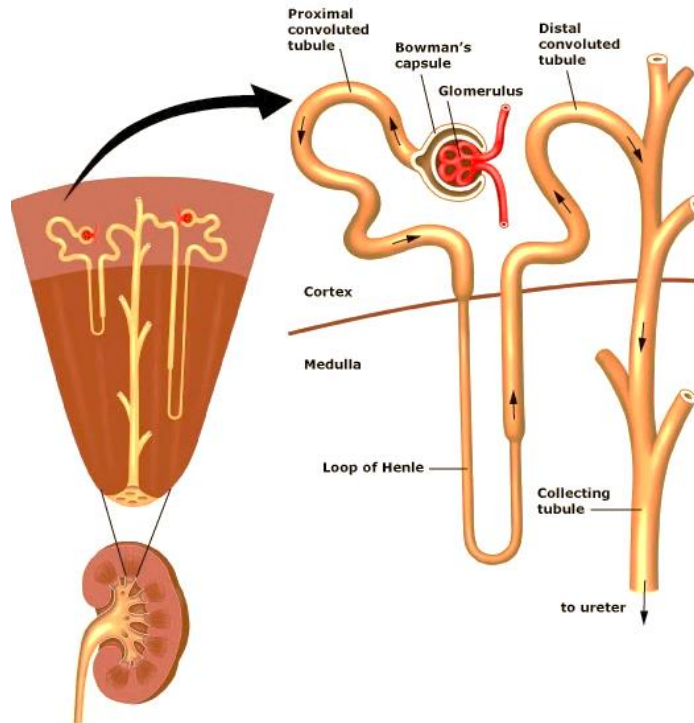


Figure 1.1: Structure and location of the nephron. The renal corpuscle is the filtration component and it is constituted by the glomerulus and the capsule. Here is where the blood is filtered. The tubule is constituted for the different segments represented in the figure, and its mission is to process and convert into urine the filtered fluid. Source: Esley A. Inker and Ronald D. Perrone, Assessment of kidney function, 2015, UpToDate [14].

1.1.3.1 The renal corpuscle

The renal corpuscle is formed by the glomerulus, a compact structure with interconnected capillary loops and the Bowman's capsule, a hollow capsule surrounding the glomerulus. Blood enters and leaves Bowman's capsule through arterioles. The Bowman's space, located inside the capsule, receives the filtered fluid. The Bowman's capsule has an outlet that leads into the first portion of the tubule.

The filtration barrier consists of three layers: the endothelium of the glomerular capillaries, the basement membrane and a single layer of

epithelial cells. The first layer consists of endothelial cells permeable to all components found in the blood except erythrocytes and leucocytes. The middle layer is the basement membrane constituted by glycoproteins and proteoglycans. The last layer is formed by podocytes, which are epithelial cells. The podocytes have structures called pedicels extended from each branch of the podocyte and embedded in the basement membrane. The pedicels of some podocytes are interdigitated with those of adjacent podocytes and the space created between the pedicels is the way by which the filtrate, once it travels through the endothelial cells and the basement membrane, passes to enter the Bowman's Space. The anatomical constitution explained so far is fundamental since it allows the filtration of large volumes of liquid from the capillaries into the Bowman's space, while it restricts the filtration of large plasma protein molecules. Finally, we find the mesangial cells in the central part of the glomerulus that act as phagocytes and remove the trapped material from the basement membrane [15, 16].

1.1.3.2 The Tubule

The renal tubule is the part of the nephron in which the filtrate from the glomerulus enters and the molecules and substances are reabsorbed or secreted. Along the different segments of the renal tubule, the single layer of epithelial cells resting on a basement membrane exhibits very large differences in morphology, protein expression patterns, and very specific activities. The different segments found in the renal tubule are [17-21]:

1.1.3.3 Proximal tubule

The proximal tubule (PT) is the first part of the renal tubule. It is divided into three segments (S1, S2 and S3) whose structural complexity

decreases from the S1 to the S3 segment. The S1 corresponds to the first half of the proximal convoluted tubules (PCT) and gets the primary urine of the glomerulus, in the renal cortex; the S2 segment includes the second half of the PCT and the first half of the proximal straight tubule (PST) [22]; the S3 is the resting half of the PST, in the medulla. The PST leads the urine to the first part of the Henle's Loop. The cells that form the PT contain brush border and strong basolateral folds. It has an acidophilic cytoplasm due to the number of mitochondria. In PT, the bulk of ion and water reabsorption takes place, important substrates like glucose and protein (amino acids) are reabsorbed, and organic anions and cations including drugs and toxicants, are secreted into the lumen. PT is also the place for important metabolic and endocrine activities. High metabolic rates and exposure to toxins make the PT more exposed to hypoxia and chemical insult than other nephron segments. Accordingly, most *in vitro* models of renal function have focused on reproducing PT function.

1.1.3.4 Loop of Henle

After filtrates leave the PT, it enters the loop of Henle. The loop of Henle has an 'U' shape and it can be found in two different loop lengths: a short loop and a long loop. The short Henle loops have a descending thin limb and a thick ascending limb. The long Henle loops have a thin descending and a thin and thick ascending limb. The loop of Henle has three parts well defined:

- Descending Thin Limb (DTL). The TDL is highly permeable to H₂O, but it has low permeability to ions and urea.
- Ascending Thin Limb (A TL). The ATL is impermeable to H₂O, but it is permeable to ions.

- Thick Ascending Limb (TAL). The TAL is the part where Na^+ , K^+ , Cl^- ions are reabsorbed from the urine by the cotransporter NKCC2. It is impermeable to the H_2O .

The DTL and the ATL are made up of flattened epithelial cells, not very specialized. The TAL is constituted of specialized epithelial cells with a huge number of mitochondria necessary for high active NaCl transport rate. The TAL includes the specialized Macula densa cells, which are in contact with the mesangial cells of the glomerulus. The Macula densa forms part of juxtaglomerular apparatus which main function is to regulate blood pressure and the filtration rate of the glomerulus.

1.1.3.5 Distal Tubule

The distal tubule (DT) is constituted by cuboidal cells without a brush border, showing an epithelium with structures (microvilli, mitochondria) that allow high absorption processes. In this segment, we can identify two parts:

- The pars recta that constitutes the start of the DT
- The pars convoluta that constitutes the end of the DT.

The principal function of the DT is reabsorbing Na^+ and Cl^- . It is relatively impermeable to H_2O but in the presence of antidiuretic hormones, its permeability to H_2O increases making urine concentrated. Aldosterone is highly active in this segment. The DT also secretes ammonium ions and hydrogen ions.

1.1.3.6 Collecting Duct

The last segment of the renal tubule is the Collecting Ducts (CD) [23]. The CD is in charge of collecting urine from the nephrons and moves it into the renal pelvis. The CD are lined with cuboidal epithelium

containing two cell types: principal cells and intercalated cells. The principal cells reabsorb Na^+ and H_2O and secrete K^+ . These functions are regulated by ADH and aldosterone. The intercalated cells participate in the acid-base homeostasis, and there are two types: α -intercalated cells secrete hydrogen ions via an apical H^+ ATPase and a H^+/K^+ exchanger and reabsorb bicarbonate. β -intercalated cells secrete bicarbonate via pendrin and reabsorb acid. The intercalated cells play important roles in the kidney's response to acidosis and alkalosis.

The Figure 1. 3 shows the different segments of the renal tubule explained in this section.

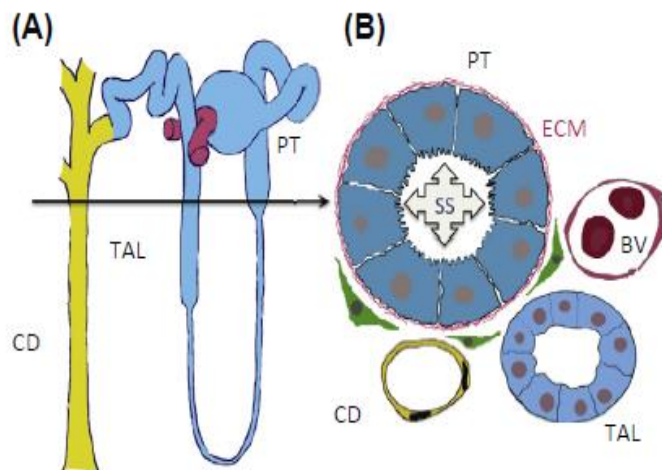


Figure 1.2: Functional 3D interactions for a renal tubule. (A) Nephrons are the kidney functional units. They consist in longitudinal tubule structures made of epithelial cells. Every nephron starts at the renal corpuscle, where it meets the vasculature and plasma is filtered through the glomerular capillaries. Then, ultrafiltrate flows along the proximal tubule (PT), the loop of Henle and the distal nephron, eventually draining into CD. Abrupt morphological changes occur at every segment transition, reflecting very different functions. (B) Cells within each tubule are exposed to four independent interactions. Luminal flow creates a shear stress (SS) over the apical surface. Binding to surrounding protein matrix (ECM, fibers) serves to sense mechanical and biochemical cues important for

tubule differentiation and function regulation. Neighboring interstitial and tubular cells send paracrine signals to modulate function and repair process (TAL, CD). Finally, oxygen, nutrients and hormones supply is ensured by blood perfusion through surrounding capillaries (BV) Source: N. Sánchez-Romero, P. Meade and I. Giménez, Microfluidic-Based 3D Models of Renal Function for Clinically Oriented Research, 2016 [24].

1.1.4 Basic processes performed by the nephrons

Urine formation and blood composition are processes that take place in the nephron, and at the same time, it involves three processes: glomerular filtration, in the glomeruli and secretion and reabsorption, in the renal tubules. These processes are going to be detailed as follows.

1.1.4.1 Glomerular Filtration

Glomerular filtration is the first step in urine formation, and it is a passive and very selective process, in which hydrostatic pressure forces fluids through the glomerular membrane. During the glomerular filtration, the blood is filtered and the molecules and waste products in this filtrate are removed from the glomerular capillaries. The glomerulus is a very efficient filter with a large surface area and extremely permeable to water and solutes. Molecules such water, glucose or amino acids are really small, usually smaller than 3 nm in diameter can pass freely from the blood into the Bowman's space. Molecules larger than 5 nm pass with greater difficulty, and they are barred from entering the tubule.

The Mechanisms of Filtration

The process by which glomerular filtration occurs is called renal ultrafiltration. The force of hydrostatic pressure in the glomerulus (HPg) is the driving force that pushes filtrate out of the capillaries and into the nephron. The osmotic pressure works against the greater force of

hydrostatic pressure, and the difference between these two determines the force by which molecules are filtered. The net filtration pressure (NFP) is the responsible for filtrate formation. The glomerular filtration rate (GFR) is directly proportional to the NFP.

Regulation of Glomerular filtration rate

GFR is regulated by intrinsic and extrinsic controls.

1. Intrinsic controls: It works by adjusting its own resistance to blood flow and it is known as renal autoregulation. The renal autoregulation entails two types of controls:

- Myogenic mechanism. The myogenic mechanism reflects the tendency of vascular smooth muscle to contract when stretched.
- Tubuloglomerular feedback mechanism. It is performed by the macula densa cells. When GFR increases, the macula densa cells release a vasoconstrictor chemical (ATP) that causes intense constriction of the afferent arteriole and a decrease of NFP and GFR. When the macula densa cells are exposed to slowly flowing filtrate with its low NaCl concentration, ATP releases is inhibited, causing vasodilation of the afferent arterioles, and an increase of the NFP and GFR.

2. Extrinsic controls: This type of control regulates the GFR maintaining the systemic blood pressure through neural and hormonal mechanisms. It entails two types of controls:

- Sympathetic nervous system controls. This control works with the goal to satisfy the needs of the body. When the volume of the extracellular fluid is normal, the sympathetic nervous system does not work and is the renal autoregulation that prevails.

- Renin-angiotensin mechanism. This mechanism is activated when various stimuli cause the granular cells to release the hormone renin. The hormone renin has to be transformed to regulate the GFR. The renine acts enzymatically on angiotensinogen, converting it to angiotensin I. This, in turn, is converted to angiotensin II by angiotensin converting enzyme. Angiotensin II acts in four ways to stabilize systemic blood pressure and extracellular fluid volume: 1. As a potent vasoconstrictor. 2. Stimulating the reabsorption of sodium. 3. Stimulating the hypothalamus to release antidiuretic hormone and activating the hypothalamic thirst center. 4. Increasing fluid reabsorption by decreasing peritubular capillary hydrostatic pressure.

It is important to mention that there are other factors affecting GFR. Usually, these factors are produced by renal cells that have the capacity to secrete a battery of chemicals, many of which act as a paracrine factor: prostaglandin E2 (PGE2), adenosine and intrarenal angiotensin II [25, 26].

The volume and solute contents of the final urine are quite different from those of the glomerular filtrate because its composition is altered through the tubular reabsorption and tubular secretion.

A combination of filtration, reabsorption, and secretion is applied specifically for each plasma substance.

1.1.4.2 Tubular reabsorption

The tubular reabsorption is a selective transepithelial process that begins when the filtrate enters the proximal tubules. The reabsorbed substances can follow the transcellular or paracellular route with the goal

to reach the blood. In the transcellular route, transported substances move through the luminal membrane, the cytosol, and the basolateral membrane of the tubule cell. In the paracellular route, the movement of substances across the tubule cells is limited because these cells are connected by tight junctions.

Sodium Reabsorption

The most abundant cations in the filtrate are Na^+ ions. The active Na^+ reabsorption is promoted by two processes:

1. Na^+ is actively transported out of the tubule cell by primary active transport through a $\text{Na}^+\text{-K}^+$ ATPase pump. Then, Na^+ is brushed along by the bulk flow of water into adjacent peritubular capillaries.
2. Active pumping of Na^+ from the tubule cells results in a strong electrochemical gradient that favors its passive entry at the luminal face via secondary active transport carriers or via facilitated diffusion through channels.

The reabsorption of Na^+ by primary active transport provides around the 80% of the energy for reabsorbing almost every other substance.

Reabsorption of Nutrients, Water, and Ions

Substances reabsorbed by secondary active transport include glucose, amino acids, lactate, and vitamins. Mechanisms for passive tubular reabsorption include osmosis, diffusion and facilitated diffusion and the substances move down their electrochemical gradients. Here, it is important to mention the role of aquaporin, transmembrane proteins that form water channels across cell membranes [27].

1.1.4.3 Tubular secretion

The tubular secretion is the process where substances such as creatinine, K^+ , H^+ , NH_4^+ , drugs and some organic acids are transferred from the peritubular capillaries into the filtrate through the tubule cells or are synthesized in the tubule cells and secreted.

The tubular secretion occurs in the opposite direction to the mechanism of reabsorption, and we can distinguish between two types of transports: passive diffusion and active transport.

Tubular secretion plays an essential role in the body to eliminate excess K^+ , to remove substances, such as certain drugs and metabolites, which are closely linked to plasma proteins, to control the pH of the blood and to discard end products, toxic products and undesirable substances that have been reabsorbed by passive processes [28].

1.1.5 The evolution of nephro pharmacology

The correct maintenance of the kidneys is essential but unfortunately, there is a high incidence of acute and chronic kidney disease (CKD), a rising global health problem with significant morbidity and mortality. These conditions affect 5–7% of the world population [29, 30]. In 2012 in the United States, total medical care expenditures for chronic kidney disease were near \$58 billion [31]. This problem emphasizes the need to explore new strategies to slow down or reversing renal disease progression. Nephro pharmacology is the discipline that studies the connection between clinical pharmacology and nephrology [32].

This discipline started almost 50 years ago, with the contribution of Kunin *et al.* in 1959 when they demonstrated the dependence of drug elimination half-life ($t_{1/2}$) on renal function. Currently, the scope in

nephropharmacology focuses on research related to specific drug therapy of renal diseases, as well as renal drug safety, because each year an estimated 18-27% of acute kidney failures are caused by drugs [33].

The development of novel drugs is both a time-consuming and cost-intensive process, and about one-third fails due to toxicological concerns and/or lack of suitable testing methods capable of predicting clinical usefulness and drug toxicity during pre-clinical development [34, 35]. For these reasons, suitable model systems for reliable pre-clinical testing are essential to validate clinical safety. Presently, the test systems in use only cover certain aspects of nephrotoxic side effects [36]. The conventional models available to study nephropharmacology include 2D PT cells cultures and animal models. The problem with these models is that they do not reliably recapitulate the *in vivo* human response to drugs, and about 7% of drug candidates fail as a consequence of undetected nephrotoxicity in pre-clinical testing with 2D cell cultures and animal models [37, 38]. At the same time, it is estimated that 30–50% of all cases of severe acute renal failure in patients are due to drug-induced nephrotoxicity [37, 39]. These facts highlight that the conventional methods used in nephropharmacology are not satisfactory enough to predict the human response. The most advanced approaches are focusing on the generation of 3D cell culture models because these models exhibit features that are closer to the physiological conditions [40, 41], and they are more realistic for translating the study findings for *in vivo* applications [42]. The generation of 3D renal cultures as suitable model systems includes the incorporation of advanced biocompatible materials or functionalized biopolymer hydrogels as matrices in combination with highly differentiated renal cells. These new technologies are expected to revolutionize our ability to understand and

predict clinically relevant renal responses for their application in kidney disease.

1.1.6 Engineered renal models for reducing animal studies

To study nephropharmacology the models currently applied include animal models [43] and test models in cell monolayer (2D) cultures [44]. Drug testing studies and toxicological screenings use different animal species like mice, rats, hamsters, rabbits, fishes (zebrafish, trout), birds (mainly chicken), guinea pigs, amphibians (*Xenopus* frogs), primates, dogs, cats, *etc.* The number of animals used in research every year has gone up with the advancement in medical technology [45]. Aside from ethical considerations, the use of animals in pharmacology preclinical testing is very time consuming, laborious and expensive [46]. These disadvantages have forced researchers to find new alternatives to decrease the time and the money involved in the studies and, of course, to decrease the number of animals used. Russell and Burch have defined these alternatives by three R's - Reduction, Refinement and Replacement [47]. These alternative strategies include a wide variety of new *in vitro* techniques, as 3D cell cultures.

No new drug can be used in patients until it has been extensively tested in animals, but the new alternative methods can help to reduce the number of animals required for nephropharmacology studies. 2D cell culture models offer the advantage of being simple, are compatible with high-throughput drug screenings and are low in cost [48]. However, in conventional 2D cell culture, cells spread mainly in the horizontal direction, resulting in flattened cells that easily dedifferentiate and are therefore less physiologically relevant compared to 3D cell culture [49, 50] (Table 1.1). The design of pharmacological studies based on 2D cell

cultures could, therefore, be biased. Another disadvantage of these models is their incapacity of recapitulating the complexity of the *in vivo* environment [51, 52]. It has been shown that 2D cell culture models require higher doses over longer time periods to induce a toxic response compared to *in vivo* and/or in humans toxicity responses[53]. These limitations could be improved using 3D cell cultures of human cells. In nephrotoxicology, the use of 3D cell culture models reflects the physiological situation better. In support, it was demonstrated that a 3D cell culture system was more sensitive to nephrotoxic compounds than the same cells grown in 2D, due to a preserved epithelial character. Additionally, long-term studies revealed the utility of the 3D model for chronic toxicity studies as well [38].

Table 1.1: Overview of conventional 2D cell culture versus 3D cell culture models

	Advantages	Disadvantages
2D cell culture	<ul style="list-style-type: none"> - Simple model - Low-cost 	<ul style="list-style-type: none"> - Flattened cells - Studies can be biased - Incapacity to mimic the physiological environment - Exposure of high dose over time to induce a toxic response
3D cell culture	<ul style="list-style-type: none"> - Improvement of physiological environment - Easy detection of biomarkers indicative for nephrotoxicity - It is a translational model from the <i>in vitro</i> to the <i>in vivo</i> situation - More sensitive to drug exposure 	<ul style="list-style-type: none"> - Novel and more relevant 3D models are still under study. - It will need time to adapt this technology to the labs and companies

1.1.6.1 Renal cells in use

The development of this Thesis is focused in a specific type of cells: The proximal tubular cells [54]. From now on, every different section of

this manuscript will be focused mainly on these cells or to the segment of the nephron where these cells are located, the PT.

Some of the most important morphological characteristics of PT cells include a columnar shape epithelium with a cobblestone formation, the presence of a brush-border and the possibility to distinguish between an apical and a basolateral membrane because of cell polarization. Also, PT cells are characterized by the differential expression and activity of specific membrane transporters and metabolizing enzymes. One of the most critical steps in the development of *in vitro* models to study nephrotoxicity is to be able to cultivate large numbers of cells with these specific phenotypical features. Below, the available sources of cells with defined renal phenotypes will be discussed, with a special focus on cells reproducing PT cells phenotype.

Renal primary cell cultures

Renal primary cell cultures are defined as cells that have been freshly isolated and derived from the original kidney or kidney explants from donors. In the last years, also isolating renal epithelial cells from human urine has successfully been achieved [55]. Renal Primary cells closely mimic the physiological state of cells *in vivo*, but the principal limitation of these cells is the process of dedifferentiation and the predetermined number of cell divisions before entering senescence. We already mentioned the PT is the best-studied segment from a clinical perspective. Thus, reports appear periodically describing new or improved methods to isolate and grow PT cells [56-58].

Immortalized Cell Lines of Renal Origin

The use of permanent cell lines began in the 1970s by renal and transport physiologists when they recognized that some of these cells

retained some kidney-specific characteristics. More recently, continuous renal cell cultures have gained importance for investigating the pharmacology of potentially nephrotoxic xenobiotics, medicines and in general, to study nephropharmacology. These studies have revealed highly robust and reproducible PT cells specific functional results over prolonged culturing [59].

Several permanent cell lines of renal origin have been established, in order to overcome the limitations of primary cells. The immortalization process is usually elicited by transfection and/or injection of Simian virus (SV40), papillomavirus (16E6/E7) genes, human Telomerase reverse transcriptase (hTERT) or transformation into primary cells of defined nephron origin; this has been carried out with renal cells from various species, including human cells. Transformed cells acquire the ability to proliferate indefinitely; however, in most cases, these cells had already suffered some dedifferentiation allowing them to grow under artificial conditions. Careful isolation, purification, and characterization have allowed for the generation of specific cell lines with adequate preservation of characteristic functional markers of defined nephron segments. In Table 1.2 the most widely used renal cell lines are represented, with a special focus on cells reproducing PT phenotype.

In addition to human cell lines, animal-derived cell lines like MDCK, LLC-PK1, NRK-52 and OK have been extremely useful for *in vitro* research of normal and altered renal epithelial function because these cells retain enough phenotypic parameters to allow for studying specific characteristics or activities, and have lesser requirements and proliferate indefinitely, unlike primary culture.

Table 1.2: Representation of the most widely used renal continuous cell lines.

Cell line	Species	Presumed Cell type origin	References
SGE-1	Wistar rat	Glomerulus	[60]
NRK-52E	Norway rat	Proximal tubule	[61]
LLC-PK1	Hampshire pig	Proximal tubule	[62]
OK	American opossum	Proximal tubule	[63]
MCT	Mouse	Proximal tubule	[64]
JTC-12	Cynomolgus monkey	Proximal tubule	[65]
HK-2	Human	Proximal tubule	[66]
CiPTEC	Human	Proximal tubule	[55]
RPTEC	Human	Proximal tubule	[67]
caki-2	Human	Renal carcinoma	[68]
mTAL	Rabbit	Medullary TAL	[69]
MDCK	Dog	Distal tubule and collecting duct	[70]
A6	Xenopus Laevis	Distal tubule and collecting duct	[71]
PAP-HT25	Rabbit	Inner medullary epithelium	[72]

1.1.7 Experimental models using renal cell cultures

The tubular structure is encased in the basement membrane (BM), a thin layer made of laminin, collagen IV, entactin/nidogen, and sulfated proteoglycans. As mentioned before, the renal tubule is a tiny tube subdivided in different segments, where the glomerular filtrate with wastes, extra fluid and other recyclable substances, like Na^+ and PO_4^{3-} , passes through.

Renal tubules are in contact with the vascular network, the interstitium, and other renal tubules. All these relationships should be kept in mind if the goal is to understand and reproduce renal function. For this reason, a recreation of the environment of the tubular structures is essential. Depending on the biological question that needs to be elucidated, multiple culture formats are available. The most relevant culture formats used in the field of nephropharmacology are discussed here in more detail.

1.1.7.1 Role of the extracellular matrix

In native kidneys, cells are embedded in a complex extracellular matrix (ECM). The ECM is a very dynamic and highly charged structure, and it plays a very important role as an active component in cell signaling, support, morphogenesis, reparation and regeneration [73]. In addition to its mechanical support function, the ECM harbors essential growth factors and signaling molecules important for tissue organization and function. The importance of cell-ECM interactions in driving differentiation towards a particular phenotype is well described [74], and an example of these interactions is found in the Human Kidney-2 (HK2) cell line, which showed an improved proximal tubular phenotype when

they were cultured on micro-scaffolds obtained by decellularizing 300 μm fragments of renal stroma [75].

The ECM is composed of basement membrane (BM) and the stromal matrix (SM): The BM is a sheet-like scaffold and comprises fibronectin, proteoglycans, laminin and collagen IV and it provides a number of physical and chemical interactions that cells need for proper self-recognition and differentiation. BM plays important roles in the kidney, illustrated by the fact that defects in renal BM are associated with kidney malfunction [76, 77]. Obviously, renal cells recognize the roughness and hardness of the BM in the same way than other tissues [78]. These properties were used in attempts to recreate artificial ECM substrates [79, 80] where it was appreciated that the topology offered by the polymeric structures could actually be more important than the bioactive signals they provide [81-83]. The SM is composed of collagen I, proteoglycans and glycosaminoglycans, which form fibrous structures providing the major structural support of the ECM. The SM is responsible for holding together nephrons, blood vessels and other elements from the kidney parenchyma [84]. Integrins, transmembrane receptors located in the PT cells play an important role as the mediators in the cell-ECM adhesion and signaling [85]. After understanding the role of ECM in cell adhesion, structure and function, it is essential to incorporate its components in a 3D model.

1.1.1.7.2 Two-and-a-half-Dimensional Renal Cell Culture

A drip culture is a cell culture format reflecting 2.5D, where the cells grow on top of an ECM and the growth medium of cells contains diluted ECM proteins. The advantage of this type of culture is the induction of a more physiological architecture than conventional 2D cultures [44, 86].

Some of the most relevant applications of this cell culture format are for imaging and antibody staining.

1.1.7.3 Two-and-a-half-Dimensional Renal Cell Culture in Transwell Devices

A Transwell is a membrane insert used for cell cultures, which ensures the formation of a compartmentalized system, allowing the cells to polarize. This also offers the possibility to work with co-cultures in independent compartments that communicate by the release of signaling molecules. However, due to the high costs and the fact that working with Transwells is laborious, these devices are extensively used in industry, but they have not been widely adopted in academia.

1.1.7.4 Three-Dimensional Renal Cell Culture on ECM-Coated Surfaces for Bioartificial Kidney Applications

The increasing incidence of end-stage renal disease, a shortage of kidney organ donors, and the significant impact on patient's life of current dialysis and hemofiltration techniques, generates an urgent need for alternative renal replacement therapies. One of the most actively pursued potential renal replacement therapies in the last years is the bioartificial kidney [35], a cell therapy based on *in vitro* culture of renal cells. It consists of the combination of a hemofilter in series with a bioreactor unit containing renal PT cells, termed a renal assist device [42]. Cells are seeded and grown as a confluent monolayer in the lumen of hollow fibers. The hemofiltrate is passed through the lumen and the blood through the space between the fibers. The goal is that cells will reabsorb biologically relevant substances from the filtrate, will secrete toxins into the filtrate, and will produce metabolic and endocrine functions of renal epithelia. In this way, the hemofilter would provide the

glomerular function while the cell-based cartridge will be delivering those functions of the tubular portion in the nephron [87, 88].

1.1.7.5 Three-Dimensional Renal Cell Culture in Hydrogel

Culture systems that better mimic the biological milieu are needed to bridge the gap between conventional cultures and complex native *in vivo* environments. Hydrogels are good tools for getting this goal. A hydrogel is a biocompatible polymer network with high water content and with physical properties that closely mimic the natural ECM. This ability to swell under biological conditions makes them an ideal class of materials for biomedical applications, such as drug delivery and tissue engineering [89-91]. A renal cell 3D culture system consists of cells embedded in an ECM gel generated by mixing the renal cells with a liquid ECM matrix at the time of seeding [86, 92]. These gels then polymerize based on physical (e.g. temperature or light) or chemical (e.g. pH or ionic strength) stimuli [93].

1.1.8 Other nephropharmacological models

The formation of a complex architecture *in vitro* and the incorporation of factors such as shear stress forces due to luminal fluid flow represent new 3D kidney model alternatives to apply in the area of nephropharmacology. These include decellularized kidney as native ECM scaffolds, kidney on a chip technology and 3D bioprinting techniques. Below all these nephropharmacological models will be discussed.

1.1.8.1 Decellularized kidney

Recent developments within the field of regenerative medicine also include the generation of bioscaffolds through organ decellularization. In this process, the ECM is isolated from a tissue by removing its inhabiting

cells and leaving a native ECM scaffold. Various researchers demonstrated that decellularized kidneys from animals or human could be used as 3D biological scaffolds. The decellularization process conserves the mechanical and biological properties of the ECM, generating a template that can maintain natural stromal architecture and some residual molecules and thus may promote attachment, differentiation and proliferation of newly grafted cells [94, 95]. Eventually, the regenerated tissue can be used as a transplantable organ. Since the kidney has one of the most complex architectures of the body, generating an efficient decellularization method that preserves the vascular networks and parenchymal anatomy of the native kidney has been a strongly pursued objective in regenerative medicine. Next to being a source for organ transplantation, decellularized-recellularized kidneys can also be used as a model to study the interaction of drugs affecting tissue failure and enhancing repair mechanisms. Currently, the principal limitation to obtain functional recellularized kidneys is the complexity of the organ, requiring advanced bioengineering processes. For recellularization, knowledge can be obtained from the rapidly evolving field of mini-organs, called kidney organoids[96-98]. These mini-organs form more sophisticated models to fill the gap between *in vitro* and *in vivo* understanding of functional kidney development and repair [99].

1.1.8.2 Bioprinting

3D kidney bioprinting is a new technology with the goal of developing functional full-size kidneys. This new emerging technology is based on the use of computers and modified printers-based technology, where biomaterials chosen to create de novo full-size kidney are used to print

layer-by-layer specific biological materials, with spatial control of the placement of functional components [100, 101]. Currently, researchers do not have the capacity for building a complex and large 3D kidney; therefore, the most relevant studies published have focused on kidney 3D bioprinting on a small scale with the generation of 'mini-tissue' building blocks [100, 101]. The creation of de novo kidneys is the goal of 3D bioprinting, but other applications include developing high-throughput 3D-bioprinted tissue models for research, such as drug discovery and toxicology.

1.1.8.3 Microfluidic devices

To recreate the physiological environment found *in vivo* in 3D cell models, the addition of bioreactor systems is essential because it will allow a continuous fluid flow on the cells. This new approach is possible with the use of microfluidic devices, such as kidney microchips. It has been the technology used for the development of this thesis.

Microchips technology is defined as a cell culture model in a system with a micrometer scale that incorporates important features like dimensional and morphological relevance, flow shear stress, mechanical strain and co-culture capabilities, among others [102]. A variety of cells of renal origin have been grown in microfluidic devices: e.g. primary human proximal tubule [49], primary inner medullary collecting duct [103] and HK-2 cells [104]. The design of the microchip depends on the desired purpose. One parameter necessary to design a microchip is the geometry of the system. The material selected for the fabrication could be a limitation, for this reason, it is necessary to choose materials very carefully. For instance, when used in combination with live imaging, materials should have optimal optical properties to avoid auto-

fluorescence. During the design phase, it is also necessary to consider whether the available microscope set up is compatible with microfluidic devices [24].

The use of microfluidic devices present some advantages compared with traditional cell culture models: 1) It saves expensive reagents because of the small volumes running through the micro-scaled chambers. 2) It could prolong culture of cells without the need for subpassaging or repeated media changes, 3) the incorporation of mechanical stimulation that can be interesting for those cells or tissues that endure such stimulation *in vivo* and respond to it by acquiring specific phenotypes.

A large part of the work with microfluidic devices demonstrated that this new technology is widely applicable in biomedical research, so this technology is highly valuable for studying renal physiology and pathology. For example, in the nephropharmacological area, Chocha-Snoub *et al.* developed a microfluidic kidney model to study the nephrotoxic effects of ifosfamide [105]. Ifosfamide is a drug metabolized by the liver into a bioactive and nephrotoxic compound. Using a liver micro-device directly linked to a kidney device, they demonstrated the interaction between the two organ systems, mimicking the sequence of events. The kidney cell toxicity was apparent only when the liver metabolized ifosfamide and then was perfused through the kidney device, but not when the order of exposure was reversed. Another relevant example was published by Jang *et al.* and they showed that the cells under fluid flow performed better at recovering from cisplatin toxicity than the cells in static culture, suggesting a role for shear-stress

in renal repair. In addition to renal toxicology, efficient cell differentiation [106] and kidney stone formation [104] have been addressed by using microfluidic devices.

1.2 HYPOTHESIS AND RESEARCH AIMS

The conventional models and tools for cell culture available are not satisfactory enough to predict the human response, basically because they cannot recreate the physiological environment where the cells grow *in vivo* and thus, this may lead to the lack of reproducibility of the cellular response against toxic and reparation mechanisms linked to renal damage.

1.2.1 Objectives

General objectives: Development and experimental validation of an innovative culture system based on microfluidics where human renal proximal cells can be grown in a biomimetic environment for studying renal damage and repairing.

Specific objectives:

1. Development of methods and procedures for the isolation and cell culture of human primary proximal tubular cells (hPTPC).
2. Phenotypic characterization of cells obtained from the primary culture at the level of gene expression, protein markers, enzymatic activity in living cells and transporters.
3. Development and validation of a new nephrotoxicity model using cisplatin for the study of cell viability and expression of specific markers implied in the bioactivation of this molecule.
4. Screening of molecules potentially repaired of the damage produced by the cisplatin.

Hypothesis and Objectives

5. Development of the protocol for differentiated proximal tubular cell cultures in a device that allows us the application of Shear Stress (SS).
6. Determination of the SS effect in the sensibility to cisplatin in hPTPC.

1.3 BIBLIOGRAPHY

- [1] M.A. Wallace, Anatomy and physiology of the kidney, *AORN J* 68(5) (1998) 800, 803-16, 819-20; quiz 821-4.
- [2] H.G. Preuss, Basics of renal anatomy and physiology, *Clin Lab Med* 13(1) (1993) 1-11.
- [3] G.J.T.a.B. Derrickson, *Principio de Anatomía y Fisiología*, 2013.
- [4] C. Langston, Managing fluid and electrolyte disorders in renal failure, *Vet Clin North Am Small Anim Pract* 38(3) (2008) 677-97, xiii.
- [5] H.M. Wadei, S.C. Textor, The role of the kidney in regulating arterial blood pressure, *Nat Rev Nephrol* 8(10) (2012) 602-9.
- [6] M.S. Lipkowitz, Regulation of uric acid excretion by the kidney, *Curr Rheumatol Rep* 14(2) (2012) 179-88.
- [7] S. Masuda, Functional characteristics and pharmacokinetic significance of kidney-specific organic anion transporters, OAT-K1 and OAT-K2, in the urinary excretion of anionic drugs, *Drug Metab Pharmacokinet* 18(2) (2003) 91-103.
- [8] H. Gibb, N.J. Sanders, R.R. Dunn, S. Watson, M. Photakis, S. Abril, A.N. Andersen, E. Angulo, I. Armbrecht, X. Arnan, F.B. Baccaro, T.R. Bishop, R. Boulay, C. Castracani, I. Del Toro, T. Delsinne, M. Diaz, D.A. Donoso, M.L. Enriquez, T.M. Fayle, D.H. Feener, Jr., M.C. Fitzpatrick, C. Gomez, D.A. Grasso, S. Groc, B. Heterick, B.D. Hoffmann, L. Lach, J. Lattke, M. Leponce, J.P. Lessard, J. Longino, A. Lucky, J. Majer, S.B. Menke, D. Mezger, A. Mori, T.C. Munyai, O. Paknia, J. Pearce-Duvet, M. Pfeiffer, S.M. Philpott, J.L. de Souza, M. Tista, H.L. Vasconcelos, M. Vonshak, C.L. Parr, Climate mediates the effects of disturbance on ant assemblage structure, *Proc Biol Sci* 282(1808) (2015) 20150418.
- [9] J.W. Adamson, Regulation of red blood cell production, *Am J Med* 101(2A) (1996) 4S-6S.
- [10] F. Perwad, A.A. Portale, Vitamin D metabolism in the kidney: regulation by phosphorus and fibroblast growth factor 23, *Mol Cell Endocrinol* 347(1-2) (2011) 17-24.
- [11] J.E. Gerich, C. Meyer, H.J. Woerle, M. Stumvoll, Renal gluconeogenesis: its importance in human glucose homeostasis, *Diabetes Care* 24(2) (2001) 382-91.
- [12] C. Yucha, Renal regulation of acid-base balance, *Nephrol Nurs J* 31(2) (2004) 201-6; quiz 207-8.

- [13] J.F. Bertram, R.N. Douglas-Denton, B. Diouf, M.D. Hughson, W.E. Hoy, Human nephron number: implications for health and disease, *Pediatr Nephrol* 26(9) (2011) 1529-33.
- [14] L.A.I.a.R.D. Perrone, Assesment of kidney function, <http://www.uptodate.com>, 2015.
- [15] M.R. Pollak, S.E. Quaggin, M.P. Hoenig, L.D. Dworkin, The glomerulus: the sphere of influence, *Clin J Am Soc Nephrol* 9(8) (2014) 1461-9.
- [16] J.A. Roth, T.D. Wilson, M. Sandig, The development of a virtual 3D model of the renal corpuscle from serial histological sections for E-learning environments, *Anat Sci Educ* 8(6) (2015) 574-83.
- [17] V. Vallon, The proximal tubule in the pathophysiology of the diabetic kidney, *Am J Physiol Regul Integr Comp Physiol* 300(5) (2011) R1009-22.
- [18] D. Pearce, R. Soundararajan, C. Trimpert, O.B. Kashlan, P.M. Deen, D.E. Kohan, Collecting duct principal cell transport processes and their regulation, *Clin J Am Soc Nephrol* 10(1) (2015) 135-46.
- [19] A.R. Subramanya, D.H. Ellison, Distal convoluted tubule, *Clin J Am Soc Nephrol* 9(12) (2014) 2147-63.
- [20] D.Y. Huang, H. Osswald, V. Vallon, Sodium reabsorption in thick ascending limb of Henle's loop: effect of potassium channel blockade in vivo, *Br J Pharmacol* 130(6) (2000) 1255-62.
- [21] D.B. Mount, Thick ascending limb of the loop of Henle, *Clin J Am Soc Nephrol* 9(11) (2014) 1974-86.
- [22] A. Galvan, T. Fladvad, F. Skorpen, X. Gao, P. Klepstad, S. Kaasa, T.A. Dragani, Genetic clustering of European cancer patients indicates that opioid-mediated pain relief is independent of ancestry, *Pharmacogenomics J* 12(5) (2012) 412-6.
- [23] M.L. MacDougall, T.B. Wiegmann, Urate excretion by the isolated perfused rat kidney and modification by drugs, *Proc Soc Exp Biol Med* 192(3) (1989) 276-80.
- [24] N. Sanchez-Romero, Meade, P. , Giménez, I., *Microfluidic-Based 3D Models of Renal Function for Clinically Oriented Research*, Elsevier 2016.
- [25] M. Franco Guevara, L.G. Navar, J. Herrera-Acosta, D. Bell, [The regulatory mechanisms of glomerular filtration: the tubuloglomerular feedback system, physiological aspects and their participation in the physiopathology of kidney diseases], *Gac Med Mex* 130(3) (1994) 139-45; discussion 146-7.

- [26] M.J. Holecek, Glomerular filtration: an overview, *Nephrol Nurs J* 30(3) (2003) 285-90; quiz 291-2.
- [27] W.J. O'Connor, Tubular reabsorption in normal renal function, *Ren Physiol* 7(4) (1984) 193-204.
- [28] E.B. Berkhin, M.H. Humphreys, Regulation of renal tubular secretion of organic compounds, *Kidney Int* 59(1) (2001) 17-30.
- [29] K.C. Leung, M. Tonelli, M.T. James, Chronic kidney disease following acute kidney injury-risk and outcomes, *Nat Rev Nephrol* 9(2) (2013) 77-85.
- [30] V. Jha, G. Garcia-Garcia, K. Iseki, Z. Li, S. Naicker, B. Plattner, R. Saran, A.Y. Wang, C.W. Yang, Chronic kidney disease: global dimension and perspectives, *Lancet* 382(9888) (2013) 260-72.
- [31] U. U.S. Renal Data System, *USRDS 2013 Annual Data Report: Atlas of Chronic Kidney Disease and End-Stage Renal Disease in the United States*, National Institutes of Health, National Institute of Diabetes and Digestive and Kidney Diseases, Bethesda, MD, 2013., 2013.
- [32] A.J. Atkinson, Jr., S.M. Huang, *Nephropharmacology: drugs and the kidney*, *Clin Pharmacol Ther* 86(5) (2009) 453-6.
- [
- [33] M. Loghman-Adham, C.I. Kiu Weber, C. Ciorciaro, J. Mann, M. Meier, Detection and management of nephrotoxicity during drug development, *Expert Opin Drug Saf* 11(4) (2012) 581-96.
- [34] I. Kola, J. Landis, Can the pharmaceutical industry reduce attrition rates?, *Nat Rev Drug Discov* 3(8) (2004) 711-5.
- [35] J.L. Stevens, T.K. Baker, The future of drug safety testing: expanding the view and narrowing the focus, *Drug Discov Today* 14(3-4) (2009) 162-7.
- [36] L. Fliedl, M. Wieser, G. Manhart, M.P. Gerstl, A. Khan, J. Grillari, R. Grillari-Voglauer, Controversial role of gamma-glutamyl transferase activity in cisplatin nephrotoxicity, *ALTEX* 31(3) (2014) 269-78.
- [37] T.C. Fuchs, P. Hewitt, Biomarkers for drug-induced renal damage and nephrotoxicity-an overview for applied toxicology, *AAPS J* 13(4) (2011) 615-31.
- [38] T.M. DesRochers, L. Suter, A. Roth, D.L. Kaplan, Bioengineered 3D human kidney tissue, a platform for the determination of nephrotoxicity, *PLoS One* 8(3) (2013) e59219.

- [39] N. Pannu, M.K. Nadim, An overview of drug-induced acute kidney injury, *Crit Care Med* 36(4 Suppl) (2008) S216-23.
- [40] C.A. Nickerson, E.G. Richter, C.M. Ott, Studying host-pathogen interactions in 3-D: organotypic models for infectious disease and drug development, *J Neuroimmune Pharmacol* 2(1) (2007) 26-31.
- [41] Y. Xia, I. Sancho-Martinez, E. Nivet, C. Rodriguez Esteban, J.M. Campistol, J.C. Izpisua Belmonte, The generation of kidney organoids by differentiation of human pluripotent cells to ureteric bud progenitor-like cells, *Nat Protoc* 9(11) (2014) 2693-704.
- [42] M. Ravi, V. Paramesh, S.R. Kaviya, E. Anuradha, F.D. Solomon, 3D cell culture systems: advantages and applications, *J Cell Physiol* 230(1) (2015) 16-26.
- [43] J.C. Gautier, B. Riefke, J. Walter, P. Kurth, L. Mylecraine, V. Guilpin, N. Barlow, T. Gury, D. Hoffman, D. Ennulat, K. Schuster, E. Harpur, S. Pettit, Evaluation of novel biomarkers of nephrotoxicity in two strains of rat treated with Cisplatin, *Toxicol Pathol* 38(6) (2010) 943-56.
- [44] J.C. Chen, J.L. Stevens, A.L. Trifillis, T.W. Jones, Renal cysteine conjugate beta-lyase-mediated toxicity studied with primary cultures of human proximal tubular cells, *Toxicol Appl Pharmacol* 103(3) (1990) 463-73.
- [45] S.K. Doke, S.C. Dhawale, Alternatives to animal testing: A review, *Saudi Pharm J* 23(3) (2015) 223-9.
- [46] D.K. Badyal, C. Desai, Animal use in pharmacology education and research: the changing scenario, *Indian J Pharmacol* 46(3) (2014) 257-65.
- [47] T. Arora, A.K. Mehta, V. Joshi, K.D. Mehta, N. Rathor, P.K. Mediratta, K.K. Sharma, Substitute of Animals in Drug Research: An Approach Towards Fulfillment of 4R's, *Indian J Pharm Sci* 73(1) (2011) 1-6.
- [48] Y. Wu, D. Connors, L. Barber, S. Jayachandra, U.M. Hanumegowda, S.P. Adams, Multiplexed assay panel of cytotoxicity in HK-2 cells for detection of renal proximal tubule injury potential of compounds, *Toxicol In Vitro* 23(6) (2009) 1170-8.
- [49] N. Ferrell, R.R. Desai, A.J. Fleischman, S. Roy, H.D. Humes, W.H. Fissell, A microfluidic bioreactor with integrated transepithelial electrical resistance (TEER) measurement electrodes for evaluation of renal epithelial cells, *Biotechnol Bioeng* 107(4) (2010) 707-16.
- [50] K.J. Jang, A.P. Mehr, G.A. Hamilton, L.A. McPartlin, S. Chung, K.Y. Suh, D.E. Ingber, Human kidney proximal tubule-on-a-chip for drug transport and nephrotoxicity assessment, *Integr Biol (Camb)* 5(9) (2013) 1119-29.

- [51] M.J. Bissell, D.C. Radisky, A. Rizki, V.M. Weaver, O.W. Petersen, The organizing principle: microenvironmental influences in the normal and malignant breast, *Differentiation* 70(9-10) (2002) 537-46.
- [52] Q. Guo, B. Xia, S. Moshiah, C. Xu, Y. Jiang, Y. Chen, Y. Sun, J.M. Lahti, X.A. Zhang, The microenvironmental determinants for kidney epithelial cyst morphogenesis, *Eur J Cell Biol* 87(4) (2008) 251-66.
- [53] M. El Mouedden, G. Laurent, M.P. Mingeot-Leclercq, P.M. Tulkens, Gentamicin-induced apoptosis in renal cell lines and embryonic rat fibroblasts, *Toxicol Sci* 56(1) (2000) 229-39.
- [54] V. Napadow, J. Liu, T.J. Kaptchuk, A systematic study of acupuncture practice: acupoint usage in an outpatient setting in Beijing, China, *Complement Ther Med* 12(4) (2004) 209-16.
- [55] M.J. Wilmer, M.A. Saleem, R. Masereeuw, L. Ni, T.J. van der Velden, F.G. Russel, P.W. Mathieson, L.A. Monnens, L.P. van den Heuvel, E.N. Levchenko, Novel conditionally immortalized human proximal tubule cell line expressing functional influx and efflux transporters, *Cell Tissue Res* 339(2) (2010) 449-57.
- [56] D.A. Vesey, W. Qi, X. Chen, C.A. Pollock, D.W. Johnson, Isolation and primary culture of human proximal tubule cells, *Methods Mol Biol* 466 (2009) 19-24.
- [57] M.J. Valente, R. Henrique, V.L. Costa, C. Jeronimo, F. Carvalho, M.L. Bastos, P.G. de Pinho, M. Carvalho, A rapid and simple procedure for the establishment of human normal and cancer renal primary cell cultures from surgical specimens, *PLoS One* 6(5) (2011) e19337.
- [58] C.C. Sharpe, M.E. Dockrell, Primary culture of human renal proximal tubule epithelial cells and interstitial fibroblasts, *Methods Mol Biol* 806 (2012) 175-85.
- [59] T.T. Nieskens, J.G. Peters, M.J. Schreurs, N. Smits, R. Woestenenk, K. Jansen, T.K. van der Made, M. Roring, C. Hilgendorf, M.J. Wilmer, R. Masereeuw, A Human Renal Proximal Tubule Cell Line with Stable Organic Anion Transporter 1 and 3 Expression Predictive for Antiviral-Induced Toxicity, *AAPS J* 18(2) (2016) 465-75.
- [60] M. Yamada, M. Kawaguchi, H. Takamiya, H. Wada, T. Okigaki, Establishment and characterization of an epithelial cell line, SGE1, from isolated rat renal glomeruli, *Cell Struct Funct* 13(6) (1988) 495-513.
- [61] J.E. de Larco, G.J. Todaro, Epithelioid and fibroblastic rat kidney cell clones: epidermal growth factor (EGF) receptors and the effect of mouse sarcoma virus transformation, *J Cell Physiol* 94(3) (1978) 335-42.

- [62] R.N. Hull, W.R. Cherry, G.W. Weaver, The origin and characteristics of a pig kidney cell strain, LLC-PK, *In Vitro* 12(10) (1976) 670-7.
- [63] H. Koyama, C. Goodpasture, M.M. Miller, R.L. Teplitz, A.D. Riggs, Establishment and characterization of a cell line from the American opossum (*Didelphys virginiana*), *In Vitro* 14(3) (1978) 239-46.
- [64] T.P. Haverty, C.J. Kelly, W.H. Hines, P.S. Amenta, M. Watanabe, R.A. Harper, N.A. Kefalides, E.G. Neilson, Characterization of a renal tubular epithelial cell line which secretes the autologous target antigen of autoimmune experimental interstitial nephritis, *J Cell Biol* 107(4) (1988) 1359-68.
- [65] Y. Takuwa, E. Ogata, Differentiated properties characteristic of renal proximal epithelium in a cell line derived from a normal monkey kidney (JTC-12), *In Vitro Cell Dev Biol* 21(8) (1985) 445-9.
- [66] M.J. Ryan, G. Johnson, J. Kirk, S.M. Fuerstenberg, R.A. Zager, B. Torok-Storb, HK-2: an immortalized proximal tubule epithelial cell line from normal adult human kidney, *Kidney Int* 45(1) (1994) 48-57.
- [67] M. Wieser, G. Stadler, P. Jennings, B. Streubel, W. Pfaller, P. Ambros, C. Riedl, H. Katinger, J. Grillari, R. Grillari-Voglauer, hTERT alone immortalizes epithelial cells of renal proximal tubules without changing their functional characteristics, *Am J Physiol Renal Physiol* 295(5) (2008) F1365-75.
- [68] J. Fogh, Cultivation, characterization, and identification of human tumor cells with emphasis on kidney, testis, and bladder tumors, *Natl Cancer Inst Monogr* (49) (1978) 5-9.
- [69] D.M. Scott, Differentiation in vitro of primary cultures and transfected cell lines of epithelial cells derived from the thick ascending limb of Henle's loop, *Differentiation* 36(1) (1987) 35-46.
- [70] C.R. Gaush, W.L. Hard, T.F. Smith, Characterization of an established line of canine kidney cells (MDCK), *Proc Soc Exp Biol Med* 122(3) (1966) 931-5.
- [71] K.A. Rafferty, Jr., R.W. Sherwin, The length of secondary chromosomal constrictions in normal individuals and in a nucleolar mutant of *Xenopus laevis*, *Cytogenetics* 8(6) (1969) 427-38.
- [72] S. Uchida, N. Green, H. Coon, T. Triche, S. Mims, M. Burg, High NaCl induces stable changes in phenotype and karyotype of renal cells in culture, *Am J Physiol* 253(2 Pt 1) (1987) C230-42.
- [73] F.T. Bosman, I. Stamenkovic, Functional structure and composition of the extracellular matrix, *J Pathol* 200(4) (2003) 423-8.

- [74] B. Lelongt, P. Ronco, Role of extracellular matrix in kidney development and repair, *Pediatr Nephrol* 18(8) (2003) 731-42.
- [75] G. Finesilver, J. Bailly, M. Kahana, E. Mitrani, Kidney derived micro-scaffolds enable HK-2 cells to develop more in-vivo like properties, *Exp Cell Res* 322(1) (2014) 71-80.
- [76] R. Timpl, Macromolecular organization of basement membranes, *Curr Opin Cell Biol* 8(5) (1996) 618-24.
- [77] J.H. Miner, Renal basement membrane components, *Kidney Int* 56(6) (1999) 2016-24.
- [78] D.H. Kim, P.P. Provenzano, C.L. Smith, A. Levchenko, Matrix nanotopography as a regulator of cell function, *J Cell Biol* 197(3) (2012) 351-60.
- [79] E.K.A. Nur, I. Ahmed, J. Kamal, M. Schindler, S. Meiners, Three-dimensional nanofibrillar surfaces promote self-renewal in mouse embryonic stem cells, *Stem Cells* 24(2) (2006) 426-33.
- [80] M. Schindler, I. Ahmed, J. Kamal, E.K.A. Nur, T.H. Grafe, H. Young Chung, S. Meiners, A synthetic nanofibrillar matrix promotes in vivo-like organization and morphogenesis for cells in culture, *Biomaterials* 26(28) (2005) 5624-31.
- [81] M.H. Kim, Y. Sawada, M. Taya, M. Kino-Oka, Influence of surface topography on the human epithelial cell response to micropatterned substrates with convex and concave architectures, *J Biol Eng* 8 (2014) 13.
- [82] J. le Digabel, M. Ghibaud, L. Trichet, A. Richert, B. Ladoux, Microfabricated substrates as a tool to study cell mechanotransduction, *Med Biol Eng Comput* 48(10) (2010) 965-76.
- [83] A.G. Sciancalepore, F. Sallustio, S. Girardo, L. Gioia Passione, A. Camposeo, E. Mele, M. Di Lorenzo, V. Costantino, F.P. Schena, D. Pisignano, A bioartificial renal tubule device embedding human renal stem/progenitor cells, *PLoS One* 9(1) (2014) e87496.
- [84] D. Kuraitis, C. Giordano, M. Ruel, A. Musaro, E.J. Suuronen, Exploiting extracellular matrix-stem cell interactions: a review of natural materials for therapeutic muscle regeneration, *Biomaterials* 33(2) (2012) 428-43.
- [85] Y.S. Kanwar, J. Wada, S. Lin, F.R. Danesh, S.S. Chugh, Q. Yang, T. Banerjee, J.W. Lomasney, Update of extracellular matrix, its receptors, and cell adhesion molecules in mammalian nephrogenesis, *Am J Physiol Renal Physiol* 286(2) (2004) F202-15.

- [86] E.R. Shamir, A.J. Ewald, Three-dimensional organotypic culture: experimental models of mammalian biology and disease, *Nat Rev Mol Cell Biol* 15(10) (2014) 647-64.
- [87] J. Jansen, M. Fedecostante, M.J. Wilmer, L.P. van den Heuvel, J.G. Hoenderop, R. Masereeuw, Biotechnological challenges of bioartificial kidney engineering, *Biotechnol Adv* 32(7) (2014) 1317-27.
- [88] F. Tasnim, R. Deng, M. Hu, S. Liour, Y. Li, M. Ni, J.Y. Ying, D. Zink, Achievements and challenges in bioartificial kidney development, *Fibrogenesis Tissue Repair* 3 (2010) 14.
- [89] J. Lee, M.J. Cuddihy, N.A. Kotov, Three-dimensional cell culture matrices: state of the art, *Tissue Eng Part B Rev* 14(1) (2008) 61-86.
- [90] M.P. Lutolf, Biomaterials: Spotlight on hydrogels, *Nat Mater* 8(6) (2009) 451-3.
- [91] S.R. Caliari, J.A. Burdick, A practical guide to hydrogels for cell culture, *Nat Methods* 13(5) (2016) 405-14.
- [92] T.M. Desrochers, E. Palma, D.L. Kaplan, Tissue-engineered kidney disease models, *Adv Drug Deliv Rev* 69-70 (2014) 67-80.
- [93] E.M. Ahmed, Hydrogel: Preparation, characterization, and applications: A review, *J Adv Res* 6(2) (2015) 105-21.
- [94] J.P. Hodde, R.D. Record, H.A. Liang, S.F. Badylak, Vascular endothelial growth factor in porcine-derived extracellular matrix, *Endothelium* 8(1) (2001) 11-24.
- [95] J. Hodde, R. Record, R. Tullius, S. Badylak, Fibronectin peptides mediate HMEC adhesion to porcine-derived extracellular matrix, *Biomaterials* 23(8) (2002) 1841-8.
- [96] R. Morizane, A.Q. Lam, B.S. Freedman, S. Kishi, M.T. Valerius, J.V. Bonventre, Nephron organoids derived from human pluripotent stem cells model kidney development and injury, *Nat Biotechnol* 33(11) (2015) 1193-200.
- [97] A.C. O'Neill, S.D. Ricardo, Human kidney cell reprogramming: applications for disease modeling and personalized medicine, *J Am Soc Nephrol* 24(9) (2013) 1347-56.
- [98] M. Takasato, P.X. Er, H.S. Chiu, B. Maier, G.J. Baillie, C. Ferguson, R.G. Parton, E.J. Wolvetang, M.S. Roost, S.M. Chuva de Sousa Lopes, M.H. Little,

Kidney organoids from human iPS cells contain multiple lineages and model human nephrogenesis, *Nature* 526(7574) (2015) 564-8.

[99] J.A. Davies, Self-organized Kidney Rudiments: Prospects for Better in vitro Nephrotoxicity Assays, *Biomark Insights* 10(Suppl 1) (2015) 117-23.

[100] A. Peloso, R. Katari, S.V. Murphy, J.P. Zambon, A. DeFrancesco, A.C. Farney, J. Rogers, R.J. Stratta, T.M. Manzia, G. Orlando, Prospect for kidney bioengineering: shortcomings of the status quo, *Expert Opin Biol Ther* 15(4) (2015) 547-58.

[101] S.V. Murphy, A. Atala, 3D bioprinting of tissues and organs, *Nat Biotechnol* 32(8) (2014) 773-85.

[102] M.J. Wilmer, C.P. Ng, H.L. Lanz, P. Vulto, L. Suter-Dick, R. Masereeuw, Kidney-on-a-Chip Technology for Drug-Induced Nephrotoxicity Screening, *Trends Biotechnol* 34(2) (2016) 156-70.

[103] K.J. Jang, K.Y. Suh, A multi-layer microfluidic device for efficient culture and analysis of renal tubular cells, *Lab Chip* 10(1) (2010) 36-42.

[104] Z. Wei, P.K. Amponsah, M. Al-Shatti, Z. Nie, B.C. Bandyopadhyay, Engineering of polarized tubular structures in a microfluidic device to study calcium phosphate stone formation, *Lab Chip* 12(20) (2012) 4037-40.

[105] L. Choucha-Snouber, C. Aninat, L. Grsicom, G. Madalinski, C. Brochot, P.E. Poleni, F. Razan, C.G. Guillouzo, C. Legallais, A. Corlu, E. Leclerc, Investigation of ifosfamide nephrotoxicity induced in a liver-kidney co-culture biochip, *Biotechnol Bioeng* 110(2) (2013) 597-608.

[106] M. Zhou, H. Ma, H. Lin, J. Qin, Induction of epithelial-to-mesenchymal transition in proximal tubular epithelial cells on microfluidic devices, *Biomaterials* 35(5) (2014) 1390-401.



CHAPTER | 2

Isolation and
characterization of
human proximal
tubular primary
cells
in culture

2.1 INTRODUCTION

The kidney is made up of more than a dozen different cell types. This cell heterogeneity is well known in terms of morphology and physiology. Among the different cell types, the PT cells play a major role in the reabsorption of filtered substances such as glucose and amino acids [1] and in the excretion of xenobiotics such as environmental chemicals, drugs, or endogenous waste products originating from metabolism, by secreting them into the urine [2]. So, the PT constitutes the segment of the nephron, where the majority of toxins and drugs are processed and here is where acute and chronic renal damage take places [3, 4].

Morphologically, the PT epithelium is made up of polarized epithelial cells [5, 6] that differentiate in two parts: the apical surface and the basolateral surface, separated by members of the epithelial barrier proteins of the tight and adherent junctions [7-9]. On the apical portion of the cell membrane, the PT cells present a brush border. The brush border morphology increases the cell surface area. This increment of the cell surface area is especially useful in reabsorptive processes, where the cells need a large surface area in contact with the substance to be efficient [10]. The cytosol of the proximal tubule cells has a big number of mitochondria per cell reflecting the high levels of intracellular energy required to play different functions. PT cells are equipped with a range of transporters, consisting of multiple carriers with overlapping substrate specificities that cooperate in basolateral uptake and luminal secretion [11]. PT cells uptake of organic anions is mediated by members of the solute carrier (*SLC*) family, known as organic anion transporter 1 and 3 (*OAT1/3*; *SLC22A6* and *A8*) and the bidirectional Organic Anion Transporting Peptide 4C1 (*OATP4C1*; *SLCO4C1*) [12, 13]. Cellular efflux of organic anions is facilitated

by members of the ATP-binding cassette (ABC) transporter family, known as the Multidrug Resistance Proteins 2 and 4 (MRP2/4; *ABCC2* and *-C4*), P-glycoprotein (*ABCB1*; MDR1/P-gp) and Breast Cancer Resistance Protein (BCRP; *ABCG2*), through ATP-dependent transport [14, 15]. The uptake of organic cations is mediated by the *SLC22* family of organic cation transporters (OCTs) present at the basolateral membrane of the PT cells. In the human kidney, OCT2 (*SLC22A2*) is considered one of the most important organic cation influx proteins. At the brush border membrane, the *SLC47* multidrug and toxin extrusion proteins (MATEs) are expressed. OCTs and MATEs transport a wide variety of structurally unrelated organic cations [16-18]. (Figure 2.1).

Biochemically, PT cells are characterized by the expression of markers as Megalin, SGLT-2, gamma glutamyl transferase (GGT1), dipeptidyl peptidase IV (DPPIV), aminopeptidase M (APM), amongst others [8, 9].

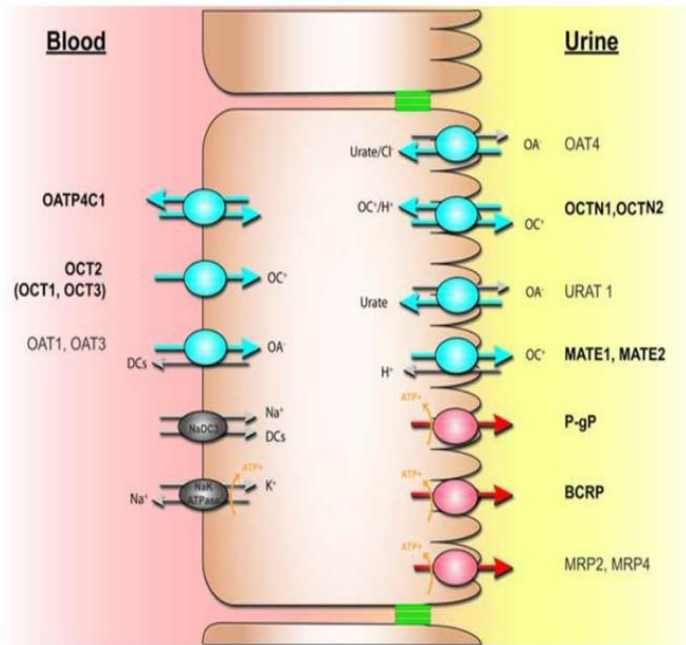


Figure 2.1: Schematic model of the major organic anion (OA⁻)/ organic cation (OC⁺) transporters in human renal proximal tubular cells. SLC transporters are depicted in blue and ABC transporters in red. Grey arrows depict the movement of driving ions. Transporters that are currently considered important for the clearance of organic cations are labeled in bold. Source: Sanchez-Romero, N., Schophuizen, C. M., Gimenez, I., Masereeuw, R. *In vitro* systems to study nephrotoxicology: 2D versus 3D models; *Eur J Pharmacol*, 2016.

Taking into account the physiological role played by these cells *in vivo*; PT cells constitute a very interesting *in vitro* model used to study different aspects of physiology or pharmacology.

Currently, there are several established cell lines of human origin available for *in vitro* models of PT (see Table 1.2 in Introduction). These cell lines have the ability to proliferate indefinitely or at least, between 20-80 passages and are used as a cost-effective tool in basic research. However, these cell lines are less used as a biologically relevant option,

basically, because important characteristics of the original tissue are lost once the cells are isolated. For example, the HK-2 cell line cannot grow if the cell confluence is higher than 60% [19], a circumstance that does not happen *in vivo*. As a consequence of these limitations, human PT primary cells constitute a good *in vitro* model to study this specific segment of the nephron and more important, they constitute a biologically more relevant tool, for this reason, many researchers are focused in the development of procedures for the isolation of PT cells.

The protocols for the isolation of these type of cells described in the literature are classified as mechanical disruption, enzymatic disruption or the mix between both procedures followed by purification steps.

The typical mechanical treatment used for isolation of PT cells is to mince the kidney into slices or small fragments [20, 21] or by using a tissue homogenizer operated by hand. The constant agitation of the tissue is also considered a mechanical treatment. Enzymatic disruption, specifically the proteolytic digestion, is the most widely applied method to isolate PT cells. Some proteolytic enzymes used are the dispase, pronase, and elastase, either alone or in combination, but the most used are collagenase and trypsin. Trypsin is considered a very aggressive enzymatic process because it digests many exoproteins in the cellular membrane. The final result can originate severely damaged cells, thus potentially hampering the subsequent attachment step. However, some primary cultures using trypsin digestion have been described [22, 23]. In the case of collagenase, it is considered the enzyme of choice for proteolytic digestion because the collagenase preparation contains a high number of hydrolytic enzymes, such as hyaluronidase, clostripain and neutral protease favoring a

complete and mild digestion of the tissue and also because the basal membrane is composed fundamentally of collagen [24].

The complex cellular architecture of the kidney, constituted by more than one dozen different cell types forces the researchers to use a purification step after the isolation procedure. The purification methods include several techniques, ranging from simple filtration to more complex methods such as immunological selection (Table 2.1).

Table 2.1: Principal isolation and purification methods used for PT cells.

Source	Enzymatic Digestion	Mechanic Disaggregation	Purification method	Ref.
Nephrectomy	Dispase Collagenase	Yes	<ul style="list-style-type: none"> Iodixanol density fraction 	[25]
Nephrectomy	Collagenase DNase	Yes	<ul style="list-style-type: none"> Cell strainer of 100 and 45 μm 	[26]
Nephrectomy	Collagenase DNase	Yes	<ul style="list-style-type: none"> Cell strainer of 120 - μm Percoll gradient Immuno-separation 	[27]
Nephrectomy	Collagenase	Yes	<ul style="list-style-type: none"> Percoll gradient Immuno-separation Flow sorting 	[28]
Nephrectomy	Collagenase Trypsin-EDTA	Yes	<ul style="list-style-type: none"> Cell strainer of 100 and 40-μm 	[29]

After the isolation, the phenotypical characterization is essential (Table 2.2 and 2.3). The characterization of the isolated cells is one of the most important and at the same time critical step of the isolation protocol since it determines the purity of the isolated cells.

Table 2.2: Expression markers for phenotypic characterization of renal epithelial cells

Marker	Technique of choice
Megalin	ICC, IF
Gamma Glutamyl Tranferasa-1 (GGT1)	ICC, WB
Alkaline Phosphatase	ICC, WB
N-acetyl-beta-D-glucosaminidase	ICC, WB
Glutamine synthetase	ICC, WB
Sodium-Phosphate transporter (NaPi)	IF, WB
Aquaporin-1 (AQP1)	IF, WB
Lectin	IHC, IF
Alanine aminopeptidase M (CD13)	IF, FC
Dipeptidyl peptidase 4 DPPIV (CD26)	IF, FC
Tetragonolobus agglutinin	IHC, IF
Sodium glucose cotransporter (SGLT2)	IH, IF, WB, qPCR
Aminopeptidase A	IHC, IF

Table 2.3: Functional markers for phenotypic characterization of renal epithelial cells.

Marker	Function
Albumin uptake	Endocytosis through the apical membrane
Gamma Glutamyl Tranferasa-1 (GGT)	Brush border enzyme
Alkaline Phosphatase	Brush border enzyme
N-acetyl-beta-o-glucosaminidase	Lysosomal enzyme
Glutamine synthetase	Cytosolic enzyme
Hormone-induced cAMP production	cAMP production dependent on expression of hormone receptor
Glucose uptake	Sodium -dependent glucose
Sodium uptake	Cotransported with glucose, amino acids, bicarbonate.

2.2 OBJECTIVES

This chapter will focus on:

- 1. Development of methods and procedures for the isolation and cell culture of human primary proximal tubular cells (hPTPC).**
- 2. Phenotypic characterization of cells obtained from the primary culture at the level of gene expression, protein markers enzymatic activity in living cells and transporters.**
3. Development and validation of a new nephrotoxicity model using cisplatin for the study of cell viability and expression of specific markers implied in the bioactivation of this molecule.
4. Screening of molecules potentially repaired of the damage produced by the cisplatin.
5. Development of the protocol for differentiated proximal tubular cell cultures in a device that allows us the application of Shear Stress (SS).
6. Determination of the SS effect in the sensibility to cisplatin in hPTPC.

2.3 MATERIAL AND METHODS

2.3.1 Source of renal tissue

The human primary proximal tubule cells (hPTPC) used in this Thesis were obtained from discarded healthy human renal tissue from surgical procedures carried out at Hospital Clínico Universitario Lozano Blesa, Zaragoza, Spain. Informed written consent was obtained from all patients.

2.3.2 Cell culture medium

hPTPC were cultured in DMEM-HAM's F12 (Lonza, BE12-719F) medium containing 2% (v/v) FCS (Sigma, F7524), 100 units/mL penicillin (BioWhittaker, 17-745H), 100 units/mL streptomycin (BioWhittaker, 17-745H), 0.25 µg/mL amphotericin (BioWhittaker, 17-745H), 5 µg/ml insulin (Sigma, I6634), 5 µg/ml transferrin (Sigma, T8027), 10 ng/mL selenium (Sigma S5261), 5×10^{-8} M dexamethasone (Sigma, D8893), 10^{-9} M tri-iodothyronine (T3) (Sigma, T5516) and 10 ng/ml EGF (Sigma, E4127). The medium and its components were filtered using a sterilized 0.22 µm filter (Fisher Sci, 10268951). From here on, this medium will be named as MCR medium (acronyms of Renal Cell Medium in Spanish).

2.3.3 Collagen coating of culture vessel surface

Cell culture plates were coated with Collagen I from calf skin (Sigma, C8919). The stock solution of Collagen I was diluted 10 times in cold MiliQ H₂O, and the resulting solution was pipetted in the cell culture plate using between 10-12 µg/cm² of this coating as a surface coverage. The cell culture plates were stored at 4°C overnight, to get a correct polymerization and after that, they were washed 2 times with MiliQ H₂O. The cell culture plates coated with Collagen I can be maintained at 4 °C for maximum 2 weeks in the fridge.

2.3.4 Protocol used in human renal cell isolation.

2.3.4.1 Preparation of materials and solutions used for the isolation of renal cells

1. Prepare the media (see Table 2.4) that we are going to use and put them to oxygenate on ice for 30 minutes before beginning the protocol. **2.** Once in the flow hood, filter all media prepared with the aid of a 20 mL syringe and a sterile 0.22 µm filter. **3.** Turn on the centrifuge and set the temperature to 4 ° C. **4.** Turn on the bath water and set the temperature to 37 ° C. **5.** Sterilize the surgical material (scissor and forceps) with a sterilizer with quartz beads.

Table 2.4: Solutions used in the isolation protocol

EBSS + collagenase 0.025%

Reagent	Stock	Working concentration	Volume needed
EBSS medium (Lonza, BE02-027F)	Liquid		25 mL
Collagenase (Sigma, C2674)	Liquid 50 mg/mL	0.025%	121,4 mL

EBSS + Bovine Serum albumin (BSA) 0.2%

Reagent	Stock	Working concentration	Volume needed
EBSS medium (Lonza, BE02-027F)	Liquid		40 mL
BSA (Lonza, A7906)	Dry powder	0.2%	0.8 g

2.3.4.2 Isolation protocol of proximal tubular cells

1. When the kidney sample arrived at the cell culture facility, it was weighed on a scale, placed in a shallow Petri dish into the flow hood and then, the capsule and fatty matter were discarded.
2. After that, sample weight was recorded to compare later the number of cells obtained versus the sample size processed.
3. To process the sample, cortical areas were dissected and minced with scissors and forceps into pieces of approximately 1 mm³.
4. The resultant fragmented tissue was transferred to a falcon tube containing ice-cold EBSS medium and centrifuged at 4°C, 400 g during 8 minutes to remove waste material.
5. After the centrifugation, the protocol continued with the resulting pellet, which was placed in a small bottle in the presence of EBSS medium with 0.025% collagenase. This bottle was incubated at 37°C in a water bath for 10 minutes with continuous agitation and oxygenation, after which the tissue fragments are allowed to sediment. The supernatant obtained contains the resulting cells after the combination of enzymatic and

mechanical dissociation, and it was centrifuged in a 50-mL falcon tube at 1000g for 10 minutes and subsequently, the pellet was resuspended and maintained in ice-cold EBSS medium and 0.2% of BSA until the purification step (7).

6. The steps explained in points 4 and 5 were repeated four times, in order to obtain a satisfactory isolation protocol with a large percentage of starting material.

7. The medium containing the BSA was sieved through a 100- μm cell strainer into a 50-mL centrifuge tube.

8. Then, the resulting filtrate was sieved through a 40- μm cell strainer into another 50-mL falcon tube. The size of 40 μm cell strainer removed tubular fragment and glomeruli respectively.

9. The medium that passed the 40 μm cell strainer (CF fraction) and the material retained in this cell strainer (C40 fraction) was used to generate the primary cultures. Cells in CF and C40 fraction were pelleted at 1000 g for 5 minutes.

10. After that, the cells of CF fraction were resuspended in 20 mL of PBS and cells of C40 fraction were resuspended in 5 mL of PBS (without $\text{Ca}^{2+}/\text{Mg}^{2+}$) (Lonza, BE17-516F) and 1 mL of each fraction was used to determine the efficacy of the isolation protocol through the tubules present in the sample (tubulocrite). Then, the cells from CF and C40 were centrifuged at 800 g for 5 minutes to remove red blood cells present in the sample. This step was repeated twice (The volume to determine the tubulocrite was drawn once).

11. In the final step, the pellet was resuspended in 5 mL of MCR medium. 1 mL of CF and C40 fraction was prepared for RNA extraction, then used to perform PCRs. The remaining volume (4 mL) in each fraction was seeded in 3 wells of a 6 wells plate (TPP, 92006) and each well was filled with a

total volume of 2 mL (MCR containing the cells and additional MCR). The cells were transferred to an incubator at 37°C, 5% (v/v) CO₂ (Figure 2.2).

12. 24 hours after the seeding the hPTPC cells were washed 2 times with PBS and then the MCR medium was renewed. After that, the cell medium was refreshed every 2-3 days till reach the confluence.

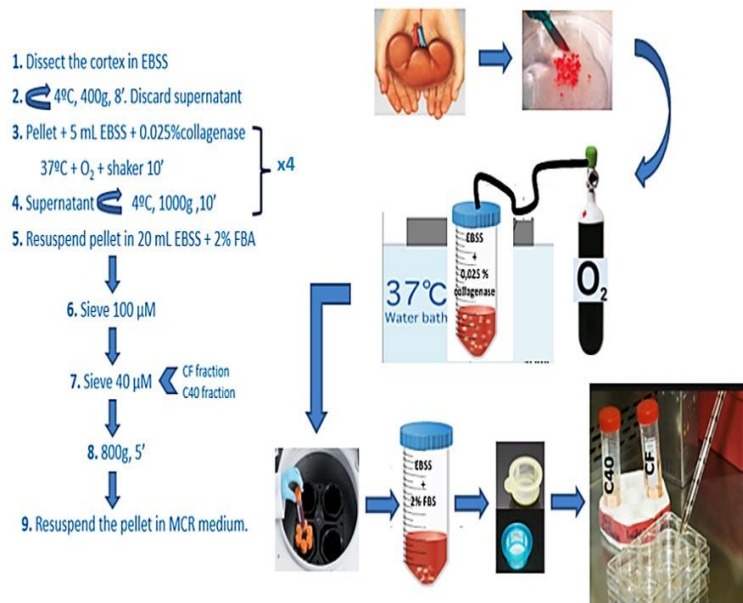


Figure 2.2: Schematic diagram of the different steps performed to obtain the hPTPC isolation.

2.3.5 Cell culture

2.3.5.1 Passage of hPTPC

Cultures of hPTPC were obtained as described previously. In passage 1, the cells were cultured on a 6 wells plate till reach 80% of confluence. Then, cells were subcultured: first, cells are washed with PBS (without Ca²⁺/Mg²⁺) and then, incubated with 0,25% trypsin (Lonza, BE02-007E) at 37°C in a 5% CO₂ incubator until the cells start to detached. After that, cells were resuspended in MCR medium to stop the effect of the trypsin, centrifuged

at 66g for 5 minutes and counted using a Neubauer camera. One mL of cell suspension was taken for RNA preparation, and 4000 cells/cm² were seeded. The growth medium was changed twice a week until confluence was reached. Doubling times for each passage were calculated and are discussed later in this chapter.

2.3.5.2 Cell freezing and thawing

Leftover cells after each trypsinization was frozen at a cell concentration of 0.5x10⁶ cells/mL in DMEM (Lonza, BE12-604F) + 20% FBS (Sigma, F7524), + 10% DMSO (Sigma, 472301). Freezing was a slow process keeping the cells in a cryocooler for 4 hours, and after that, cells were transferred liquid nitrogen until their use.

Thaw process was very quick. The cryovial with cells was submerged in a bath water at 37°C, once thawed, cells were resuspended in 5 mL MCR medium, centrifuged at 66g for 5 minutes and seeded at the desired concentration.

2.3.6 Analysis of phenotypic markers expression by Reverse transcriptase-polymerase chain reaction (RT-PCR)

2.3.6.1 RNA isolation

RNA isolation was performed with 1mL of cell suspension (unknown cell number) in the isolation protocol and 25.000 cells in culture from passages 1-4, with the commercial kit Total RNA Purification (Norgen Biotek, 37500) according to manufacturer's instructions. A sample human kidney tissue was used as a control. The RNA isolation for the control was performed using TriZol reagent (Invitrogen, 15596-026) according to manufacturer's instructions. Isolated RNA was quantified using a Nanodrop spectrophotometer (Thermo Sci., Nanodrop 2000) and its

integrity was tested using a 1% agarose gel with TBE buffer (Fisher Sci., 15881-044). The isolated RNA was kept at -80°C to avoid degradation.

2.3.6.2 cDNA synthesis

The isolated RNA was retrotranscribed into cDNA through the commercial kit High-Capacity cDNA Reverse Transcription Kit (Applied Biosystems, 4387406) according to manufacturer's instructions.

2.3.6.3 RT-PCR

Twelve pairs of primers were combined in a multiplex PCR (Table 2.5).

Table 2.5: Multiplex primers.

Mix	Primer	Sequence	Amplicon	Location
1	Megalin	PF:CATCCAAGCGAATGGATCTG PR:CAGTACAATCCACATCGCCATC	185 bp	TP
	KSP	PR:TCCCATGCCTACCTCACCTT PF:TTGCAGCGACACACGATCA	125 bp	Kidney-specific cadherin
	DPPIV	PF:TACTACTGGCTGGGTTGGAAG PR:TGTCTGTAACCTTCTTCATTGCTG	102 bp	TP
2	APN	PF:GAACGATCTCTTCAGCACATCAG PR:GAAGAGGGTGTGTTTCAGCG	232 bp	TP
	GADPH	PF:TTGACGCTGGGGCTGGCATT PR:GTGCTCTTGCTGGGGCTGGT	157 bp	Endogenous control
	GGT1	PF:TGAGCCCAGAAGTGAGAGCAGT PR:ATGTCCACCAGCTCAGAGAGGG	185 bp	TP

3	THP	PF: GAGTGTCACCTGGCGTACTG PR: CATGGGTTTCATTCTCGTCAAC	358 bp	TAL
	α SMA	PF: CAGGCATGGATGGCATCAATCA PR: ACTCTAGCTGTGAAGTCAGTGTC	172 bp	Myofibroblast
	SGLT-2	PF: ACGCCTGATTCCCGAGTTCT PR: AGAACAGCACAAATGGCGAAGT	110 bp	TP
4	AQP-2	PF: ATCACGCCAGCAGACATCC PR: AGCACGTAGTTGTAGAGGAGG	350 bp	CD
	NKCC2	PF: GGGGAGTCATGCTCTTCATTTCGC PR: CCACGAACAACCCGTTAGTTG	149 bp	TAL
	NCC	PF: CACCAAGAGGTTTGAGGACATG PR: GACAGTGGCCTCATGCCTTGAA	70 bp	DT

RT-PCR was set up using the commercial kit DSF-Taq (Bioron, 101005). The final volume of the reaction mixture was 20 μ L, and 1 μ L of cDNA was added (Table 2.6).

Table 2.6: Reagents and working concentration for mixes of PCR

Reagent (concentration)	Working concentration
Buffer incomplete 10x	1x
Mg ²⁺ 4 mM	0.16 mM
dNTP 10 mM	200 μ M
Primers 4 mM	0.5 μ M
Taq polymerase	5*10 ⁻⁴ U

RT-PCR cycles were as follows (Table 2.7):

Table 2.7: PCR procedure

Cycle repetitions	Temperature	Time	Process
1x	94°C	2'	Initialization step
40x	94°C	45''	Denaturation step
40x	62°C	30''	Annealing step
40x	72°C	1.30'	Elongation step
1x	74°C	5'	Final elongation:
1x	4°C	∞	Final hold

The PCR products were separated on a 2% agarose gel with TBE buffer and stained with ethidium bromide (Sigma, E7637). The gels were visualized using a camera GBOX (Sygene) with an ultraviolet light integrated.

2.3.7 Analysis of phenotypic markers by Immunofluorescence

Cells were plated at a concentration of 8.000 cells/cm² on glass coverslips (VWR, ecn 631-1577) covered with Collagen I from calf skin. Confluent monolayers were fixed with 4% paraformaldehyde for 10 minutes and then washed with PBS [30]. The fixed cells were permeabilized with 0.2% Triton-X 100 (Sigma, X100), incubated for 10 minutes and washed with PBS. Afterward, cells were incubated for 10 minutes in a quenching solution, using 50 mM NH₄Cl, and then washed again. The blocking solution, PBS, 0.1% Tween 20 (Sigma, P5927), 0.1 % BSA and 10 % Goat Serum (Sigma, G6767), was incubated for 30 minutes at room temperature (RT) and then, cells were incubated with primary

antibodies in blocking solution overnight at 4°C. The primary antibodies used were ZO-1 (1:40; Santa Cruz Biotechnology, SC-10804) and acetylated tubulin (1:100, Sigma, T6793). Cells were incubated with secondary anti-mouse Alexa 555 (1:1000; Invitrogen, A31621) or anti-rabbit antibodies, Alexa 488 (1:100; Invitrogen, A-11008) for 1 hour in blocking solution buffer at room temperature. Coverslips were mounted in Vectashield Hard Set TM Mounting Medium (VectorLabs, H-1400) with DAPI (1:1000). Coverslips were examined under a fluorescence microscope (Olympus IX81). Control cells without primary antibody were used to detect the unspecific binding of the secondary antibody.

2.3.8 Analysis of phenotypic markers by Immunocytochemistry

8.000 cells/cm² were plated on glass coverslips coated with type I Collagen from calf skin. Confluent monolayers were fixed with 4% paraformaldehyde for 10 minutes at RT and permeabilized with 0.1% Triton X100 for 10 minutes [31]. After the permeabilization step, cells were washed with PBS and incubated with 3% H₂O₂ (quenching solution for endogenous peroxidase activity) for 5 minutes. Non-specific binding sites were blocked by incubation with Vectastain Elite ABC kit (VectorLabs, PK-6100) according to manufacturer's instructions and finally, cells were incubated overnight at 4°C with GGT1 (1:50), Megalin (1:50; SantaCruz Biotechnology, SC-47025), Calbindin 28 (1:50, Sigma C9848) and α -SMA (1:50, Sigma, A5228) primary antibodies. Afterward, coverslips were washed and then exposed to their corresponding biotinylated secondary antibodies (1:200) for 1 hour at RT. The protocol continued with the incubation of the reagents from Vectastain Elite ABC kit (VectorLabs, PK6100) to create the Avidin/Biotinylated Complex, followed by the incubation with Sigmafast DAB kit (Sigma, D0246), the precipitated

substrate system to peroxidase, till the cells changed the color. Cells were counterstained with hematoxylin-eosin (Vector, H3404), mounted in Vectashield Hard Set TM Mounting Medium and examined in an inverted microscopy (Olympus IX81). Unspecific binding and residual background peroxidase activity could be detected in control cells processed without the primary antibody.

2.3.9 Cytochemical demonstration of GGT1 activity

2.3.9.1 Gamma Glutamyl Transpeptidase (GGT1) cytochemical staining

This assay let us visualize the GGT activity obtained through the reaction between a diazonium salt and the naphthylamine released by hydrolysis of a syntactic GGT substrate, γ -glutamyl-4-methoxy-2-naphthylamide (GMNA).

Cells were fixed for 10 min with ice-cold methanol (Fisher Sci. M/3950/21) and ice-cold acetone (Sigma, 90872) (1:1) and washed with 0.85% NaCl (Saline solution). Then, cells were incubated with the working solution (Table 2.8) for 20 minutes in the dark and again, they were washed with saline solution. To stop the reaction, cells were incubated with a 0.1 M solution of cupric sulfate (Sigma, C1297) for 2 min and then, washed with a saline solution [32]. The pictures were taken using an inverted microscope (Olympus IX81).

Table 2.8: Working substrate solution for a volume of 5 mL

Substrate solutions*	Working concentration	Volume
GMNA solution 2.5 mg/mL (SC, 215216)	0,25 mM	0,25 mL
Tris buffer, pH 7.4	0.1 M	1,25 mL
NaCl (Saline solution)	0.85%	3,5 mL
Glycylglycine (Sigma, G3915)	3,78 mM	2,5 mg
Fast blue salt hemi zin chloride (Sigma, F3378)	1,20 mM	2,5 mg

**The substrate solution was filtered through a Whatman N^o. 1 filter paper just before use to remove any insoluble aggregates of the substrate.*

2.3.10 Analysis of phenotypic markers by flow cytometry

Confluent monolayers were washed twice with PBS. For detachment, cells were incubated with 0.25% trypsin until they were completely detached. Aliquots with a cell suspension of 5×10^5 cells were resuspended in 50 μ L PBS and incubated for 1 hour at RT with 50 μ L of labeled antibodies CD10⁺(Immunostep, 10A-100T), CD13⁺(Acris, SM1856FT), CD26⁺ (Acris, SM2264RT [33]. Cells were pelleted by centrifugation at 262g for 10 minutes and resuspended in 500 μ L PBS twice. The resulting pellet was resuspended in 250 μ L PBS and incubated with propidium iodide to check the cell viability. The specificity of these antibodies was shown by isotype labeling. The labeled cells were analyzed using a flow cytometer (BD, FACSAria) [34]. Some experiments were performed using the triple positive population of sorted cells by FACS. The separated cells were

seeded, and 7 days after the seeding, they were analyzed by multiplex-PCR. All the performed flow cytometry analysis included negative controls to quantify and subtract the autofluorescence profile.

2.3.11 Determination of Enzyme activity in live cultured cells.

The enzyme activity of GGT1 and DPPIV were analyzed by measuring the conversion of a specific enzyme substrate: GGpN and GPpN respectively. The reaction of these enzymes consisted in the enzymatic conversion of the substrate gamma glutamyl-p-nitroanilide (Sigma, G6133) and glycyl glycine, a glutamyl acceptor and Gly-pro-p-nitroanilide (Sigma, G0513) in the presence of the specific enzyme GGT1 and DDPIV respectively. The liberated reaction product, p-nitroaniline, is a yellow-colored compound whose rate of formation is determined optically as the measure of the gamma-glutamyl transferase (GGT1) and dipeptidyl transferase IV (DPPIV) activity (Figure 2.3).

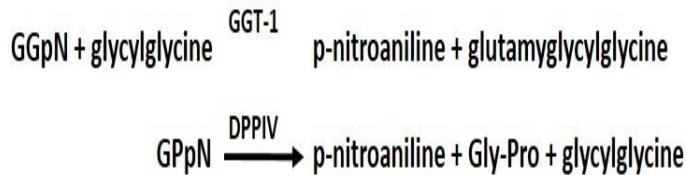


Figure 2.3: GGpN and GPpN reaction

To determine the activity of gamma-glutamyltransferase 1 (GGT1, CD224) and dipeptidyl peptidase IV (DPPIV, CD26) as marker enzymes for the proximal tubule, 8000 cells/ cm² were grown in 96 wells plate (TPP, 92096). When confluence was reached, the cells were rinsed with HBSS buffer and the substrate solutions were prepared:

1. The GGT1 activity was assessed using 2 mM γ -glutamyl-p-nitroanilide and 50 mM glycylglycine as a substrate, in 1 mL PBS. This preparation was incubated during 1h at 37°C in a plate reader [35].
2. The activity of DPPIV was determined using 1 mM Gly-Pro-p-nitroanilide as a substrate in 1 mL PBS. This preparation was incubated during 1h at 37°C in a plate reader [36].

The resulting product, p-nitroaniline, in both reactions is directly proportional to the enzyme presents in the sample. P-nitroaniline concentration was measured at 410 nm using a microplate reader (BioTek, Synergy HT) and the measures were taken every 20 minutes during an hour. The result was represented as absorbance at 410 nm. To determine the activity, a standard curve with 3 known concentrations for p-nitroaniline (Sigma, 185310) was performed, and the results were expressed as mmol p-nitroaniline/min/cm² or mmol p-nitroaniline/h/cm² (Figure 2.4).

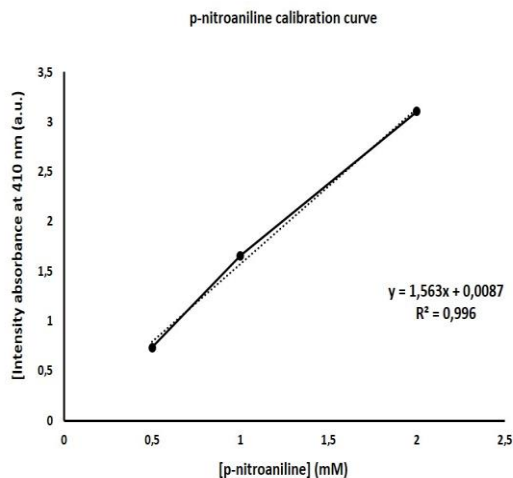


Figure 2.4: . p-nitroaniline calibration curve.

2.3.12 Transporter Assays

2.3.12.1 How do the fluorescence-based experiments work?

To evaluate xenobiotic handling in *in vitro* systems, fluorescent based functional assays are performed. These assays are based on the use of fluorescent probes that can pass the plasma membrane by diffusion or by using transporters. Usually, these fluorescent probes are substrates for certain transporters or precursors [37-39], so when the substrate comes in, the fluorescence in the cells can be quantified. At the same time, these substrates can be combined with apical/basolateral transporter inhibitors and consequently, the resulting decreasing or increasing of intracellular fluorescence can be measured and correlated to transport activity (Figure 2.5). The transporters activity in hPTPC were investigated analyzing the presence of two important basolateral transporters, OAT1 and OCT2 and three apical transporters, BCRP, MRP4 and P-gp. To this end, cells were exposed to ASP+ (influx basolateral OCT2 transporter), calcein-AM (influx cell membrane and efflux apical BCRP, MRP, P-gp transporters) and fluorescein (influx basolateral OAT1 transporter and efflux apical MRP/BCRP transporters), in the presence or absence of model inhibitors for OAT1 (Probenecid), BCRP (KO143), P-gp (PSC833) and MRPs (MK571).

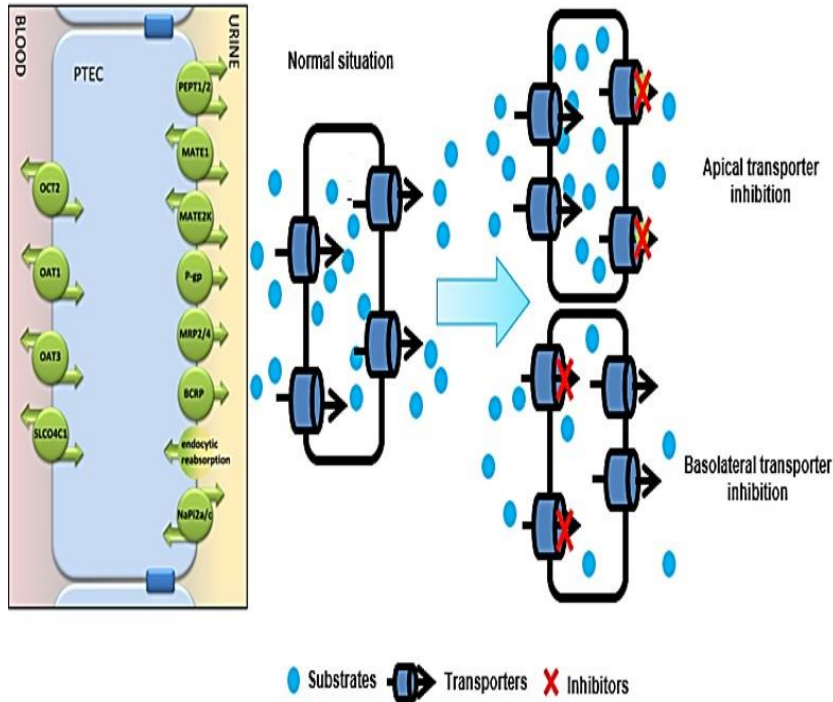


Figure 2.5: Graphic presentation of substrate handling and transport inhibition.

2.3.12.2 Cell culture

hPTPC were seeded at a density of 8000 cells per cm² in 96 wells plates and cultured in MCR medium at 37 °C. in a 5% CO₂ atmosphere during 7 days until confluence was reached.

2.3.12.3 Organic anion transporter 1 (OAT1)

Confluent cells were washed twice with HBSS buffer (Lonza, BE10-527F). To determine the uptake by the OAT1 transporter [40], cells were incubated in a concentration gradient of Fluorescein 0-100 μM (Sigma, F6377) during 40 minutes. To evaluate the inhibition of the transporter, some wells with cells were pre-incubated using 100 μM probenecid

(Sigma, P8761) during 15 minutes, and then, the cells were incubated with the inhibitor and fluorescein (6 μ M), during 40 minutes at 37°C. After the incubation time in presence or absence of inhibitors, cells were washed with HBSS buffer, lysed with 0.1 M NaOH and shaken for 20 minutes. The fluorescence was measured in a plate reader at 485 nm of excitation and 535 nm of emission.

2.3.12.4 BCRP

Fluorescein is a known fluorescent substrate of ABC transporter family [19]. This substrate can enter into the cell through OAT1, and the exit could be possible by MRP and BCRP. Here, we evaluated BCRP transporter. Cells were washed twice with HBSS buffer and pre-incubated with 15 μ M KO143 (Sigma, K2144), a specific inhibitor of BCRP for 15 minutes. After the incubation with the inhibitor, cells were exposed to 5 μ M of fluorescein in the absence and presence of the inhibitor for 40 minutes at 37°C. Before reading the results, the cells were washed with HBSS and lysed with 0.1 M NaOH. The fluorescence was measured in a plate reader at 485 nm of excitation and 535 nm of emission.

2.3.12.5 P-glycoprotein transporter (P-gp) and Multidrug resistance protein (MRP)

The activity of the ABC efflux transporters P-gp and MRP was performed by measuring the accumulation of the typical cell viability substrate calcein-AM (Sigma, 17783)[41]. Cells were washed twice with HBSS buffer and incubated with 1.25 μ M calcein-AM in HBSS buffer, in the presence or absence of the inhibitors PSC-833 (6 μ M; Tocris, 121584-18-7) or MK571 (50 μ M; Tocris, 115104-28-4) at 37°C for 40 minutes. After the incubation, cells were washed with HBSS buffer and lysed with a solution containing 1% Triton X100. The lysate was kept in agitation for 20

minutes. The resulting fluorescence was measured in a plate reader at 488 nm of excitation and 518 nm of emission.

2.3.12.6 Organic Cation Transporter 2 (OCT2)

The activity of the renal OCT2 transporter was investigated in hPTPC by using a method adapted from Brown *et al.* [2]. Cells were washed twice with HBSS buffer and then, they were incubated in solutions containing a concentration gradient between 0-100 μ M for the fluorescent OCT2 substrate, ASP+ (4-(4-(dimethylamino)styryl)- N-methylpyridinium iodide); Sigma, D3418), in HBBS at 37°C during 30 minutes. After the incubation, the cells were washed with HBSS and the accumulation of substrate by hPTPC was measured using a plated reader by the analysis of fluorescence intensity (excitation 450 nm, emission 642 nm).

2.3.13 Statistics

Differences between groups were considered to be statistically significant when $p < 0.05$ using two-tailed Student's t-test in Excel.

2.4 RESULTS

2.4.1 Protocol of hPTPC isolation

Forming colonies of attached hPTPC could not be identified easily 24 hours after the seeding, as a consequence of the waste material (erythrocytes, cells no attached) present in the well plate. By 48 hours, small cellular colonies were identified (Figure 2.6). Small colonies were constituted approximately by 20 cells, and these cells presented the typical cuboidal epithelial shapes with large, spherical and central nuclei.

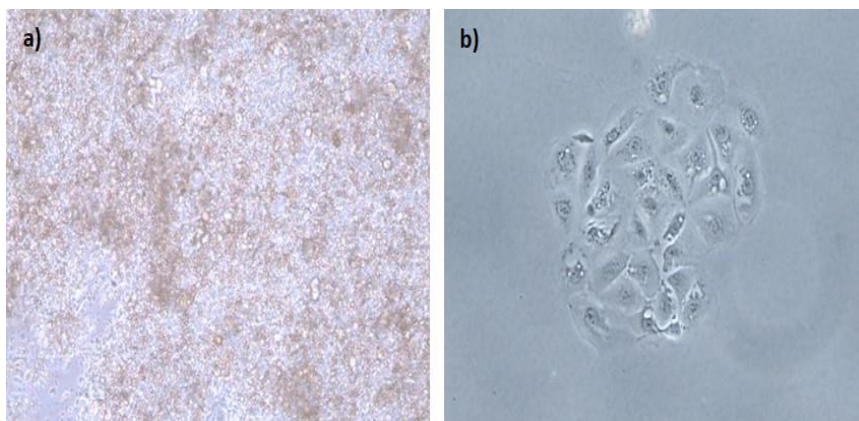


Figure 2.6: a) Representation of the status of the cell culture 24 hours after the seeding, with abundant waste material. On the left bottom side, can be identified some single cells. b) The picture shows a small cellular colony of hPTPC 48 hours after the seeding.

The efficiency of isolation was calculated as follow:

$$\text{Tubulocrite \%} = \text{mg Tubules} / \text{resuspended volume} \times 100$$

The result of tubulocrite percentage for CF fraction was 1.5 % (+/- 1.18 %) and for C40 fraction was 1.6 % (+/-3.17 %). These results were

expressed as the average of the 36 samples processed over the last three years +/- SD.

2.4.2 Evolution of hPTPC morphology and doubling time through subcultivation

All kidney samples from nephrectomies processed to isolate proximal tubular cells contained viable single cells with the ability to proliferate into cell colonies and form a confluent cell monolayer.

Small colonies formed two days after isolation. To observe a confluent cell monolayer, cells needed to grow an average of approximately 7 days in each cell passage. Primary cultures showed the classic cobblestone appearance of epithelial cells in passage 1, 2 and 3 and a heterogeneous morphology in passage 4 (Figure 2.7 and 2.8).

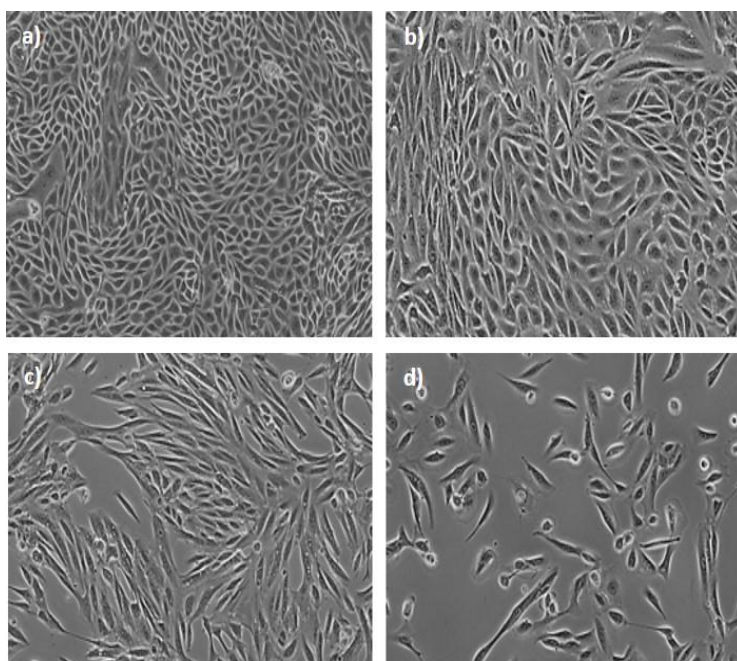


Figure 2.7: Evolution of morphology in hPTPC cultured from fraction CF. Representative phase contrast image of primary cells in passage 1 (a), passage 2 (b), passage 3 (c) and passage 4 (d). Cells maintain epithelial morphology and form a characteristic monolayer till passage 3.

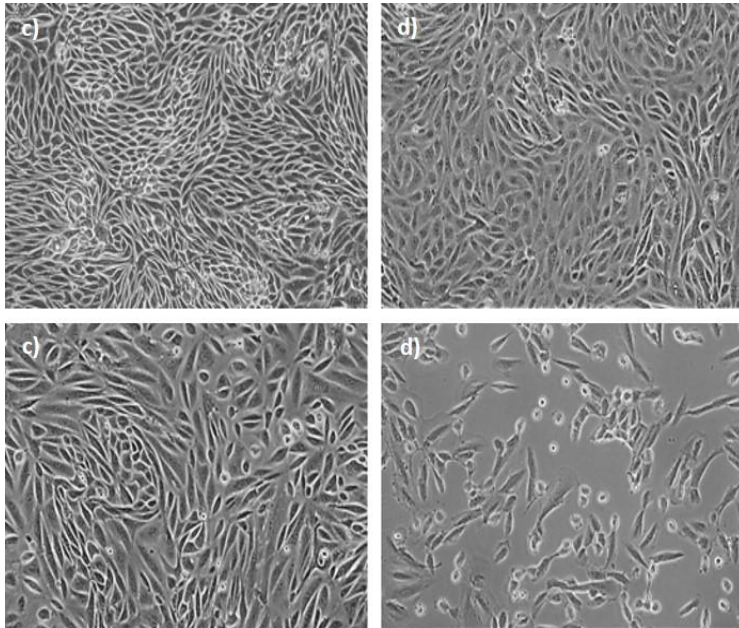


Figure 2.8: Evolution of morphology in hPTPC cultured from fraction C40. Representative phase contrast image of primary cells in passage 1 (a), passage 2 (b), passage 3 (c) and passage 4 (d). Cells maintain epithelial morphology and form a characteristic monolayer till passage 3.

We observed an *in vitro* lifespan of approximately one month per cell passage, and the cells lost their proliferative activity at passage 4. We could not observe any morphological differences between the cells in CF and C40 fraction by phase contrast microscopy. The doubling time was determined in each fraction (Figure 2.9), as well as the number of collected cells per fraction (Figure 2.10).

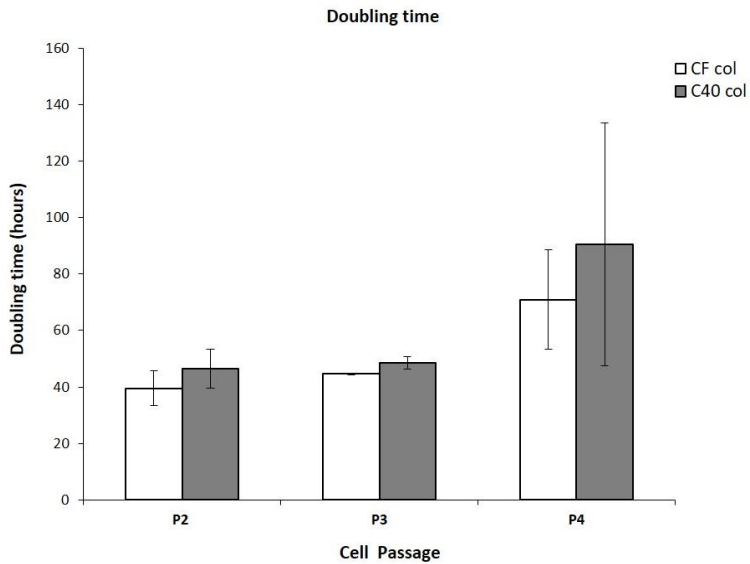


Figure 2.9: Doubling time (hours). Graph comparing doubling times between CF and C40 fraction. 7 days after the seeding, cells were harvested and counted via Neubauer camera. Doubling time was calculated as: number of cells obtained after cell passage/ number of cells seeded=2^{number of divisions}. Data are shown as mean \pm S.D, n=3

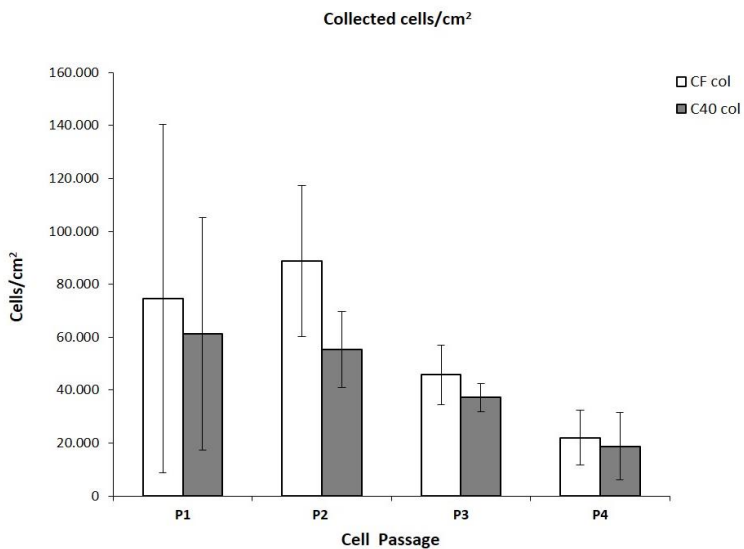


Figure 2.10: Cells number per area surface. Graph comparing the number of harvested cells per square centimeter in each passage. Data are shown as mean \pm SD, n=3.

2.4.3 Transcriptional expression of phenotypic markers in hPTPC

The multiplex PCR was designed to overcome a potential problem with the use of microfluidic devices, the limited number of harvested cells. A multiplex PCR offers the possibility to amplify several different DNA sequences simultaneously from the same sample. In this case, 12 reactions were combined in 4 mixes of 3 targets each, one included an endogenous control. The selected primers were specific for PT, for other segments of the nephron and also for dedifferentiation.

The purity of the isolated hPTPC was evaluated by using multiplex RT-PCR. Single cells from the protocol of isolation were analyzed at passage 0, with the goal to determine the initial purity of the fractions (Figure 2.11). The cultured cells used for the experiments were analyzed from passage 1-4 (Figure 2.12) to determine the phenotypic stability of the cells over time.

In agreement to their *in vivo* expression, the RT-PCR results showed that hPTPC cells were positive for Megalin, KSP-Cad, DPPIV, SGLT-2, APN and GGT1, all of them specific marker for PT at passages 1, 2, 3 and 4, indicating that these cells are phenotypically stable at least over four passages. In addition, over four passages, NCC and NKCC2 expression was persistent, indicating cell contamination from others segments from the nephron. However, the expression of THP and AQP2 was lost from passage 2. RNA from whole human kidney was positive for all markers tested. There were not observed differences in the expression of markers between the CF and C40 fraction.

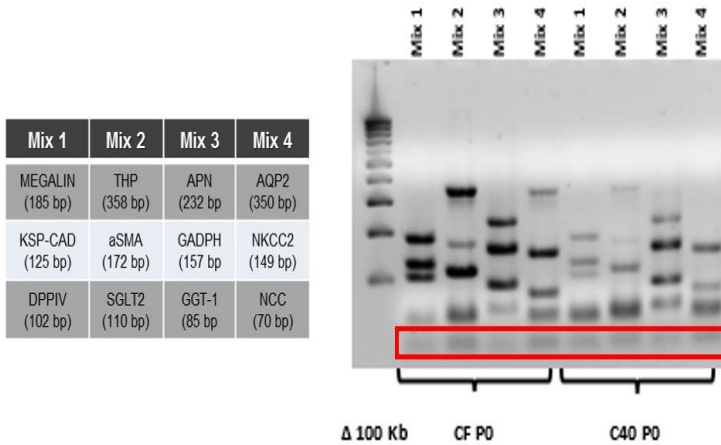


Figure 2.11: Multiplex RT-PCR. Analysis of initial purity comparing CF and C40 fraction. There was not different in the expression of the markers between fractions. The red box showed primer dimer.

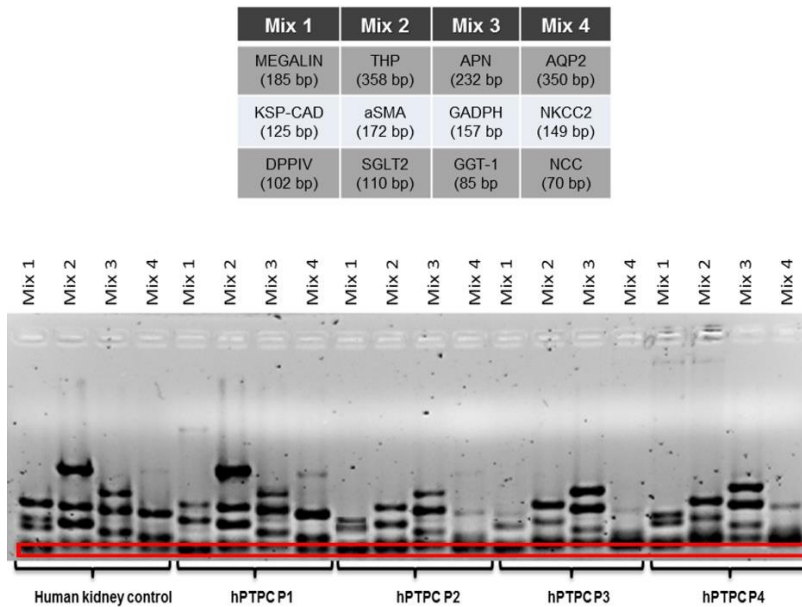


Figure 2.12: Multiplex RT-PCR. Expression of the different markers analyzed from passage 1 -4. The positive control was the RNA from the whole kidney. The principal markers from PT cells were maintained from P1 to P4. However, the expression of NCC and NKCC2 was also maintained over cell passages, indicating this is not a 100% pure culture for PT cells. The red box showed the primer dimers.

The Megalin marker supposed a problem in the multiplex RT-PCR analysis because it was not positive consistently. We think this loss of expression may be due to the small starting amount of cDNA from passage 1-4 used to perform the RT-PCR, because analyzing this mix separately, megalin was positive (Figure 2.13) and with another type of techniques, as an IF, it was also positive.

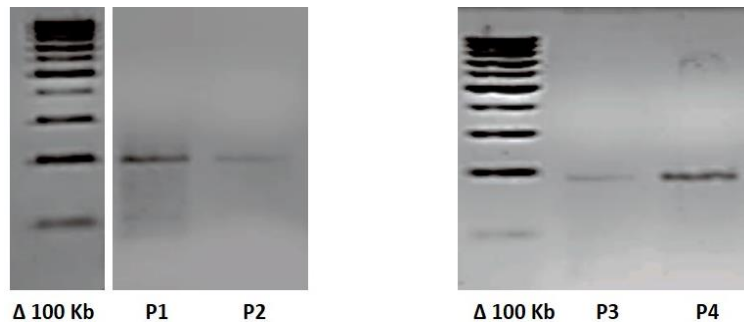


Figure 2.13: Megalin expression by RT-PCR. The cDNA analyzed in the Figure 2.12 (P 1-4) by multiplex PCR was also analyzed for Megalin as a single primers pair in the RT-PCR reaction. The hypothesis of the small starting amount of cDNA to perform the RT was confirmed with this result since in the multiplex RT-PCR Megalin was not detected.

2.4.4 Immunofluorescence analysis by using epithelial markers

The immunofluorescence of the hPTPC was performed 7 days after the seeding when cells reached the confluence to demonstrate the epithelial origin of these cells by using the antibody ZO-1 and acetylated tubulin. The immunofluorescences were performed until passage 3.

The analysis using ZO-1 was performed to confirm the epithelial origin of cells, emphasizing their cell polarity [42]. The expression of ZO-1 showed a linear distribution of the tight junction protein (Figure 2.14a). We also observed different morphologies present in the cell culture, although ZO-1 was expressed in all cells.

We used acetylated tubulin to detect primary cilia. These organelles are present in epithelial cells, and they are fundamentals for fluid mechanosensing and regulation of tubular morphology [43]. When we examined the expression of acetylated tubulin, we detected the typical structure of this cell type: the primary cilia (Figure 2.14b).

The culture of hPTPC revealed a well-defined confluent monolayer with the positive expression of the ZO-1 protein and acetylated tubulin, both specific markers of epithelial cells.

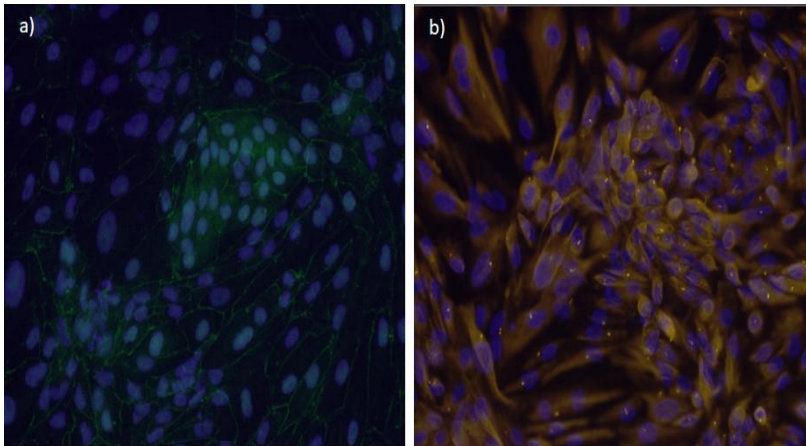


Figure 2.14: Proximal tubular epithelial origin of hPTPC. The hPTPC seeded on coverslips coated with collagen I were analyzed by IF, 7 days after the seeding. The analyzed cells belonged to CF fraction of a cell culture in passage 2. a) Expression of epithelial marker ZO-1 [44] confirmed the formation of tight junctions. b) The analysis of acetylated tubulin showed the expression of primary cilia (brighter dots in yellow).

2.4.5 Immunocytochemistry characterization

Markers for proximal tubule (GGT1 and Megalin), distal tubule (CB-28) and Myofibroblast (α SMA) [45] were tested for the first three passages in both fractions. Immunocytochemistry showed different levels of expression of the specific stains between the cells in all cell passages. No

differences were found in marker expression between the fractions CF and C40.

Gamma-glutamyl transpeptidase (GGT1) is a glycoprotein located in the brush border of proximal tubular cells. GGT1 cleaves gamma-glutamyl peptide bonds in glutathione and other peptides and transfers the gamma-glutamyl group to acceptors [46]. This glycoprotein was studied with different techniques to show its expression for 2 reasons: the first one is because in the kidney it is specific for PT cells. The second reason is for the role played in nephrotoxicity area (explained in chapter 3). The result obtained for this marker in hPTPC confirmed a high expression. Approximately, the 80-90% of the cells showed positive staining for this marker (Figure 2.15a).

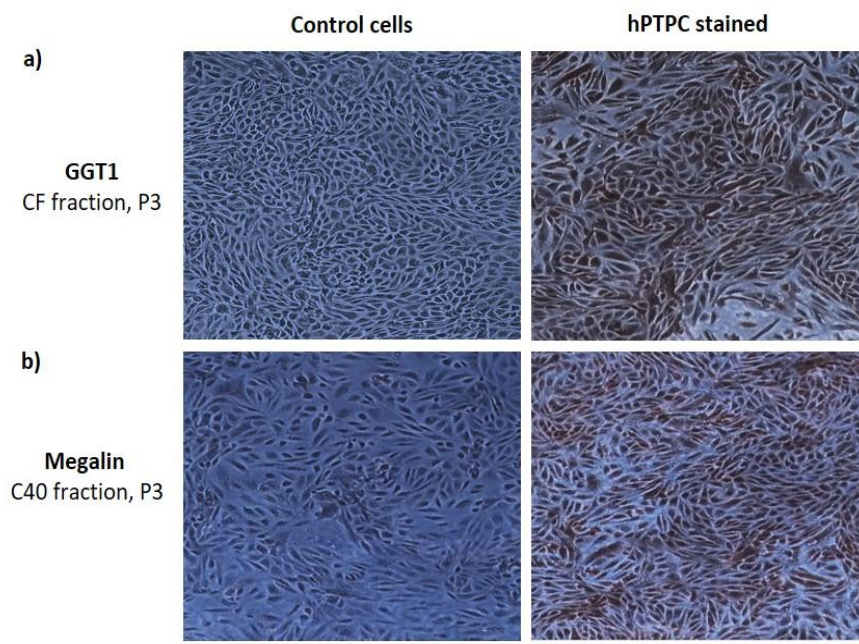
Megalin is a multiligand receptor belonging to the low-density lipoprotein receptor family gene. It is expressed and localized in the brush border and the endocytic pathway of the renal proximal tubule epithelium. Megalin plays a specific key role in the proximal tubular uptake of glomerular-filtered albumin and other low-molecular-weight-protein [47, 48]. The immunocytochemistry using this receptor showed that between the 80-90% of the hPTPC had a positive expression (Figure 2.15b).

Calbindin-28 (CB28) is an intracellular calcium-binding protein. In the kidney, this protein is exclusively localized in the distal tubule and the proximal part of the collecting ducts [49]. The expression of Calbindin 28 in hPTPC was slightly positive only in some cells, representing a 5% of positive staining in the cell culture. This result showed that the human primary cell culture is heterogeneous (Figure 2.15c).

The alpha smooth muscle actin (α SMA) is a typical marker of myofibroblasts [50]. The expression of this marker was confirmed over the

cell passages, indicating some degree of epithelial–mesenchymal transition [51] has taken place (Figure 2.15d).

It is very important to highlight that the level of expression of CB-28 and α SMA was weak, compared with the higher expression of GGT and Megalin.



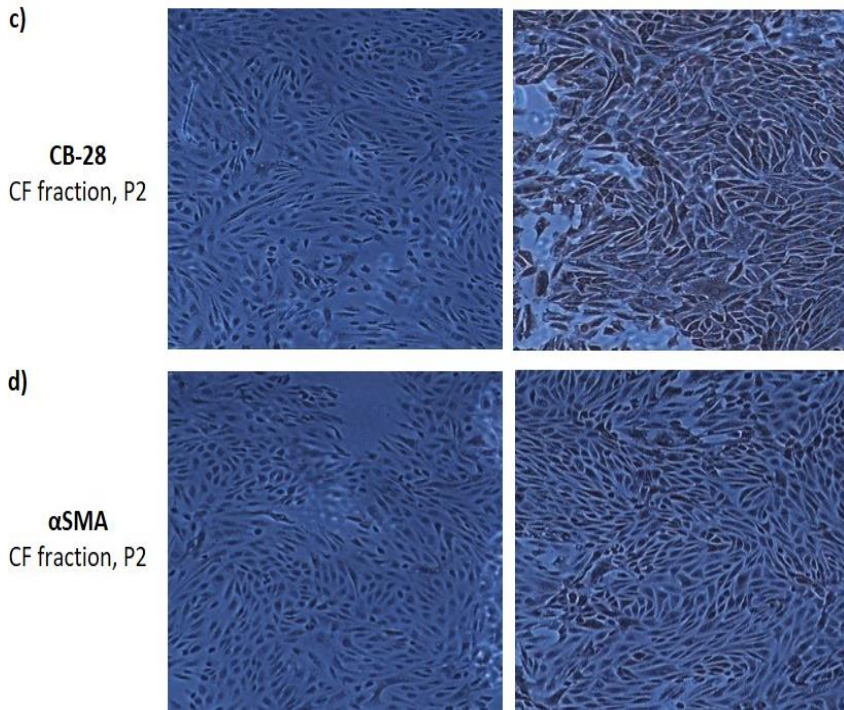


Figure 2.15: Representative immunocytochemical images. a) hPTPC, CF fraction, cell passage 3 stained with GGT1. The expression of the brush border enzyme GGT1 was highly positive compared with the control. b) hPTPC C40 fraction cell passage 3 stained with Megalin. The expression of this marker was also very high. The positive expression of GGT1 and Megalin confirmed the proximal tubular origin of the hPTPC. c) CB-28 was used to stain the hPTPC CF fraction cell passage 2. The expression of this marker was weakly positive, compared with the control. This result indicated contamination of distal cells in our human primary cell culture. d) The marker α SMA is a specific marker of Myofibroblast. Its positive expression in hPTPC CF fraction cell passage 2 confirmed a possible EMT.

2.4.5.1 Cytochemical demonstration of GGT1 activity

The presence of proximal tubular brush border enzyme GGT1 in hPTPC was confirmed using an enzyme cytochemistry assay previously described by Rutenburg *et al.* [1]. GMNA cytochemical staining is a simultaneous coupling azo dye method for the histochemical demonstration of γ -glutamyl transpeptidase activity using the substrate GMNA. The reaction caused the precipitation of an insoluble, reddish-brown dye, at cell sites containing enzyme activity. The intensity of the staining was variable, with areas of intense reddish-brown staining next to areas of less intensity, or absent staining. The positive reddish brown staining of hPTPC can be observed in Figure 2.16.

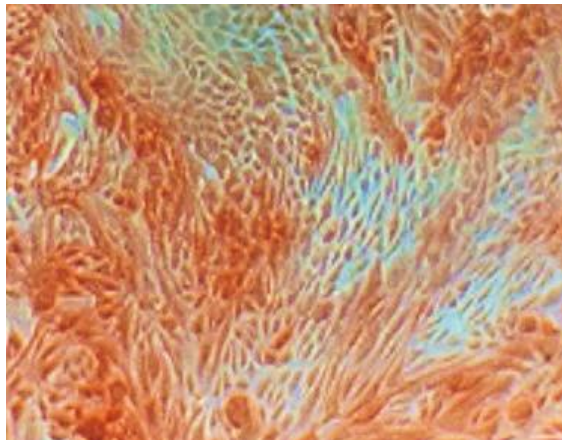


Figure 2.16: Light microscopy of GGT1 staining of hPTPC.

2.4.6 Flow cytometry analysis

The flow cytometry was used to get a pure population of PT cells. By using this technique, we quantified the relative expression of three specific markers expressed in the brush border of the proximal tubule cells: CD13⁺ (Aminopeptidase N, APN), CD10⁺ (Acute lymphocytic leukemia antigen, CALLA) and CD26⁺ (Dipeptidyl peptidase IV, DPPIV). We decided

to perform the flow cytometry analysis using these antibodies previously described in the literature where it was reported that cells double positive for CD10/CD13 constitute a pure, functional and stable proximal tubular epithelial cell population [28, 33, 52], and exactly the same happened for CD26⁺ [52]. After the gating, the average percentage of CD13⁺, CD26⁺, CD10⁺, the double positive for CD13/CD26 and the triple positive for the three markers were calculated and represented as mean \pm SD (Table 2.9) These results confirmed the expression and the presence in the cell culture of these typical proximal tubule markers (Figure 2.17).

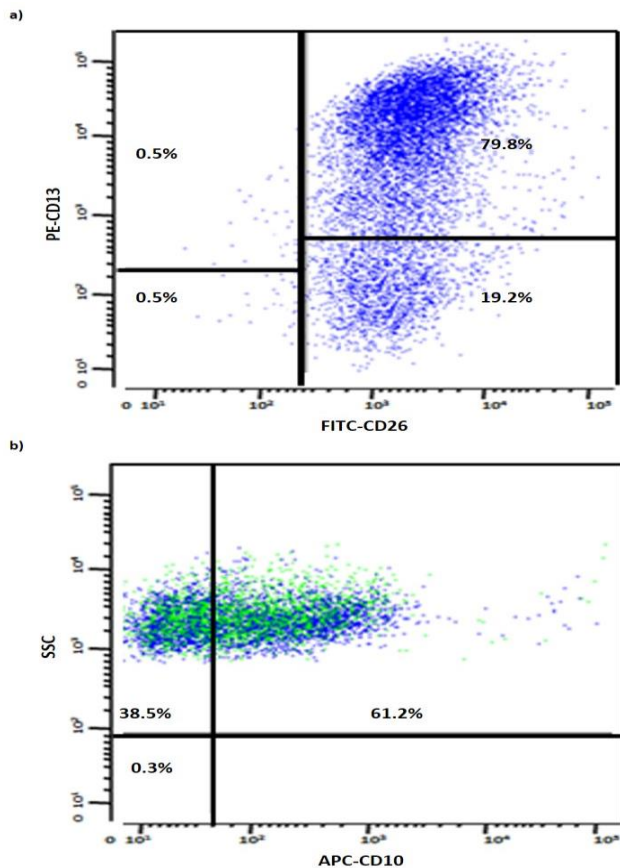


Figure 2.17: a) Flow cytometry analysis revealed about a 79.8% double positive cell population labeled with antibodies against CD26 (FITC) and CD13 (PE). b) The double positive cell population was also analyzed for CD10 (APC) obtaining a 61.2% of the triple positive cell population.

Table 2.9: Cells markers analyzed by flow cytometry

	CD13	CD26	CD10
Mean (%) ± SD	86.15 ± 7.59 (n=4)	98.675 ± 0.77 (n=4)	61.95 ± 1.48 (n=2)

	CD13/CD26	CD13/CD26/CD10
Mean (%) ± SD	82.6 ± 6.77 (n=3)	61.1 ± 0.14 (n=2)

Positive triple cells were separated by FACS and seeded and 7 days after the seeding, a multiplex RT-PCR was performed. The markers not specific of PT cells remained positive (Figure 2.18). So, the goal to obtain a 100% pure population of PT cells was not reached with this method.

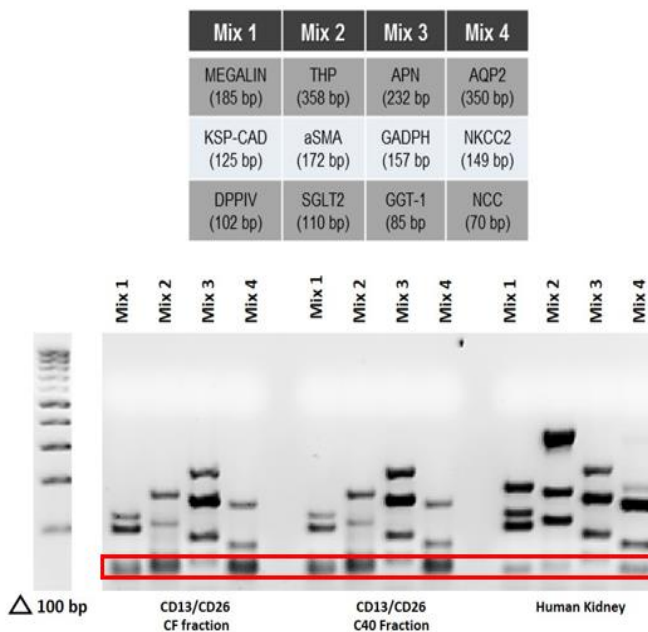


Figure 2.18: Analysis of markers by multiplex PCR. The sorted cells double positive for CD13/CD26 were seeded and 7 days after the seeding, a multiplex PCR was performed. No differences were observed compared with results of multiplex PCR where the cells were not previously sorted. The red box showed dimer primer.

2.4.7 Determination of Enzyme activity in live cultured cells

The activity of GGT1 and DPPIV was quantified in hPTPC by measuring the liberation rate of p-nitroaniline from specific substrates (GGpN and GpN, respectively). This technique was not an end point assay, so it let us study the changes in the enzymatic activity along the time with a specific cell culture. The use of this technique will be very useful in the microfluidic devices, where it is convenient follow the progression of cells along time.

Then, to verify that the measures for hPTPC corresponded with what would be expected from PT, a validation was carried out by performing a test comparing the p-nitroaniline accumulation using the substrate GGpN in the presence of different cell types. The chosen cell types were BEC (biliary epithelial cells), cells with high expression of GGT1, BMC (bone marrow stromal cells), cells without expression of GGT1 and the hPTPC (Figure 2.19). The results were consistent with what we expected.

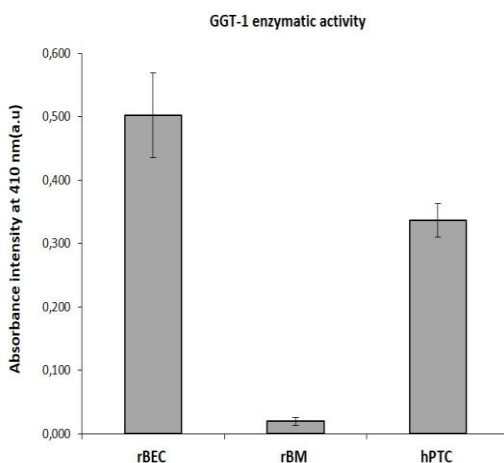


Figure 2.19: Absorbance intensity of GGpN. The graph showed the absorbance intensity of the liberated p-nitroaniline in BEC, BMC and hPTPC cells demonstrating the specificity of the product. The data were represented as mean +/- SD (n=2).

In hPTPC, a linear increase in the absorbance produces for p-nitroaniline

was observed over 60 min (Figure 2.20), with an end activity of approximately 110 and 83.87 mmol p-nitroaniline/h/cm² respectively (Figure 2.21). These results showed the presence of GGT1 and DPPIV, specific enzymes for PT cells, in the hPTPC.

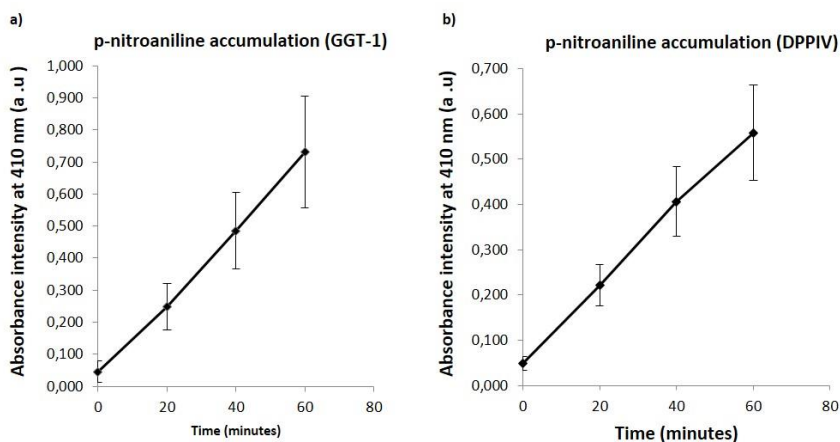


Figure 2.20: Determination of enzymatic activity. GGT1 and DPPIV activity was determined by measuring the p-nitroaniline liberated from the artificial substrates GGpN (n=23) and GPpN (n=4) respectively, over 60 min. The absorbance was represented as mean +/- SD.

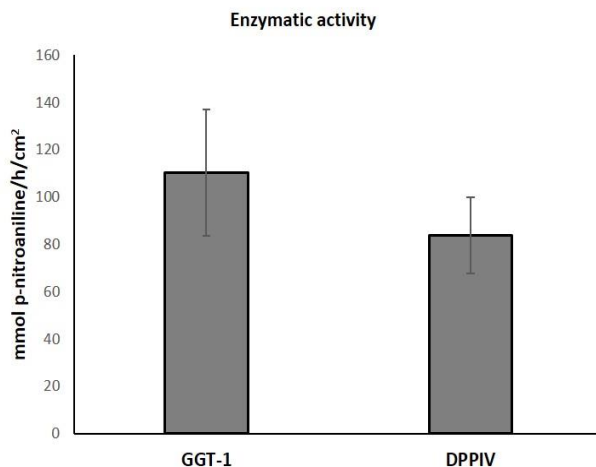


Figure 2.21: Determination of GGT1 and DPPIV activity by p -nitroaniline concentration. GGT1 and DPPIV activity was determined by measuring the p-nitroaniline liberated from the artificial substrates GGpN (n=23) and GPpN (n=4) respectively, after of 60 min incubation. The concentration was calculated from p-nitroaniline calibration curve as mean +/- SD.

Usually, GGT1 enzymatic activity was analyzed 7 days after seeding. However, some experiments were analyzed 14 days after seeding (Figure 2.22) showing an increased activity compared with GGT1 activity at 7 days.

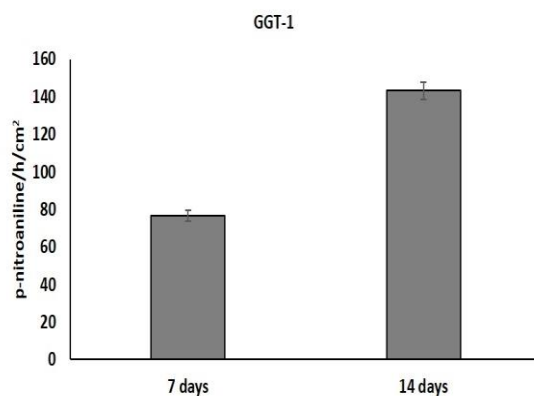


Figure 2.22: GGT1 enzymatic activity. The enzymatic activity of GGT1 was analyzed in culture 7 and 14 days after the seeding. GGT1 increased its activity almost the double after 14 days in culture, compared with the result at 7 days

2.4.8 Transporter Assays

2.4.8.1 Organic anion transporter 1 (OAT1)

OAT-mediated fluorescein transport was investigated using a concentration gradient of the substrate. This assay helped us to determine if there was uptake by the OAT1 transporter and also if the uptake was substrate concentration dependent (Figure 2.23).

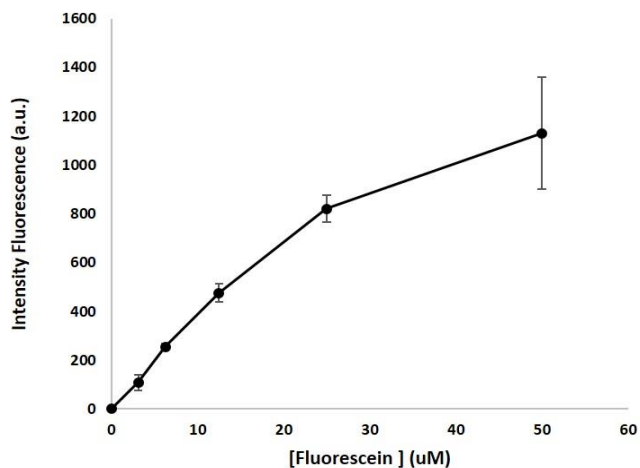


Figure 2.23: OAT1 activity. The fluorescence intensity indicated that the fluorescein was uptake by OAT1 in a concentration-dependent way. Data were expressed as mean \pm SD of two independent experiments.

To demonstrate the uptake was transporter mediated, specific inhibition of fluorescein uptake in the presence of probenecid was studied (Figure 2.24).

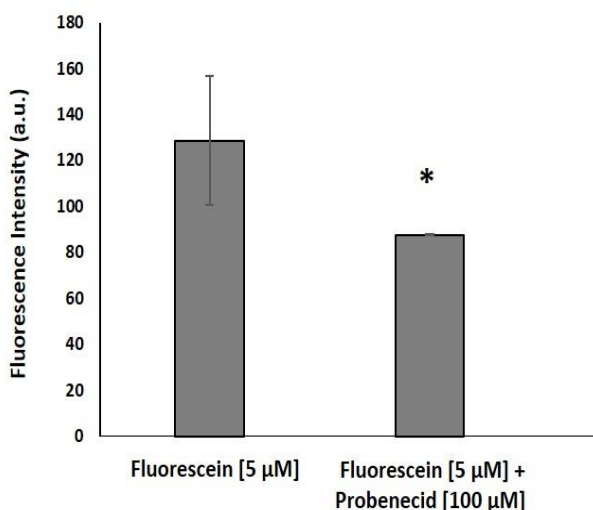


Figure 2.24: OAT1 inhibition. The use of probenecid, an inhibitor of OAT1, produced a reduction in the fluorescence intensity, indicating the uptake of fluorescein is transporter mediated. Data were expressed as mean \pm SD of two independent experiments. * $p=0.01$

The uptake of fluorescein and also its inhibition demonstrated the OAT1-mediated fluorescein transport. These results demonstrated the presence of OAT1 in hPTPC.

2.4.8.2 ABC transporter family

As we mentioned before, the uptake of fluorescein is OAT1 mediated. Here, we studied the fluorescein efflux by using an inhibitor of BCRP (KO143) activity. The use of this inhibitor increased the retention of fluorescein in a ratio of 1.3. (Figure 2.25).

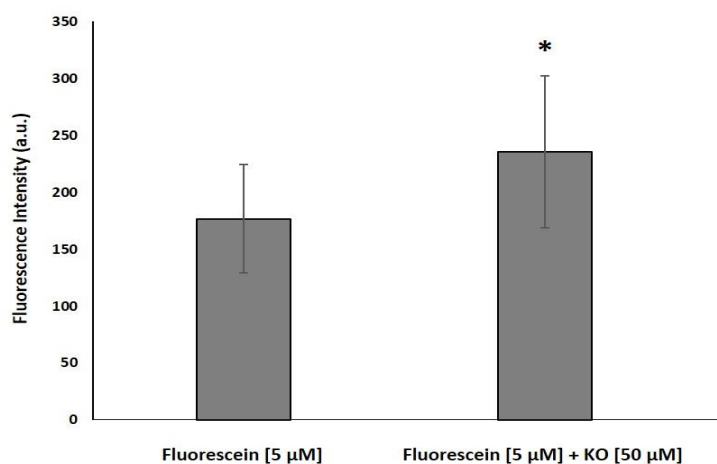


Figure 2.25: BCRP activity. The fluorescein was accumulated in the cells in the presence of KO143 inhibitor. Data were expressed as mean \pm SD of two independent experiments. * $p=0.02$.

2.4.8.3 Activity of P-glycoprotein transporter (P-gp) and Multidrug resistance protein (MRP)

The activity of P-gp and MRP transporter was determined by using the lipophilic non-fluorescent substrate calcein-AM. Calcein-AM penetrates the cell membrane and once inside, it is metabolized by esterases activity to render a fluorescent substrate, calcein. To determine the fraction of calcein efflux through P-gp and MRP transporters, hPTPC cells were

incubated with Calcein-AM in the presence of inhibitors PSC833 (P-gp) and MK571 (MRP). As represents the Figure 2.26, an increase in the fluorescence intensity was observed when cells were incubated with Calcein-AM, indicating that the molecule penetrated the cell membrane and was converted into a fluorescent substrate. The use of inhibitors promoted much more the intracellular accumulation of calcein. PSC833, inhibitor of P-gp transporter increased the fluorescence intensity in a ratio of 1.98, meanwhile MK571, inhibitor of MRP, increased the accumulation of fluorescence in a ratio of 1.70 compared with the substrate in absence of inhibitors. These results showed the presence of MRP and PgP in our hPTPC.

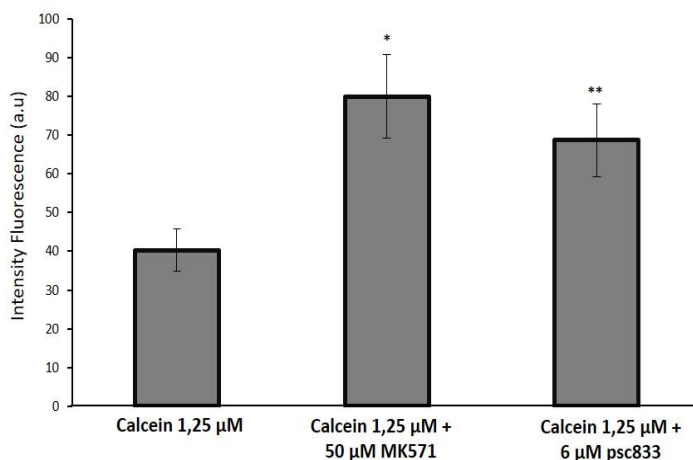


Figure 2.26: Fluorescent substrates accumulate in hPTPC in the presence of efflux transport blockers. An increase in fluorescence was observed when cells were incubated with the fluorescent substrates without inhibitors or in the presence of inhibitors. Inhibitors promoted the intracellular accumulation of the fluorescent substrates, as depicted in the bar graphics. Data were expressed as mean \pm SD of four independent experiments. *- $p=5,11E-11$ **- $p=3.34E-09$

2.4.8.4 Organic Cation Transporter 2 (OCT2)

The ability of hPTPC cells to transport nephrotoxics as the cisplatin (it will be discussed in chapter 3) was studied by the activity of the basolateral transporter OCT2. The fluorescent molecule used to study this transporter was ASP⁺. The concentration dependency of ASP⁺ uptake by hPTPC cells (Figure 2.27) was demonstrated. Thus, the expression of OCT2 in hPTPC cells was confirmed.

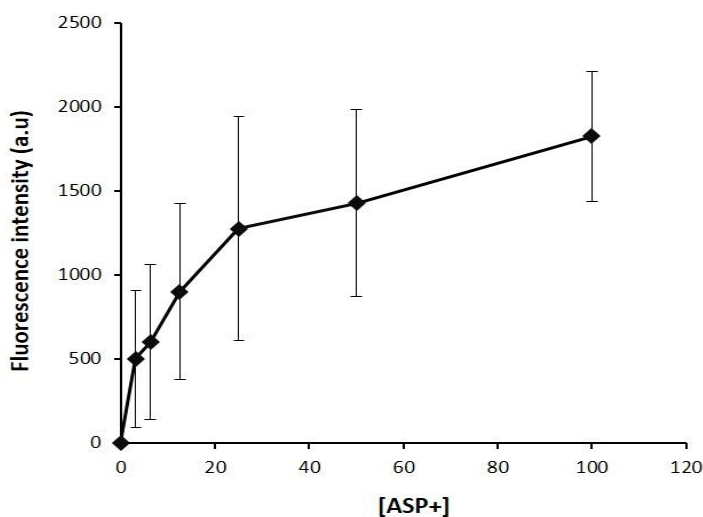


Figure 2.27: Organic cation transporter 2 (OCT2) activity in hPTPC. The activity of OCT2 analyzed by measuring the fluorescence accumulation of transported 4-(4-(dimethylamino)styryl)-N-methylpyridinium iodide (ASP⁺) as a concentration gradient. Data were expressed as mean \pm SD of two independent assays.

2.5 DISCUSSION

Cultured Proximal tubular cells are a valuable *in vitro* model that can be used to study various aspects of physiology and pathology, drug-drug interaction, drug metabolism or mechanisms of cytotoxicity. Accordingly, most *in vitro* models of renal function have focused on reproducing PT cells function. Here, it has been described the protocol to isolate proximal tubular cells from human nephrectomies and its posterior characterization.

The protocol used in this Thesis for the isolation of human proximal tubular cells was adapted from preceding reports by John J. Gildea *et al.* [24], Sharpe C.C. *et al.* [53], David A. Vesey *et al.* [54], Paul A. Glynne [29] and Patrick Salmon [55] with modifications. The principal modifications included were the presence of O₂ during the protocol isolation, four repeats of the digestion process, the washing step and low-speed centrifugation to remove the red blood cells present in the sample, and finally the determination of the tubulocrite. The reviewed literature of protocols for isolation of PT cells did not show a method to determine the initial purity of the starting material [25, 26, 33, 54, 56-60].

Although the amount of starting material was really small, it was not a problem to expand the cells and work with them.

The following steps were critical to get an effective isolation protocol:

- The size of the fragmented tissue has to be small in order to facilitate the digestion of the tissues in the presence of collagenase.
- Appropriate collagenase treatment is crucial for proximal tubular preparation because this enzyme helps to disrupt basement membrane, leading to the isolation proximal tubular cells.

- The combination of the enzymatic treatment with collagenase and the mechanical process with the continuous agitation favored the digestion of the renal tissue
- It is very important to be cautious 24h after the seeding when it is necessary to refresh the growth medium because the hPTPC are still relatively fragile and can be easily damaged or disrupted by direct contact; pipette only down the side of the well, and never directly on top of the cells.

To evaluate the phenotype of the isolated cells, further characterization was performed by analyzing specific markers from PT and also markers from others segments of the nephron through morphological identification, RT-PCR, immunofluorescence, immunocytochemistry, cytochemical staining, FACS, functional assays and transporters assays. After this exhaustive analysis, we observed that the hPTPC retained the epithelial morphology and a reasonable doubling time till passage 3. Some scientific publications have reported the maintenance of primary PT cells from human, at least, till passage 7 [33, 52, 61]. The problem of these reported work was that they did not show cell morphology pictures along passages, so it hindered us the comparison with the morphology of hPTPC at passage 4. Similarly, they did not also measure the presence of cells from other segments of the nephron, making impossible to evaluate the purity of their isolated cell populations.

Based on cell morphology, we decided to perform the characterization of these cells till passage 3, although in the RT-PCR there are data until cell passage 4. The analysis of the results confirmed sustained expression of PT putative markers. However, expression of NCC, NKCC2 and CB-28 confirmed the presence of other segments of the nephron, DT, TAL and DT, respectively. The expression of α SMA, indicated the presence of

myofibroblasts, although α SMA expression was present in the starting material of the isolation protocol. The published literature about α SMA expression in PT cells describes that the appearance of myofibroblasts is a normal response to kidney injury [62-64]. Here, it is important to remember that our hPTPC were isolated from human nephrectomies and consequently, the expression of α SMA might be reflected in the cell culture described here as a response of hPTPC to organ disruption and artificial *in vitro* conditions [65, 66]. The expression of other specific markers for other segments of the nephron indicated that the hPTPC cell culture was heterogeneous. When I compared the results of the analyzed markers in hPTPC with other publications using human proximal tubular primary cells, I detected a problem: The other publications only analyze specific markers for PT, and usually, they have expression of the analyzed markers [33, 52, 54, 67-70]. This type of analysis can induce to a big mistake since researchers affirm they have pure PT cell culture, however, they did not analyze other segments from the nephron, as we did it.

The intensity of the GMNA staining was variable, with areas of intense reddish-brown staining by the side of other areas with less intensity, or absent staining. The area without staining was probably constituted by cells from another segment of the nephron different from the PT. The area with different intensities can be explained as a consequence of cell aging. Assays based on GGT1 enzymatic activity were performed 7 and 14 days after seeding showing very different levels of GGT1 expression. Considering this, we concluded that the cells cultured for longer periods of time have higher staining intensity.

In FACS analysis, we used three specific PT epithelial cell surface markers CD10, CD13 and CD26. Previous studies demonstrated that the

cell populations that express double positive for CD10/CD13 or just CD26 were a pure population of PT cells [28, 52]. Based on these studies, a cell sorting for the triple positive cells were performed. However, the markers not specific of PT cells remained positive by RT-PCR. Different explanations can be suggested for the obtained results: the gating for the FACS analysis was not very well adjusted, and it introduced cells from other segments of the nephron; a partial process of transdifferentiation was presented in the hPTPC, so even using the specific PT markers, the presence of markers from others segment of the nephron were expressed.

The fluorescent-based assays to study transporter activity were easy to handle, and the data obtained with these assays were fast and reproducible. We tested the influx of different substrates (ASP+ and fluorescein) in hPTPC demonstrating an increase in the fluorescence intensity that was concentration-dependent. These data suggested the presence of OCT-2 and OAT1 [39, 71]. Also, we tested the efflux of different substrates (Calcein-AM and fluorescein) in the presence of several known inhibitors (KO143, MK571, and PSC833). Our efflux data showed that the substrates were not specific just for one transporter [39] because calcein-AM efflux depends on P-gp and MRP and fluorescein efflux depends on BCRP and MRP. However, the partial inhibition obtained with the use of the inhibitors let us study transporters activity, confirming the presence of BCRP, MRP and P-gp in hPTPC.

Currently, all the knowledge we have about the mentioned transporters was obtained by using cellular models with the overexpression of transporters or vesicles derived from such cell lines [72-74]. The study of these transporters should be similar to what we find in physiological situations, however, they do not express all the individual

transporters [75, 76]. Due to this problem, the search for new cellular models keeps going [39, 40, 77], since they constitute an indispensable tool to study transport systems of the proximal tubule, including absorption, disposition and detoxification of drugs in a more physiological way. A very well characterized cell line of human proximal tubular origin is ciPTEC. This cell line has been thoroughly described, and they express the majority of the described transporter [39, 77]. These characteristics have made these cells one of the best *in vitro* cell line model to study PT function. Considering this, our human proximal tubular primary cells, hPTPC, constitute an improved model, since they expressed a majority of transporters simultaneously.

The hPTPC isolated and used throughout this Thesis, showed many characteristics of PT, including monolayer organization, cell polarization with the expression of tight junction and primary cilia, expression of specific protein of PT, as Megalin and SGLT-2, among others. They also expressed enzymatic activity for DPPIV, as well as, GGT1. hPTPC also expressed transporter activity for OCT2, OAT1, P-gp, MRP and BCRP. The characterization of our cells confirmed the putative markers of the proximal tubule and the expression of multiple endogenous organic ion transporters mimicking renal reabsorption and excretion. However, we can confirm that hPTPC was not a 100 % pure culture with proximal tubule cells. Nevertheless, I believe that we achieved a highly-enriched cell culture with proximal tubular cells (>85%). Hence, these results constitute a powerful tool for future *in vitro* transport studies in pharmacology, physiology and also kidney bioengineering.

2.6 BIBLIOGRAPHY

[1] M. Gekle, Renal tubule albumin transport, *Annu Rev Physiol* 67 (2005) 573-94.

[2] C.D. Brown, R. Sayer, A.S. Windass, I.S. Haslam, M.E. De Broe, P.C. D'Haese, A. Verhulst, Characterisation of human tubular cell monolayers as a model of proximal tubular xenobiotic handling, *Toxicol Appl Pharmacol* 233(3) (2008) 428-38.

[3] J.B. Hook, J.H. Smith, Biochemical mechanisms of nephrotoxicity, *Transplant Proc* 17(4 Suppl 1) (1985) 41-50.

[4] G.F. Rush, J.H. Smith, J.F. Newton, J.B. Hook, Chemically induced nephrotoxicity: role of metabolic activation, *Crit Rev Toxicol* 13(2) (1984) 99-160.

[5] A.L. Trifillis, Isolation, culture and characterization of human renal proximal tubule and collecting duct cells, *Exp Nephrol* 7(5-6) (1999) 353-9.

[6] H. Toutain, J.P. Morin, Renal proximal tubule cell cultures for studying drug-induced nephrotoxicity and modulation of phenotype expression by medium components, *Ren Fail* 14(3) (1992) 371-83.

[7] A.S. Fanning, L.L. Mitic, J.M. Anderson, Transmembrane proteins in the tight junction barrier, *J Am Soc Nephrol* 10(6) (1999) 1337-45.

[8] K.J. Andersen, A.B. Maunsbach, E.I. Christensen, Biochemical and ultrastructural characterization of fluid transporting LLC-PK1 microspheres, *J Am Soc Nephrol* 9(7) (1998) 1153-68.

[9] M.J. Ryan, G. Johnson, J. Kirk, S.M. Fuerstenberg, R.A. Zager, B. Torok-Storb, HK-2: an immortalized proximal tubule epithelial cell line from normal adult human kidney, *Kidney Int* 45(1) (1994) 48-57.

[10] M.A. Venkatachalam, D.B. Jones, H.G. Rennke, D. Sandstrom, Y. Patel, Mechanism of proximal tubule brush border loss and

regeneration following mild renal ischemia, *Lab Invest* 45(4) (1981) 355-65.

[11] F.G. Russel, R. Masereeuw, R.A. van Aubel, Molecular aspects of renal anionic drug transport, *Annu Rev Physiol* 64 (2002) 563-94.

[12] H.K. Kleinman, J. Graf, Y. Iwamoto, G.T. Kitten, R.C. Ogle, M. Sasaki, Y. Yamada, G.R. Martin, L. Luckenbill-Edds, Role of basement membranes in cell differentiation, *Ann N Y Acad Sci* 513 (1987) 134-45.

[13] K.J. Pienta, B.C. Murphy, R.H. Getzenberg, D.S. Coffey, The effect of extracellular matrix interactions on morphologic transformation in vitro, *Biochem Biophys Res Commun* 179(1) (1991) 333-9.

[14] S. Terryn, F. Jouret, F. Vandenabeele, I. Smolders, M. Moreels, O. Devuyst, P. Steels, E. Van Kerkhove, A primary culture of mouse proximal tubular cells, established on collagen-coated membranes, *Am J Physiol Renal Physiol* 293(2) (2007) F476-85.

[15] D.A. Volpe, Application of method suitability for drug permeability classification, *AAPS J* 12(4) (2010) 670-8.

[16] Y. Sato, M. Terashima, N. Kagiwada, T. Tun, M. Inagaki, T. Kakuta, A. Saito, Evaluation of proliferation and functional differentiation of LLC-PK1 cells on porous polymer membranes for the development of a bioartificial renal tubule device, *Tissue Eng* 11(9-10) (2005) 1506-15.

[17] M. Ni, J.C. Teo, M.S. Ibrahim, K. Zhang, F. Tasnim, P.Y. Chow, D. Zink, J.Y. Ying, Characterization of membrane materials and membrane coatings for bioreactor units of bioartificial kidneys, *Biomaterials* 32(6) (2011) 1465-76.

[18] H. Lee, S.M. Dellatore, W.M. Miller, P.B. Messersmith, Mussel-inspired surface chemistry for multifunctional coatings, *Science* 318(5849) (2007) 426-30.

- [19] S.E. Jenkinson, G.W. Chung, E. van Loon, N.S. Bakar, A.M. Dalzell, C.D. Brown, The limitations of renal epithelial cell line HK-2 as a model of drug transporter expression and function in the proximal tubule, *Pflugers Arch* 464(6) (2012) 601-11.
- [20] R.G. Spiro, Studies on the renal glomerular basement membrane. Preparation and chemical composition, *J Biol Chem* 242(8) (1967) 1915-22.
- [21] J.O. Norgaard, A new method for the isolation of ultrastructurally preserved glomeruli, *Kidney Int* 9(3) (1976) 278-85.
- [22] J. Berman, A. Perantoni, H.M. Jackson, E. Kingsbury, Primary epithelial cell culture of adult rat kidney, enhancement of cell growth by ammonium acetate, *Exp Cell Res* 121(1) (1979) 47-54.
- [23] M.G. Cherian, Rat kidney epithelial cell culture for metal toxicity studies, *In Vitro Cell Dev Biol* 21(9) (1985) 505-8.
- [24] J.J. Gildea, H.E. McGrath, R.E. Van Sciver, D.B. Wang, R.A. Felder, Isolation, growth, and characterization of human renal epithelial cells using traditional and 3D methods, *Methods Mol Biol* 945 (2013) 329-45.
- [25] S.C. Presnell, A.T. Bruce, S.M. Wallace, S. Choudhury, C.W. Genheimer, B. Cox, K. Guthrie, E.S. Werdin, P. Tatsumi-Ficht, R.M. Ilagan, R.W. Kelley, E.A. Rivera, J.W. Ludlow, B.J. Wagner, M.J. Jayo, T.A. Bertram, Isolation, characterization, and expansion methods for defined primary renal cell populations from rodent, canine, and human normal and diseased kidneys, *Tissue Eng Part C Methods* 17(3) (2011) 261-73.
- [26] S. Kroening, E. Neubauer, B. Wullich, J. Aten, M. Goppelt-Struebe, Characterization of connective tissue growth factor expression in primary cultures of human tubular epithelial cells: modulation by hypoxia, *Am J Physiol Renal Physiol* 298(3) (2010) F796-806.

- [27] A. Verhulst, P.C. D'Haese, M.E. De Broe, Inhibitors of HMG-CoA reductase reduce receptor-mediated endocytosis in human kidney proximal tubular cells, *J Am Soc Nephrol* 15(9) (2004) 2249-57.
- [28] M.J. Helbert, S.E. Dauwe, I. Van der Biest, E.J. Nouwen, M.E. De Broe, Immunodissection of the human proximal nephron: flow sorting of S1S2S3, S1S2 and S3 proximal tubular cells, *Kidney Int* 52(2) (1997) 414-28.
- [29] P.A. Glynn, Primary culture of human proximal renal tubular epithelial cells, *Methods Mol Med* 36 (2000) 197-205.
- [30] C.J. Gottardi, M. Arpin, A.S. Fanning, D. Louvard, The junction-associated protein, zonula occludens-1, localizes to the nucleus before the maturation and during the remodeling of cell-cell contacts, *Proc Natl Acad Sci U S A* 93(20) (1996) 10779-84.
- [32] A.M. Rutenburg, H. Kim, J.W. Fischbein, J.S. Hanker, H.L. Wasserkrug, A.M. Seligman, Histochemical and ultrastructural demonstration of gamma-glutamyl transpeptidase activity, *J Histochem Cytochem* 17(8) (1969) 517-26.
- [33] C. Van der Hauwaert, G. Savary, V. Gnemmi, F. Glowacki, N. Pottier, A. Bouillez, P. Maboudou, L. Zini, X. Leroy, C. Cauffiez, M. Perrais, S. Aubert, Isolation and characterization of a primary proximal tubular epithelial cell model from human kidney by CD10/CD13 double labeling, *PLoS One* 8(6) (2013) e66750.
- [34] B.D. Uhal, X. Li, A. Xue, X. Gao, A. Abdul-Hafez, Regulation of alveolar epithelial cell survival by the ACE-2/angiotensin 1-7/Mas axis, *Am J Physiol Lung Cell Mol Physiol* 301(3) (2011) L269-74.
- [35] P. Wlodek, M. Sokolowska, O. Smolenski, L. Wlodek, The gamma-glutamyltransferase activity and non-protein sulfhydryl compounds levels in rat kidney of different age groups, *Acta Biochim Pol* 49(2) (2002) 501-7.

- [36] N. Glube, A. Giessl, U. Wolfrum, P. Langguth, Caki-1 cells represent an in vitro model system for studying the human proximal tubule epithelium, *Nephron Exp Nephrol* 107(2) (2007) e47-56.
- [37] K.M. Bircsak, C.J. Gibson, R.W. Robey, L.M. Aleksunes, Assessment of drug transporter function using fluorescent cell imaging, *Curr Protoc Toxicol* 57 (2013) Unit 23 6.
- [38] A. Mahringer, J. Delzer, G. Fricker, A fluorescence-based in vitro assay for drug interactions with breast cancer resistance protein (BCRP, ABCG2), *Eur J Pharm Biopharm* 72(3) (2009) 605-13.
- [39] P. Caetano-Pinto, M.J. Janssen, L. Gijzen, L. Verscheijden, M.J. Wilmer, R. Masereeuw, Fluorescence-Based Transport Assays Revisited in a Human Renal Proximal Tubule Cell Line, *Mol Pharm* 13(3) (2016) 933-44.
- [40] T.T. Nieskens, J.G. Peters, M.J. Schreurs, N. Smits, R. Woestenenk, K. Jansen, T.K. van der Made, M. Roring, C. Hilgendorf, M.J. Wilmer, R. Masereeuw, A Human Renal Proximal Tubule Cell Line with Stable Organic Anion Transporter 1 and 3 Expression Predictive for Antiviral-Induced Toxicity, *AAPS J* 18(2) (2016) 465-75.
- [41] F.M. van de Water, J.M. Boleij, J.G. Peters, F.G. Russel, R. Masereeuw, Characterization of P-glycoprotein and multidrug resistance proteins in rat kidney and intestinal cell lines, *Eur J Pharm Sci* 30(1) (2007) 36-44.
- [42] B.M. Denker, E. Sabath, The biology of epithelial cell tight junctions in the kidney, *J Am Soc Nephrol* 22(4) (2011) 622-5.
- [43] V. Raghavan, Y. Rbaibi, N.M. Pastor-Soler, M.D. Carattino, O.A. Weisz, Shear stress-dependent regulation of apical endocytosis in renal proximal tubule cells mediated by primary cilia, *Proc Natl Acad Sci U S A* 111(23) (2014) 8506-11.

- [44] B.S. Kwon, L.P. Gangarosa, Sr., K. Green, J.M. Hill, Kinetics of ocular herpes simplex virus shedding induced by epinephrine iontophoresis, *Invest Ophthalmol Vis Sci* 22(6) (1982) 818-21.
- [45] M.T. Zuber, D.E. Smith, G.A. Neumann, S. Goossens, J.C. Andrews-Hanna, J.W. Head, W.S. Kiefer, S.W. Asmar, A.S. Konopliv, F.G. Lemoine, I. Matsuyama, H.J. Melosh, P.J. McGovern, F. Nimmo, R.J. Phillips, S.C. Solomon, G.J. Taylor, M.M. Watkins, M.A. Wiczorek, J.G. Williams, J.C. Jansen, B.C. Johnson, J.T. Keane, E. Mazarico, K. Miljkovic, R.S. Park, J.M. Soderblom, D.N. Yuan, Gravity field of the Orientale basin from the Gravity Recovery and Interior Laboratory Mission, *Science* 354(6311) (2016) 438-441.
- [46] L. Fliedl, M. Wieser, G. Manhart, M.P. Gerstl, A. Khan, J. Grillari, R. Grillari-Voglauer, Controversial role of gamma-glutamyl transferase activity in cisplatin nephrotoxicity, *ALTEX* 31(3) (2014) 269-78.
- [47] X.Y. Zhai, R. Nielsen, H. Birn, K. Drumm, S. Mildenerberger, R. Freudinger, S.K. Moestrup, P.J. Verroust, E.I. Christensen, M. Gekle, Cubilin- and megalin-mediated uptake of albumin in cultured proximal tubule cells of opossum kidney, *Kidney Int* 58(4) (2000) 1523-33.
- [48] S. De, S. Kuwahara, A. Saito, The endocytic receptor megalin and its associated proteins in proximal tubule epithelial cells, *Membranes (Basel)* 4(3) (2014) 333-55.
- [49] C. Hemmingsen, Regulation of renal calbindin-D28K, *Pharmacol Toxicol* 87 Suppl 3 (2000) 5-30.
- [50] A. Sebe, S.K. Leivonen, A. Fintha, A. Masszi, L. Rosivall, V.M. Kahari, I. Mucsi, Transforming growth factor-beta-induced alpha-smooth muscle cell actin expression in renal proximal tubular cells is regulated by p38beta mitogen-activated protein kinase, extracellular signal-regulated protein kinase1,2 and the Smad signalling during epithelial-myofibroblast transdifferentiation, *Nephrol Dial Transplant* 23(5) (2008) 1537-45.

[51] G. Litscher, R.C. Niemtow, L. Wang, X. Gao, C.H. Urak, Electrodermal mapping of an acupuncture point and a non-acupuncture point, *J Altern Complement Med* 17(9) (2011) 781-2.

[52] P.C. Baer, W.A. Nockher, W. Haase, J.E. Scherberich, Isolation of proximal and distal tubule cells from human kidney by immunomagnetic separation. Technical note, *Kidney Int* 52(5) (1997) 1321-31.

[53] C.C. Sharpe, M.E. Dockrell, Primary culture of human renal proximal tubule epithelial cells and interstitial fibroblasts, *Methods Mol Biol* 806 (2012) 175-85.

[54] D.A. Vesey, W. Qi, X. Chen, C.A. Pollock, D.W. Johnson, Isolation and primary culture of human proximal tubule cells, *Methods Mol Biol* 466 (2009) 19-24.

[55] P. Salmon, Generation of human cell lines using lentiviral-mediated genetic engineering, *Methods Mol Biol* 945 (2013) 417-48.

[56] K.J. Jang, A.P. Mehr, G.A. Hamilton, L.A. McPartlin, S. Chung, K.Y. Suh, D.E. Ingber, Human kidney proximal tubule-on-a-chip for drug transport and nephrotoxicity assessment, *Integr Biol (Camb)* 5(9) (2013) 1119-29.

[57] B.M. Grabias, K. Konstantopoulos, Epithelial-mesenchymal transition and fibrosis are mutually exclusive responses in shear-activated proximal tubular epithelial cells, *FASEB J* 26(10) (2012) 4131-41.

[58] Z.Y. Oo, R. Deng, M. Hu, M. Ni, K. Kandasamy, M.S. bin Ibrahim, J.Y. Ying, D. Zink, The performance of primary human renal cells in hollow fiber bioreactors for bioartificial kidneys, *Biomaterials* 32(34) (2011) 8806-15.

[59] K.L. Price, S.A. Hulton, W.G. van't Hoff, J.R. Masters, G. Rumsby, Primary cultures of renal proximal tubule cells derived from

individuals with primary hyperoxaluria, *Urol Res* 37(3) (2009) 127-32.

[60] M. Wieser, G. Stadler, P. Jennings, B. Streubel, W. Pfaller, P. Ambros, C. Riedl, H. Katinger, J. Grillari, R. Grillari-Voglauer, hTERT alone immortalizes epithelial cells of renal proximal tubules without changing their functional characteristics, *Am J Physiol Renal Physiol* 295(5) (2008) F1365-75.

[61] C.J. Detrisac, M.A. Sens, A.J. Garvin, S.S. Spicer, D.A. Sens, Tissue culture of human kidney epithelial cells of proximal tubule origin, *Kidney Int* 25(2) (1984) 383-90.

[62] S. Ishibe, L.G. Cantley, Epithelial-mesenchymal-epithelial cycling in kidney repair, *Curr Opin Nephrol Hypertens* 17(4) (2008) 379-85.

[63] H. Zhang, S.F. Lau, B.F. Heng, P.Y. Teo, P.K. Alahakoon, M. Ni, F. Tasnim, J.Y. Ying, D. Zink, Generation of easily accessible human kidney tubules on two-dimensional surfaces in vitro, *J Cell Mol Med* 15(6) (2011) 1287-98.

[64] C. Badid, N. Mounier, A.M. Costa, A. Desmouliere, Role of myofibroblasts during normal tissue repair and excessive scarring: interest of their assessment in nephropathies, *Histol Histopathol* 15(1) (2000) 269-80.

[65] J. Yang, Y. Liu, Dissection of key events in tubular epithelial to myofibroblast transition and its implications in renal interstitial fibrosis, *Am J Pathol* 159(4) (2001) 1465-75.

[66] J. Slyne, C. Slattery, T. McMorrow, M.P. Ryan, New developments concerning the proximal tubule in diabetic nephropathy: in vitro models and mechanisms, *Nephrol Dial Transplant* 30 Suppl 4 (2015) iv60-7.

[67] B.S. Cummings, J.M. Lasker, L.H. Lash, Expression of glutathione-dependent enzymes and cytochrome P450s in freshly

isolated and primary cultures of proximal tubular cells from human kidney, *J Pharmacol Exp Ther* 293(2) (2000) 677-85.

[68] A.L. Trifillis, A.L. Regec, B.F. Trump, Isolation, culture and characterization of human renal tubular cells, *J Urol* 133(2) (1985) 324-9.

[69] C. van Kooten, S. Lam, M.R. Daha, Isolation, culture, characterization and use of human renal tubular epithelial cells, *J Nephrol* 14(3) (2001) 204-10.

[70] I. Van der Biest, E.J. Nouwen, S.A. Van Dromme, M.E. De Broe, Characterization of pure proximal and heterogeneous distal human tubular cells in culture, *Kidney Int* 45(1) (1994) 85-94.

[71] J. Jansen, M. Fedecostante, M.J. Wilmer, J.G. Peters, U.M. Kreuser, P.H. van den Broek, R.A. Mensink, T.J. Boltje, D. Stamatialis, J.F. Wetzels, L.P. van den Heuvel, J.G. Hoenderop, R. Masereeuw, Bioengineered kidney tubules efficiently excrete uremic toxins, *Sci Rep* 6 (2016) 26715.

[72] J.E. Karlsson, C. Heddle, A. Rozkov, J. Rotticci-Mulder, O. Tuveson, C. Hilgendorf, T.B. Andersson, High-activity p-glycoprotein, multidrug resistance protein 2, and breast cancer resistance protein membrane vesicles prepared from transiently transfected human embryonic kidney 293-epstein-barr virus nuclear antigen cells, *Drug Metab Dispos* 38(4) (2010) 705-14.

[73] A.A. El-Sheikh, R. Greupink, H.M. Wortelboer, J.J. van den Heuvel, M. Schreurs, J.B. Koenderink, R. Masereeuw, F.G. Russel, Interaction of immunosuppressive drugs with human organic anion transporter (OAT) 1 and OAT3, and multidrug resistance-associated protein (MRP) 2 and MRP4, *Transl Res* 162(6) (2013) 398-409.

[74] H.G. Wittgen, J.J. van den Heuvel, P.H. van den Broek, H. Dinter-Heidorn, J.B. Koenderink, F.G. Russel, Cannabinoid type 1 receptor antagonists modulate transport activity of multidrug resistance-associated proteins MRP1, MRP2, MRP3, and MRP4, *Drug Metab Dispos* 39(7) (2011) 1294-302.

[75] D. Gartzke, G. Fricker, Establishment of optimized MDCK cell lines for reliable efflux transport studies, *J Pharm Sci* 103(4) (2014) 1298-304.

[76] J. König, F. Müller, M.F. Fromm, Transporters and drug-drug interactions: important determinants of drug disposition and effects, *Pharmacol Rev* 65(3) (2013) 944-66.

[77] M.J. Wilmer, M.A. Saleem, R. Masereeuw, L. Ni, T.J. van der Velden, F.G. Russel, P.W. Mathieson, L.A. Monnens, L.P. van den Heuvel, E.N. Levtchenko, Novel conditionally immortalized human proximal tubule cell line expressing functional influx and efflux transporters, *Cell Tissue Res* 339(2) (2010) 449-57.



CHAPTER

3

Generation and
validation of a new
nephrotoxicity
model based in the
use of cisplatin in
hPTPC

3.1 INTRODUCTION

Cisplatin (also known as CDDP)[1] is a chemotherapeutic tetracoordinated drug based on platinum, and it is widely used against solid tumors [2] including head and neck, lung, testis ovary and breast cancers [3]. Regarding its history, cisplatin was described by Michael Peyrone in 1845 and 115 years later, in 1960, the group headed by Barnett Rosenberg discovered its antitumoral potential [4]. The first time that cisplatin was approved for clinical use was in 1978 in the US [5] after the studies carried out by Hill's group to demonstrate its clinical efficacy [6]. The mechanism of action of cisplatin works through the formation of DNA adducts. This formation leads the interference with DNA synthesis, and at the same time, it produces the cell death during cell division [7].

As many other anticancer drugs, cisplatin is highly active and toxic for proliferating cells [8]. Side effects associated with the treatment with cisplatin include nephrotoxicity, ototoxicity, neurotoxicity, among others. However, it is necessary to highlight that the major dose-limiting factor is renal toxicity, affecting around 25-35% of patients after a single dose treatment [3], as a consequence of an increase in the glomerular filtration. Therefore, the treatments must often be stopped [9]. To reduce the nephrotoxicity and allow a dose escalation therapeutic level, hydration protocols were developed and implemented in the treated patients [10]. However, these prevention protocols were not effective. This side effect limits cisplatin use in cancer therapy [11], and consequently, only 60% of patients complete three of four cisplatin cycles. In the kidney, particularly the proximal tubule, accumulates high amounts of cisplatin compared to other organs [12]. A study carried out

by Kulmann *et al.* [13], showed that the cisplatin concentration in proximal tubular cells is about 5 times the serum concentration. Therefore, this accumulation contributes to the nephrotoxicity.

The mechanisms by which cisplatin kills PT cells have been investigated for many years. Although PT cells do not proliferate under normal conditions, these cells present properties that make them particularly exposed to cisplatin toxicity: PT cells are involved in the blood clearance mechanism and reabsorption of essential metabolites. This segment of the nephron is where the majority of toxins and drugs are processed and here is where acute and chronic renal damage take places [14, 15]. It is also remarkable, the pharmacological activation of cisplatin in PT cells since it is bioactivated into a more potent metabolite [16, 17].

So, these two reasons underlie the susceptibility to cisplatin of quiescent PT cells. The uptake of cisplatin takes place via organic cation transporter 2 (OCT2), and also via copper transporter 1 (CTR1) [1, 18, 19], both transporters expressed on the basolateral side of PT cells [18, 20]. Once cisplatin is into the cells, it binds to DNA, or the cisplatin forms glutathione-conjugates by GSH-transferase [21, 22]. The dissociation of one of the chlorines from the cisplatin molecule results in a positive charge on the platinum that will attract the negatively charged sulfur on the cysteine moiety of the glutathione molecule. This process form the platinum-glutathione (GSH) conjugates [23, 24] reducing the amount of platinum available to bind to DNA and protecting dividing cells from cisplatin toxicity. The platinum-glutathione (GSH) conjugate is transported to the PT lumen via MATE1 and MRP2, respectively [25, 26]) and it is here where extracellular biotransformation occurs [17]

dependent on these steps: [21-24]The platinum-GSH conjugates are cleaved into platinum-cysteinyl-glycine-conjugates by the enzyme GGT1 [17, 27]. Next, platinum-cysteinyl-glycine-conjugates are metabolized into platinum-cysteine-conjugates by DPPIV. So far, the described processes take place extracellularly. The platinum-cysteinyl-glycine-conjugates can be transported back into the cells, although the mechanisms for this reabsorption are not well-known. Observations in carcinoma cells showed that neutral amino acid transporter complexes might mediate the influx [28]. However, additional studies are needed to identify carrier involved in PT cells. Once the platinum-cysteinyl-glycine-conjugates is transported into the cells, it is converted into reactive platinum-thiols by cysteine-S-conjugate beta-lyase [17]. The cisplatin-induced nephrotoxicity includes the activation of multiple pathways, including p53-mediated responses and the intrinsic and extrinsic apoptosis pathways, the responses to oxidative stress and ER stress and lysosomal toxicity [12, 29] (Figure 3.1).

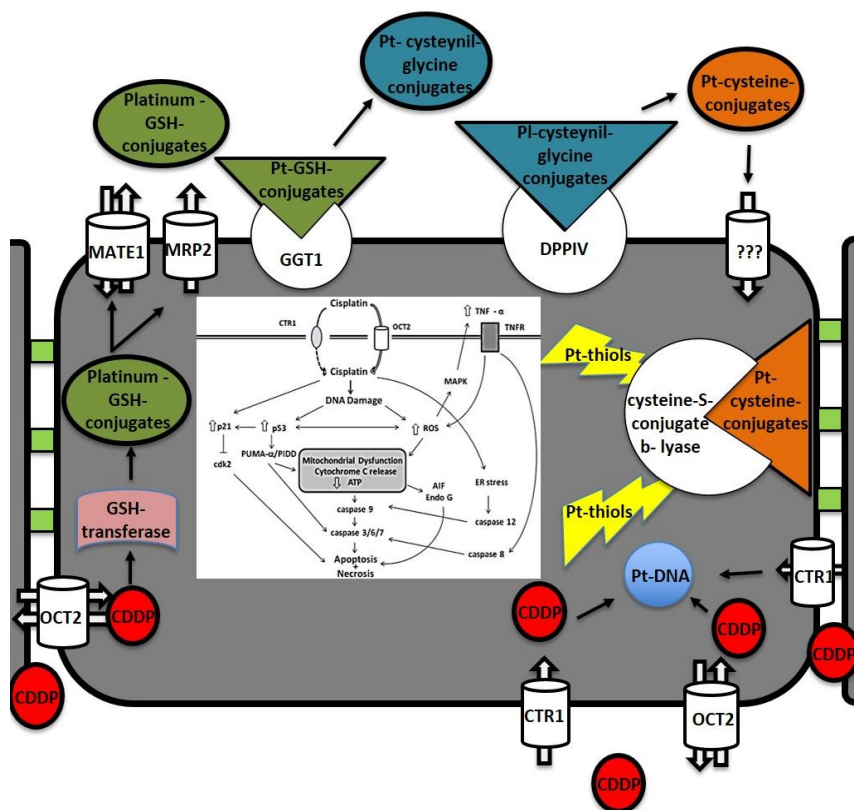


Figure 3.1: Role of cisplatin in hPTPC. The image represents the principal transporters implied in the uptake of cisplatin, as well as the routes followed to get the conversion of cisplatin into a more toxic molecule. In the middle of the picture, there is a diagram of activation (adapted from Miller, R.P. *et al.*[3]) of the nephrotoxicity induced by cisplatin and mediated by multiple pathways.

3.2 OBJECTIVES

The Specific Aims worked out in this chapter were:

1. Development of methods and procedures for the isolation and cell culture of human primary proximal tubular cells (hPTPC).
2. Phenotypic characterization of cells obtained from the primary culture at the level of gene expression, protein markers, enzymatic activity in living cells and transporters.
- 3. Development and validation of a new nephrotoxicity model using cisplatin for the study of cell viability and expression of specific markers implied in the bioactivation of this molecule.**
- 4. Screening of molecules potentially repaired of the damage produced by the cisplatin.**
5. Development of the protocol for differentiated proximal tubular cell cultures in a device that allows us the application of Shear Stress (SS).
6. Determination of the SS effect in the sensibility to cisplatin in hPTPC.

3.3 MATERIAL AND METHODS

3.3.1 Cell culture

The hPTPC were the cells used for all the experiments, derived from human nephrectomies and characterized as a cell line enriched with PT cells (see chapter 2.). Cells were cultured in MCR medium. hPTPC cytotoxicity assays were performed with cells seeded at a density of 8.000 cells per cm² in 96 wells plates (TPP, 92096) and cultured during 7 days until reaching the confluence, at 37 °C in a 5% CO₂ atmosphere. One row of the 96 wells plate was left empty and used to measure controls and standards (Figure 3.2, Row A).

3.3.2 Experimental design

7 days after the seeding, the hPTPC were exposed to different concentrations of cisplatin (1 concentration per row; Rows C-H, Figure 3.2) during 8 hours. Cells without cisplatin exposure were used as control (Row A, Figure 3.2). After the treatment time, MCR medium containing cisplatin was replaced by fresh MCR medium and cells were kept in the incubator at 37 °C in a 5% CO₂ atmosphere, during 40 h, before the effects of cisplatin were evaluated by determining the GGT1 enzymatic activity, the cell viability and the total amount of proteins.

3.3.3 Cisplatin exposure

For this aim, a stock solution of 3.33 mM of cisplatin (Sigma, P4394) dissolved in a NaCl solution 140 mM was prepared. The working concentrations were 300, 100, 50, 30, 15, and 5 µM. The higher concentration of cisplatin, 300 µM, was prepared in MCR culture medium from the stock solution, and the other concentrations were serially diluted in culture medium from the higher concentration.

Each row of the 96 wells plate was exposed to a 100 μ L of a different cisplatin concentration during 8 hours in the incubator.

3.3.4 Small molecules treatment.

The small molecules tested were Cimetidine, Genistein and β -Lapachone. The organic cation transporter OCT2 contributes to cisplatin uptake in renal tubular cells [18]. Cimetidine, a pharmacological inhibitor of OCT2, has been reported to reduce cisplatin uptake in cultured renal tubular cells [1, 18]. Genistein is a nonsteroidal isoflavonoid with estrogen-like activity. Previous studies have shown that genistein regulates genes that are related in controlling cell proliferation, cell cycle, apoptosis [30] and also, genistein has antioxidant effect. This antioxidant effect may counteract the effect of ROS generated by cisplatin [31]. β -Lapachone is a quinone that modulates (increasing) the NAD metabolism. This was correlated with an increased SIRT1 enzymatic activity that ameliorated cisplatin nephrotoxicity and nutrient, metabolic and redox state of the cell [32].

For small molecules treatment, the 96 wells plate was divided into four parts, once the cells reached the confluence (Figure 2.29). Each part was constituted for three columns of the plate and a different treatment: cisplatin, cisplatin + cimetidine (Sigma, C-4522), cisplatin + genistein (Sigma, G8649) and cisplatin + β -Lapachone (Sigma, L2037). The chosen concentrations to test the small molecules were: 10 or 100 μ M for Cimetidine and Genistein and 0.1 or 1 μ M for β -Lapachone. Cells located in the division of the plate to be treated with the small molecules were pretreated with them for 1 hour. After this treatment, cells were incubated in the presence of small molecules and cisplatin or

just cisplatin for 8 hours. The wells incubated only with cisplatin contained the maximum volume of the vehicle used to dissolve the small molecules (Figure .3.2).

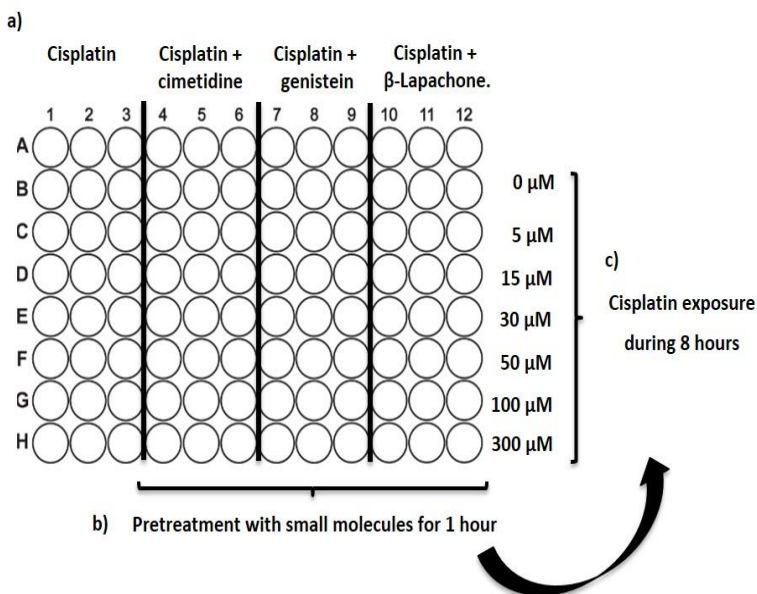


Figure 3.2: Experimental design for the treatment with small molecules in hPTPC.

3.3.5 Assays to evaluate the effects of cisplatin in hPTPC

3.3.5.1 Cell viability assay

PrestoBlue reagent is a resazurin-based solution that functions as a cell viability indicator by using the reducing power of living cells. The PrestoBlue reagent contains a cell-permeant compound that is blue in color and virtually nonfluorescent. When added to cells, the PrestoBlue reagent resazurin is modified to resafurin by the reducing environment of the viable cell and turns red in color and becomes highly fluorescent.

Cells were washed with HBSS buffer (Lonza, BE10-527F) to remove the cell culture medium. The assay solution was prepared containing:

1/10 PrestoBlue reagent (TermoFisher Scientific, A13262) in 1 mL DMEM (Lonza, BE12-917F). Cells were incubated in a plate reader (BioTek, Synergy HT) at 37°C for 1 h, taking measures every 20 minutes. The formation of resafurin was monitored (ex.530 nm / emm.590 nm). The PrestoBlue working solution was added to three wells without cells and incubated under the same conditions to determine and later subtract the background

The kinetics for cisplatin cytotoxicity were analyzed using GraphPad (GraphPad Software, San Diego, CA, USA). A non-linear regression analysis of dose-dependent inhibition was applied to calculate the IC50 for each independent experiment. Data were represented as mean \pm SD.

3.3.5.2 GGT1 functional assay.

GGT1 enzyme activity in cultured hPTPC was analyzed by measuring the enzymatic conversion of the substrate gamma glutamyl-p-nitroanilide (GGpN) in the presence of glycyl glycine, a glutamyl acceptor. The liberated reaction product, p-nitroaniline, is a yellow-colored compound whose rate of formation is determined optically as the measure of the gamma-glutamyl transferase (GGT1) [33].

To perform this assay, cells were washed with HBSS buffer to remove the cell culture medium. The assay solution was prepared containing: 2 mM γ -glutamyl-p-nitroanilide (Sigma, G6133) + 50 mM glycylglycine (Sigma, G3915) in 1 mL DMEM. Cells were incubated in a plate reader at 37°C during 1 h. The resulting product, p-nitroaniline, is directly proportional to the enzyme activity present in the sample. The activity was measured at 410 nm using a microplate reader and the measures were taken every 20 minutes during an hour. Three wells without cells were incubated with the assay solution mentioned before to subtract

the background of the assay. The final result was represented as intensity absorbance at 410 nm and enzyme activity per culture area (see Page 92, Chapter 2 for details).

3.3.5.3 BCA Protein Assay Kit

After the determination of GGT1 enzymatic activity and cell viability, total protein amount per well was determined by using the BCA method. This assay was essential in the evaluation of the effects produced by cisplatin because it helped to normalized the previous performed assays, letting know in a very precise way, the enzymatic activity and the cell viability per well, based on the protein concentration.

This method of protein quantification is based on bicinchoninic acid (BCA) reaction, combining the well-known reduction of Cu^{+2} to Cu^{+1} by protein in an alkaline medium with the highly sensitive and selective colorimetric detection of the cuprous cation. For this goal, cells were washed with HBSS, lysed with 25 μL /well with lysis buffer containing cComplete mini 7x (Roche, 04693124001), APS 5x (Sigma, 09913), Triton X100 2% (Sigma, X100) and H_2O MiliQ and incubated at RT during 20 minutes with agitation. A BSA protein standard curve was performed to determine the protein concentration present in the wells, adding 25 μL /well of each BSA concentration and using duplicates. 200 μL /well of the working reaction were added by mixing 50 parts of BCA (Life Technology, 23225) reagent A (sodium carbonate, sodium bicarbonate, bicinchoninic acid and sodium tartrate in 0.1M sodium hydroxide) with 1 part of BCA reagent B (4% cupric sulfite) (50:1, Reagent A: B) and it was incubated at 37°C during 30 minutes. The results were measured in a plate reader at 562 nm absorbance.

3.3.5.4 Crystal Violet

The Crystal Violet assay was based on the method of Saotome *et al.* [34] Crystal violet is a dye able to stain the DNA of cells. It is a very useful method to observe the number of cells per plate, after cisplatin treatment, using a microscope. Then, it can be dissolved in acid to obtain a very good estimate of the total number of cells in each well. After the cisplatin exposure, cells were washed with PBS buffer, fixed with 4 % Paraformaldehyde during 15 minutes at RT and then washed with PBS to eliminate the rest of the fixative. After that, cells were stained with 0.1% crystal violet solution (Sigma, C0775) in PBS buffer for 30 minutes at RT. After the incubation, the excess of dye was removed by extensive washing with tap water. Pictures were taken using an inverted microscope. For quantitative measurements, formed crystals were dissolved by using 10% acetic acid, and the crystal violet concentration was measured using a plate reader at 590 nm absorbance.

Next, Figure 3.3 shows a representation of the used methods explained in this section.

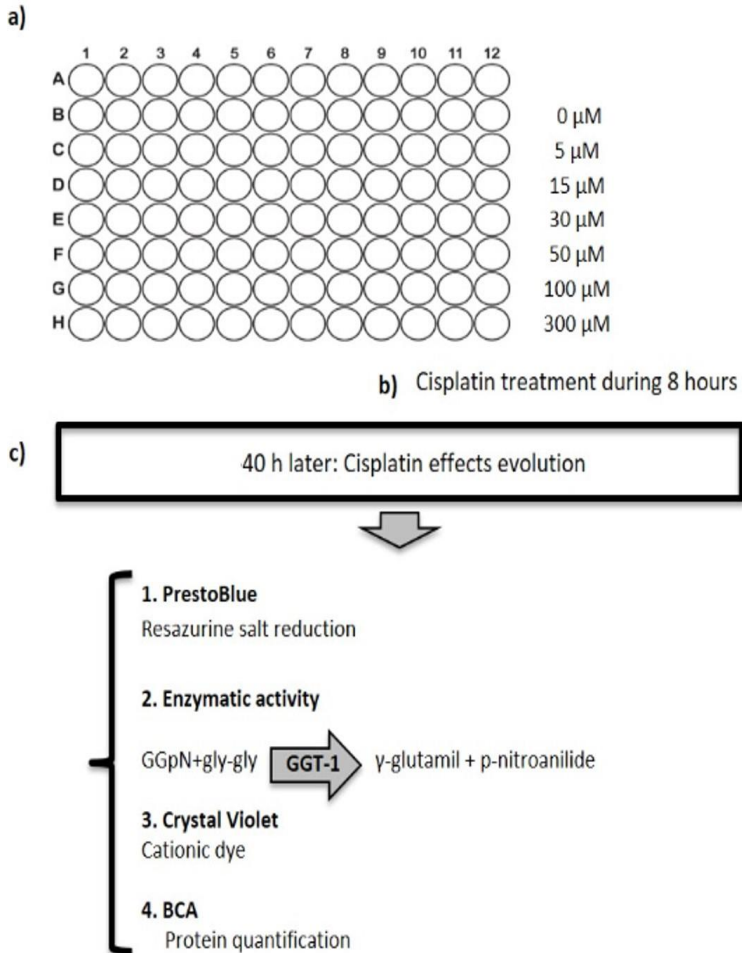


Figure 3.3: Schematic representation of the methods. a) Cells are seeded in a 96 wells plate b) Once the cells reached the confluence are exposed to different cisplatin concentration during 8h. c) 40 h after cisplatin treatment was evaluated the effects of this nephrotoxic by using different assays.

3.3.5.5 Gamma Glutamyl Transpeptidase (GGT1) cytochemical staining

This assay let us to visualize the GGT activity obtained through the reaction between a diazonium salt and the naphthylamine released by

hydrolysis of a synthetic GGT substrate, γ -glutamyl-4-methoxy-2-naphthylamide (GMNA).

Cells were fixed for 10 minutes with ice-cold methanol (Fisher Sci. M/3950/21) and ice-cold acetone (Sigma, 90872) (1:1) and washed with 0.85% NaCl (Saline solution). Then, cells were incubated with the working solution (Table 3.1) for 20 minutes in the dark and again, they were washed with saline solution. To stop the reaction, cells were incubated with a 0.1 M solution of cupric sulfate (Sigma, C1297) for 2 minutes and then, washed with a saline solution [35]. The pictures were taken using an inverted microscope (Olympus IX81).

Table 3.1: Working substrate solution for a volume of 5 mL

Substrate solutions*	Working concentration	Volume
GMNA solution 2.5 mg/mL (SC, 215216)	0,25 mM	0,25 mL
Tris buffer, pH 7.4	0.1 M	1,25 mL
NaCl (Saline solution)	0.85%	3,5 mL
Glycylglycine (Sigma, G3915)	3,78 mM	2,5 mg
Fast blue salt hemi zinc chloride (Sigma, F3378)	1,20 mM	2,5 mg

**The substrate solution was filtered through a Whatman N^o. 1 filter paper just prior to use to remove any insoluble aggregates of the substrate.*

3.4 RESULTS

3.4.1 96 wells plate nephrotoxicity model

3.4.1.1 Cisplatin causes dose-dependent cell death in hPTPC

Confluent monolayers of hPTPC cells were incubated with cisplatin (0, 5, 15, 30, 50, 100 and 300 μM) during 8 h. After the incubation, cisplatin was removed and fresh MCR medium was added to the cells. Cell morphology and survival was checked 40 hours after the cisplatin treatment under an inverted microscope (Olympus IX81). All the different cisplatin concentrations were compared with the control. 40 hours after the cisplatin treatment, the cell morphology at 5 and 30 μM was not very different compared to the control. However, cell survival was relatively lower as concentration increased (Figure 3.4). At 50 μM , 100 μM and 300 μM , the cell morphology and cell survival changed drastically compared to the control: cells showed a rounding shape with the cytoplasm full of granules and cells were detached from the cell culture plate. These observations increased in a concentration-dependent way.

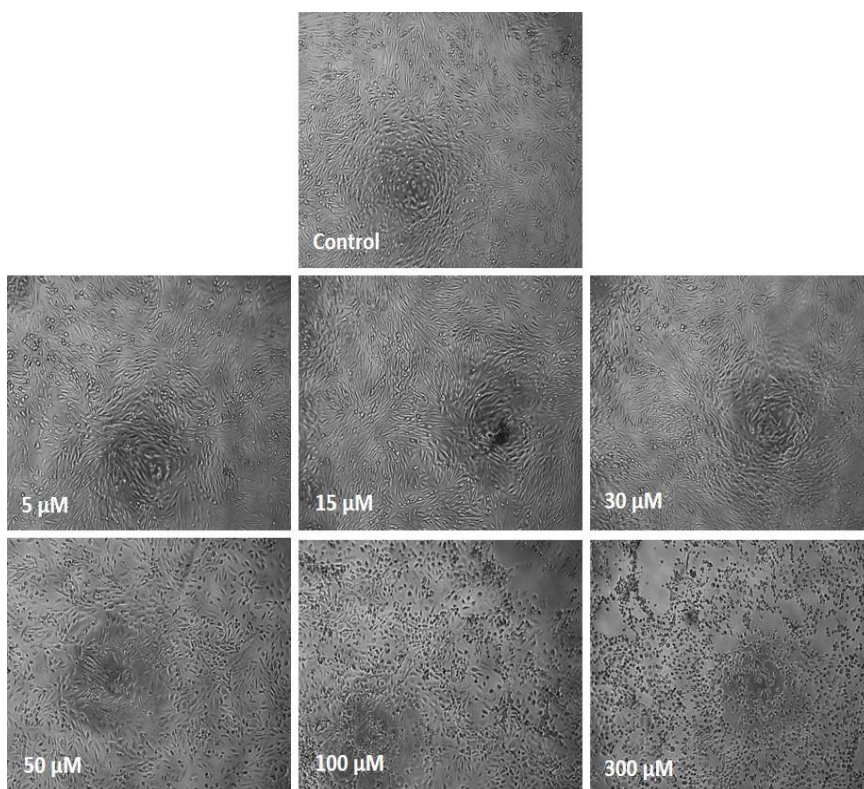


Figure 3.4: Cell morphology and survival: 40 hours after cisplatin treatment, cells exposed to different concentrations of cisplatin were compared to the control. Morphological and survival changes were clearly visible from 50 μM of cisplatin.

After the cisplatin treatment, we performed the crystal violet assay. The formed crystals were not solubilized, and it allowed us to visualize with the microscope the nuclear stain of the cells presents per wells treated with a different cisplatin concentration. These images let us estimate the cell number per well, showing a high nuclear stain in control cells compared to the cells treated with 300 μM cisplatin, where the number of cells (identified by its stained nuclei) is really low (Figure 3.5).

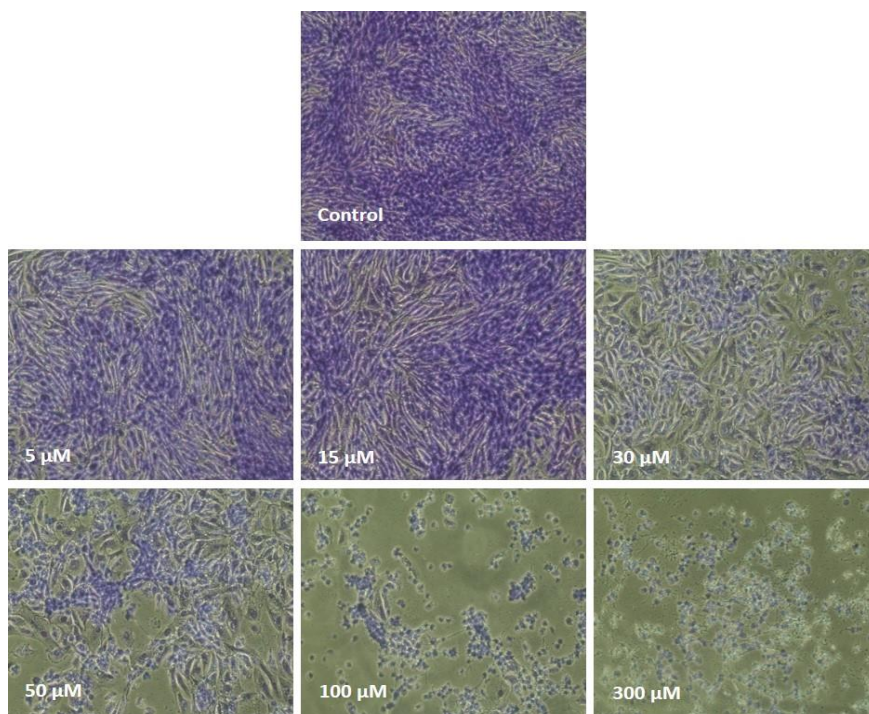


Figure 3.5: Crystal Violet assay after cisplatin exposure. Images were taken under an inverted microscope.

3.4.1.2 GGT1 activity and cell viability in hPTPC exposed to cisplatin

The cytotoxic effects caused by the cisplatin treatment in hPTPC were evaluated through the combination of three optical assays: GGT1 enzymatic activity, PrestoBlue cell viability, and BCA. These assays based on optical measurements will let us work with microfluidic devices (Chapter 4), where the number of cells is very limited, so the use of optical assays is useful to obtain results.

The GGT1 enzymatic activity was expressed in the graphs as the result of the normalized absorbance, and it was also expressed as mmol p-nitroaniline/h/cm². PrestoBlue Cell viability assay was expressed as normalized fluorescence, and BCA protein content per well was

expressed as normalized mg/mL protein (Figure 3.6). The graphs of Figure 3.6 showed that the cytotoxic effects caused by the cisplatin treatment in hPTPC are dose-dependent, consistent with the previous results observed under the microscope. The GGT1 enzymatic activity was maintained without changes compared with control cells until 15 μM , however, from 30 μM the enzymatic activity suffered a reduction. The graphs for the evaluation of cell viability and protein concentration showed a similar behavior: a reduction in the normalized fluorescence for PB and also, in the normalized absorbance for BCA was observed from 5 μM of cisplatin.

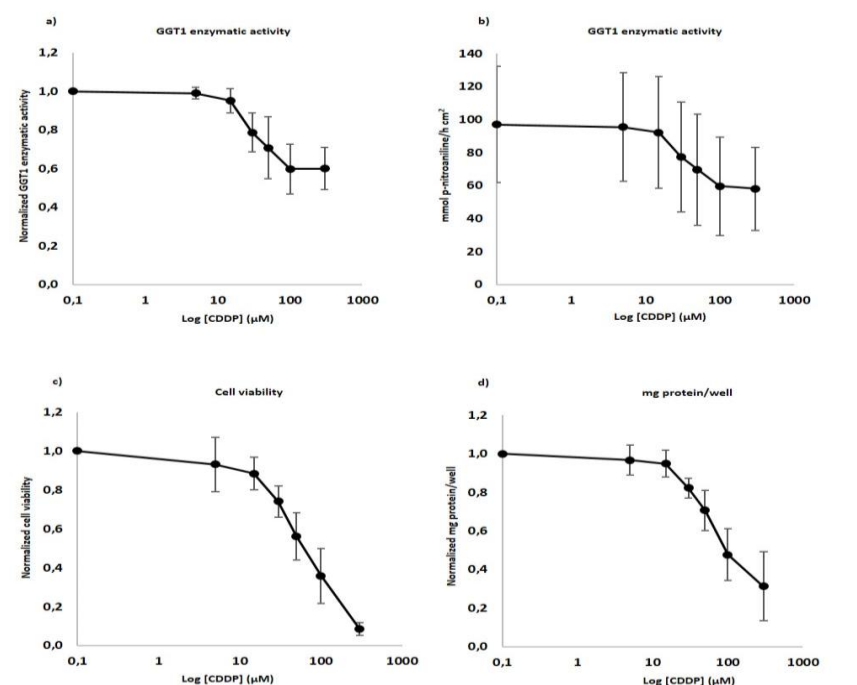


Figure 3.6: Evaluation of the cisplatin effects. a) GGT1 enzymatic activity b) mmol p-nitroaniline/h/cm². Both graphs showed a decrease in the dose response curve from the concentration 30 μM of cisplatin. c) PrestoBlue assay. d) BCA protein assay kit. The dose response curves for PrestoBlue and BCA showed a decrease from the concentration 5 μM of cisplatin. The results were expressed as mean \pm SD of three separate experiments performed with 6 repetitions.

To calculate the drug potency, the EC50 value was calculated. EC50 let us know determine the concentration of cisplatin inducing 50% of the effect observed at the maximum cisplatin concentration. This concentration was $64 \pm 29 \mu\text{M}$ (mean \pm SD, $n=3$)

GGT1 enzymatic activity and PrestoBlue were normalized with total protein amount (BCA) using the absolute data once the background was subtracted of each assay (Figure 3.7). The normalized assays with the total protein amount revealed that GGT1 presented more relative enzymatic activity in the biggest cisplatin concentrations: 100 and 300 μM and PrestoBlue showed a concentration-dependent curve.

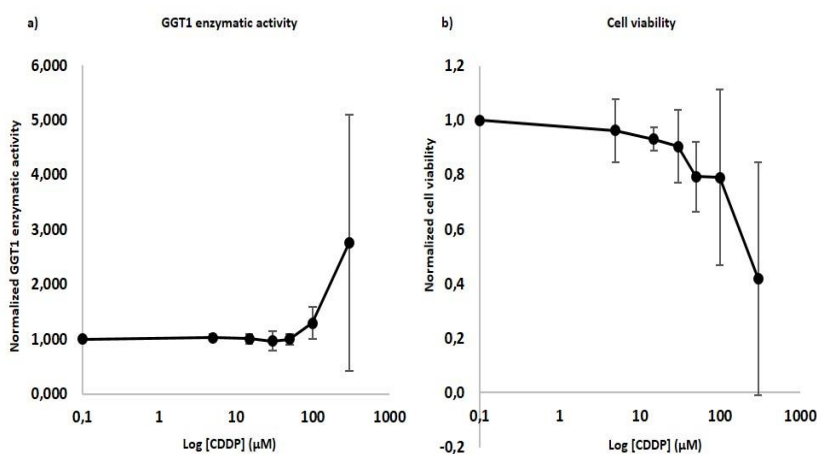


Figure 3.7: GGT1 enzymatic activity and Presto blue normalized with total protein amount (BCA). a) Normalized GGT1 enzymatic activity. b) Normalized PrestoBlue. The results were expressed as mean \pm SD of three separate experiments performed with 6 repetitions.

3.4.2 The heterogeneous increase in GGT1 activity in cisplatin-treated hPTPC cells.

GGT1 cytochemical staining was performed to confirm the phenotype of PT cells and also to determine the activity of the enzyme after cisplatin exposure. The activity was dependent on the number of cells present in each well treated with a different cisplatin concentration (Figure 3.8). The intensity of the staining was variable, with areas of intense reddish-brown staining by the side of other areas of less intensity and it can be explained as a consequence of cell aging. At 300 μM of cisplatin, the cells still attached to the well plate showed a very intense reddish brown staining evenly. This data supported the increase in the GGT1 activity normalized with BCA (Figure 3.7).

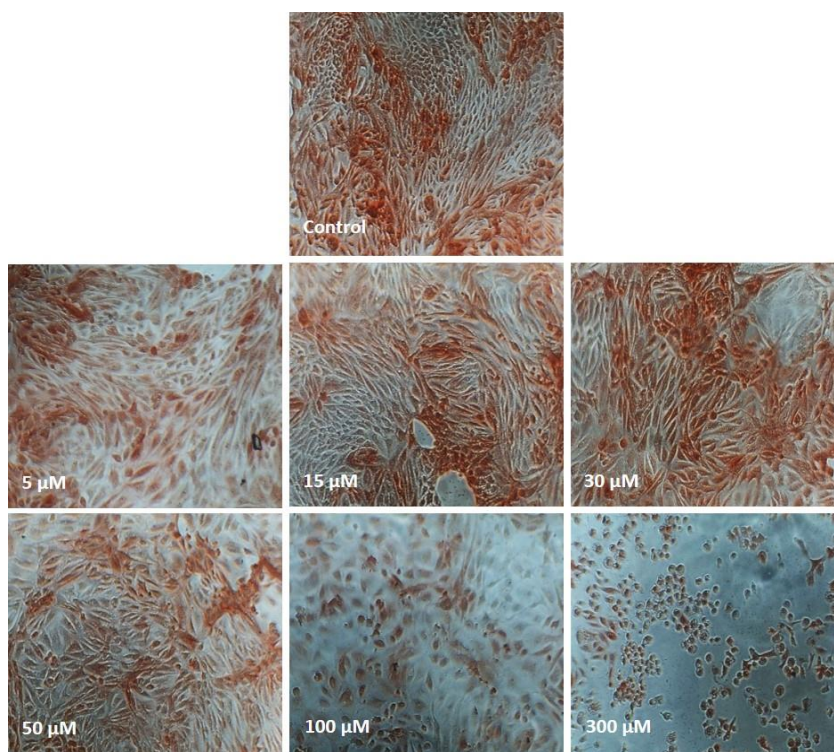


Figure 3.8: GGT1 cytochemical staining. The images show the GGT1 expression after cisplatin exposure. Auto-Regeneration capacity of the hPTPC after cisplatin treatment.

3.4.3 The effects of cisplatin in hPTPC are irreversible

The effects caused by cisplatin were analyzed through the experiments discussed so far. Usually these experiments were performed 40 hours after cisplatin exposure. However, we did not know whether the cisplatin effects to the cell viability over time and if hPTPC cells are capable of auto-regeneration after the cisplatin insult. For this aim, cells were exposed during 8 hours to different cisplatin concentrations once the confluence was reached, and every 72-96 hours PrestoBlue assay was performed. The evaluation of cell viability by using PrestoBlue reagent was very useful since it was not an end point assay, it did not affect the cells, and under sterility, the assay can be repeated with the same cells along time. The graph showed the cell viability 18 days after cisplatin exposure and the results did not show the ability of auto regeneration in hPTPC because while in the cell control, the cell viability is maintained, in cells treated with cisplatin, the cell death increases over time even at the lowest concentration used (Figure 3.9).

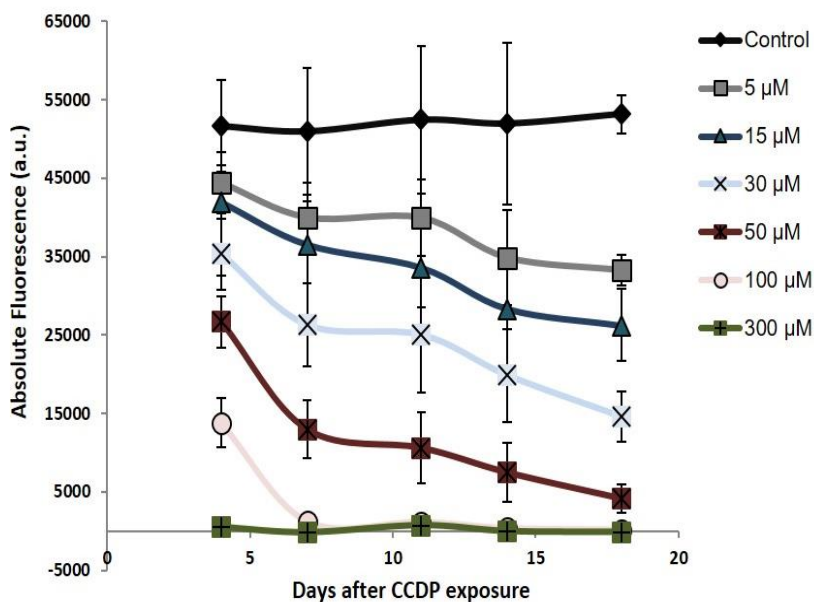


Figure 3.9: PrestoBlue assay performed every 72-96 h after cisplatin exposure. The cisplatin treatment showed a toxicity dose-dependent and time-dependent and the cells did not show auto regeneration capacity. The results were expressed as mean \pm SD.

3.4.4 Model validation: testing for small molecules with potential anti-cisplatin effects

The previous results showed that hPTPC did not possess the auto-regenerative capacity to avoid the death cell produced by cisplatin exposure. With the aim to reduce the effects caused by this molecule, cells were incubated with small molecules in the presence of Cisplatin.

Before starting to work with the small molecules, we thoroughly reviewed the literature in which these molecules have been used to establish different concentrations to use in our model. We tested 10 and 100 μ M for Cimetidine and Genistein and 0.1, 1 and 10 μ M for β -Lapachone. As we explained before, the small molecules were incubated

1 hour before to the cisplatin exposure and then, they were incubated with cisplatin during 8 hours. 40 hours after the cisplatin exposure, the effects of this nephrotoxic were firstly evaluated through the microscopic observation (Figure 3.10). Control and cimetidine cells showed the same behavior and the maximum morphological changes in this picture were observed at 100 μ M of cisplatin. Genistein and β -Lapachone also showed a similar behavior and the control cells were not observed as confluent, so it could indicate the molecules presented toxicity for the hPTPC. When cells were exposed to a high concentration of cisplatin, they showed a round shape and were detached from the cell culture plate. The treatment with cisplatin in the presence of Genistein and β -Lapachone produced the detachment of the cells and the loss of the cell monolayer even at small concentrations of cisplatin.

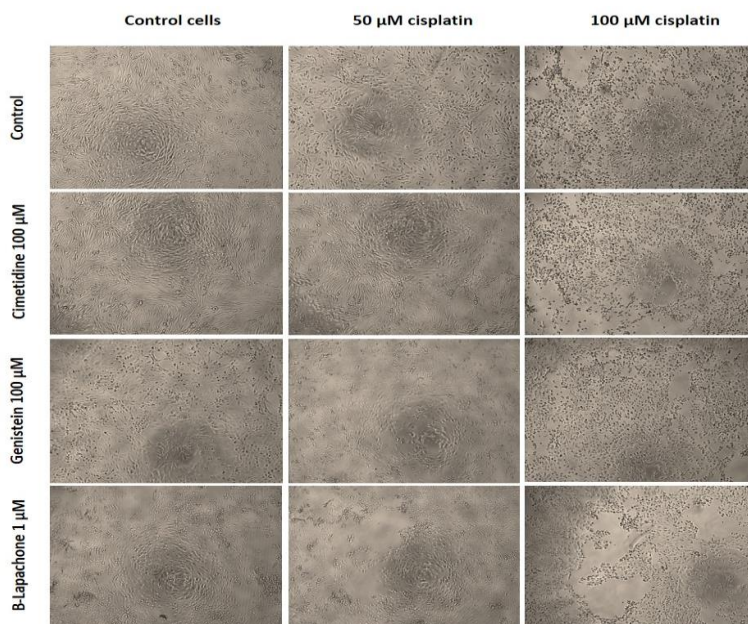


Figure 3.10: Morphological changes after cisplatin exposure and cisplatin combined with small molecules exposure. Cells were exposed to cisplatin during 8 hours, and the morphological changes showed in the pictures were reported 40 hours after cisplatin exposure.

After the microscope observation, GGT1 enzymatic activity, cell viability, and protein/well content were analyzed (Figure 3.11). The PrestoBlue assay showed a dose-response curve for the control and the small molecules. Genistein had less cell viability than the rest of the tested small molecules, even in the control, so it indicated that the used concentration of this molecule was toxic for the cells. GGT1 enzymatic activity showed a similar behavior for the control and cimetidine curves with an increase of GGT1 enzymatic activity at 300 μM of cisplatin in both cases. The dose-response curve for Genistein started with a decreased value of GGT1 enzymatic activity for the control (0 μM cisplatin) and the different cisplatin concentrations, supporting the data obtained for the cell viability assay, but this molecule also presented an increase in GGT1 enzymatic activity at 100 and 300 μM of cisplatin. β -Lapachone represented a dose response curve without an increase of GGT1 at the higher concentration of cisplatin. The tested small molecules did not improve cell viability after cisplatin exposure, as indicated by EC50 (Table 3.2).

Table 3.2: EC50 of cisplatin in the presence of the different small molecules tested.

	Cisplatin	Cisplatin + Cimetidine	Cisplatin + Genistein	Cisplatin + β -Lapachone
Mean	48.14	46.60	33.60	14.80
\pm SD (μM)	\pm 59.71	\pm 53.88	\pm 28.85	\pm 15.91

The protein content /well analyzed by BCA protein kit assay showed negative results in the wells treated with the different concentrations of

cisplatin in the presence of Genistein and β -Lapachone. The negative values obtained from BCA suggested us that maybe this is not the best method to normalize the other performed assays especially, when cell number was reduced, or cells were very damaged, as a consequence of cisplatin treatment.

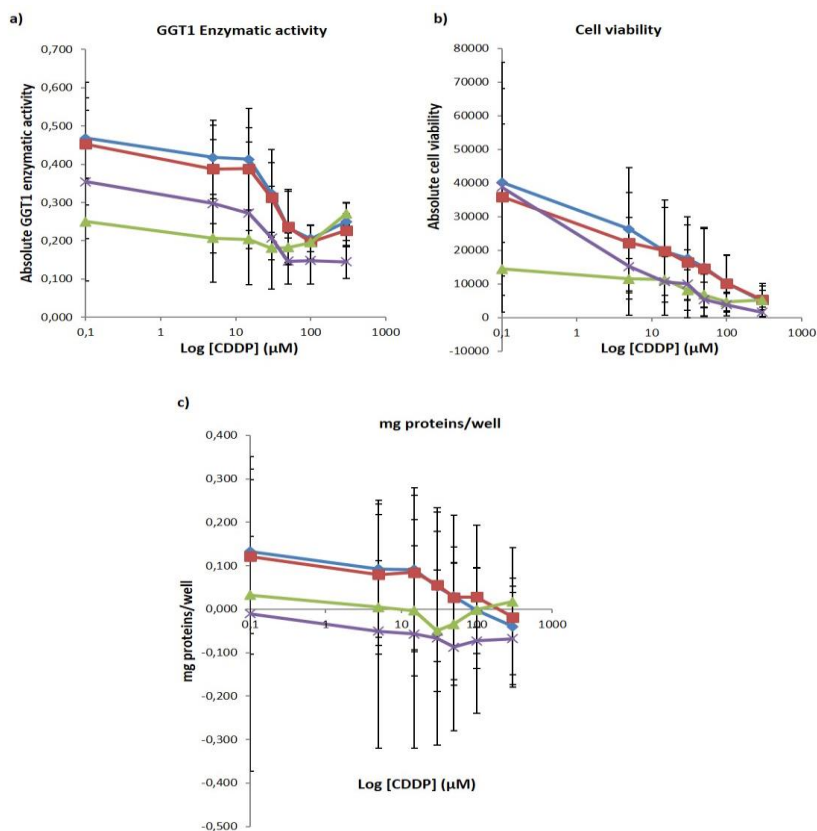


Figure 3.11: Evaluation of cisplatin effects in presence of the small molecules. a) GGT1 enzymatic activity. b) PrestoBlue Cell viability assay. c) BCA protein assay kit. The use of small molecules did not decrease or improve the effects produced by the cisplatin. The results were expressed as mean \pm SD of three separate experiments performed by triplicated. Blue: cisplatin; Red: cisplatin + 100 μ M cimetidine; Green: cisplatin + 100 μ M Genistein; Purple: cisplatin + 1 μ M β -Lapachone.

3.5 DISCUSSION

A model reproducing the physiological environment of PT cells will be useful in several contexts, from basic biological research to translational approaches. From a clinical standpoint, an unmet need is the ability to model the response to potential nephrotoxics by PT cells. Primary cultures will provide the optimal biological material while fluidic devices will help to generate more physiologically relevant conditions. However, it has already been discussed in the previous chapter the risk that a small number of cells growing in the fluidic channel poses for appropriate phenotyping, and thus also for evaluating a potential nephrotoxicant. On the other hand, it was interesting to be able to use interrogation procedures that could be applied repeated times. This would allow for long-term assessment that is required for evaluation of regeneration mechanisms and/or therapies after an acute PT insult. Here, we have focused in the creation and optimization of a consistent and reproducible nephrotoxicity model based in the use of cisplatin with the goal to transfer this knowledge to fluidic devices that let reproduce a more physiological environment for cells.

Cisplatin was used as a nephrotoxicant model because its effects on PT have been extremely well documented and appear to be more consistent than other damaging agents (e.g. gentamicin). Moreover, *in vitro* studies to evaluate cisplatin-induced nephrotoxicity using PT primary cell culture systems are limited. Usually, the *in vitro* nephrotoxicity models based into study cisplatin effects described in the literature, use continuous cell lines [11, 216-220]. Thus, our results can add further knowledge about cisplatin mechanisms of action under more representative experimental conditions. This work was performed on hPTPC, cells isolated and

characterized as explained in Chapter 2. hPTPC cells are a primary culture of human renal cells highly enriched in PT cells and extensively characterized with the expression of the principal markers of PT and the expression of multiple organic ion transporters, mimicking renal reabsorption and excretion. The use of these cells constitutes a clear advance over the use of continuous cell lines, which should improve our ability for predicting a toxic drug effects in human kidney.

The experimental design was chosen to reproduce the conditions used *in vivo*. Typically, cisplatin treatment consists in the administration of 20-150 mg cisplatin/m² given as a bolus injection or as several-hour long infusion [223-226]. 50% of the administered dose can appear in urine during the 24h following administration. The majority, is excreted during the few first hours. Cisplatin clearance is around 50 mL/min/m², thus exceeding that of creatinine, indicating tubular secretion. Although several cycles of cisplatin treatment are administered, renal toxicity can be observed already in the first cycle. The period of 8 hours used for the exposure to cisplatin in this model represents an average *in vivo* exposure [227]. The information on cisplatin concentrations in serum and ultrafiltrate is very sparse. Clearance of cisplatin also depends on individual characteristic. Thus, the dose-response curve of cisplatin for the creation of the nephrotoxicity model comprised a broad interval of concentrations, including low, medium and high concentrations of this molecule reviewed from the literature, where it was possible to observe different effects in the hPTPC depend on the used concentration [221, 222].

hPTPC grown on 96 wells plate exhibited cell death when exposed to increasing concentrations of cisplatin. The evaluation of cell morphology

through direct observation under the phase microscope showed a cell cytoplasm completely full of granules and cells detached from the cell culture plate, as the cisplatin concentration increased. The morphology of cells exposed to cisplatin was always compared with the control cells. Although I did not evaluate the mechanism of death induced by cisplatin in these cells, it is well known that concentration up to 30 μM caused a cell death with the characteristics of apoptosis, meanwhile concentrations equal or higher than 300 μM caused a cell death with the characteristic of necrosis and at 100 μM , both apoptotic and necrotic cells coexist [226, 228].

For quantification, two optical assays were chosen for repeated evaluation of the cisplatin effects. Cell viability can be easily determined by quantifying the reduction of a resazurin salt. Among the available alternatives, a commercial solution (PrestoBlue) was chosen because is optimized to produce a fast readout, thus reducing the time are exposed to the reagents. The other assay consisted in determining GGT1 enzymatic activity. This activity is relevant because besides being a marker of PT phenotype, is one of the defenses against oxidant and toxic agents. At the beginning, PrestoBlue assay and GGT1 functional assay were performed separately. We detected a decrease in the number of cells because of the wash processes and considering that the last goal of the nephrotoxicity model is to transfer it to the fluidic devices, where the number of cells is limited, and the aim was to allow for repeated measurements, we decided to perform these two assays simultaneously. For this goal, the first thing that we checked was the spectrum of both reagents, and we concluded that there is not spectral interference between the used reagents. Also, we performed the GGT1 and PrestoBlue assays sequentially (each assay performed per separated) and simultaneously (both experiments

performed at the same time) obtaining similar dose-response curves. The combined PB-GGT1 substrate reagent turned out to be an excellent assay for determining cell viability and GGT1 activity simultaneously.

Cells were exposed to cisplatin during 8 hours and 40 hours after cisplatin exposure, the effects of cisplatin were analyzed with the cell viability-GGT1 assay and protein/well content. GGT1 enzymatic activity, cell viability and protein/well content in the primary culture of hPTPCs exposed to cisplatin showed a dose-dependent decrease. This confirmed the morphological observation that cisplatin produced a response dependent on the concentration employed in our cell culture. Under the experimental conditions of our model, we calculated the IC₅₀ for cell viability in hPTPC, and it was 64±29 μM. This is very similar to a previous observation by J.X. Huang *et al.*, who reported that IC₅₀ after cisplatin exposure for HK2 cell line was 15±2 μM and for human PT primary cells was 48±2 μM [229]. The IC₅₀ comparison between a continuous and a primary cell line after cisplatin exposure showed a big difference in the obtained results, which may explain the difficulty in translating *in vitro* results to *in vivo* applications [59-63].

We could not determine the IC₅₀ for the cisplatin effects on GGT1 activity. This is because cisplatin exhibited a biphasic effect. While lower doses reduced GGT1 in a concentration-dependent manner, GGT1 activity in hPTPC cells exposed to doses above 100 μM was higher than the expected from the cell viability values. The normalization of GGT1/ BCA actually demonstrated a relative increase in the enzymatic activity of the GGT1 in those cells. The GGT1 cytochemical staining (GMNA) also showed a high activity of the enzyme at the higher concentrations of cisplatin. This result was represented with a very intense reddish brown staining in the

cells that were still on the plate. Hence, to determine an absolute explanation about the increase of GGT1 dependent on the concentration observed in this model is not easy, as a consequence of the controversial role played by this enzyme [12]: Some studies showed that several tumorigenic cell lines possessed an increased GGT activity and a reduced sensitivity to cisplatin [230]. However, there are some published studies where the GGT addition increased the sensitivity to cisplatin, and its inhibition decreased it, suggesting that GGT is the enzyme that activates and enhances cisplatin nephrotoxicity [231, 232]. We propose other theory to this increase of GGT1: The cells get cysteine provided by GGT1 through the breakdown of extracellular GSH. This fact favors to the reconstitution of the intracellular GSH and also to its homeostasis. Thus, the result of an increased GGT1 activity accompanied in a decreased cell viability as a consequence of the cisplatin toxicity could also be explained as a defense mechanism: GGT1 can offer resistance to the oxidative stress. As the cisplatin concentration increases, the oxidative stress does too, and it could suppose the increase of the enzymatic activity, but at the same time, this increase activates and enhances cisplatin nephrotoxicity producing a fall in cellular viability.

Cisplatin induces moderated renal damage that can be recovered in weeks-months. Thus, we studied whether hPTPC were able to recover from cisplatin treatment. For this study, we took advantage of the ability to repeatedly assess cell viability using the Presto Blue reagent. The hPTPC did not show self-regeneration after cisplatin exposure and the graphs obtained for this result showed that the cisplatin is dose-and time-dependent, and even in the smallest concentration, cisplatin caused toxicity over time. With the goal to revert or just improve the effects caused by cisplatin exposure, we studied different small molecules.

Cimetidine, an inhibitor of the OCT2 basolateral transporter, was tested at 10 and 100 μM in the presence of cisplatin, but we could not see an improved response in the effects caused by the nephrotoxic molecule, compared with the control (cells only treated with cisplatin). The lack of effect cannot be attributed to the absence of OCT2 expression in hPTPC cells. ASP+ influx experiments in Chapter 1 demonstrated hPTPCs express functional OCT2 transport. On the other hand, our model of one-compartment (apical) is not the best suited to evaluate the physiological transport of Cisplatin, which might be entering through other transporters. Also, the conditions used in the experiment might not be the more adequate, requiring higher doses of cimetidine [211, 233]. Genistein, a nonsteroidal isoflavonoid did not show improved in GGT1, PrestoBlue or BCA at 10 μM compared with the cells without the treatment of this molecule. However, at 100 μM , the data from cell viability assays showed a higher toxicity in all the cisplatin concentrations treated with this molecule. At this concentration, genistein presented toxicity even in control cells. This data supported the study published by *Khoshyomn et al.* [234] where they proved that genistein can significantly enhance the antiproliferative and cytotoxic action of cisplatin. The quinone β – Lapachone, was highly toxic at 10 μM causing the cell death of all cells, for this reason, we tried the concentrations of 0.1 and 1 μM . We did not observe any changes in the assays evaluated with this small molecule. The small molecules tested in the presence of cisplatin in hPTPC were not valid, at least in the way used in our group, to decrease or prevent the cisplatin nephrotoxicity.

The determination of protein by the BCA assay in the small molecules section gave us negative values. These negative values did not let us normalize the GGT1 and PrestoBlue results. This fact prompted us to study

the reasons for this phenomenon, and one of the explanations found was the detection of interferences in the results of the protein quantification when Triton was used as a component of the lysis buffer. As an alternative assay to normalize the other results, we optimized the crystal violet assay, and currently, it is the method used in the nephrotoxicity model.

The optimization of this nephrotoxicity model based in cisplatin is easily reproducible and the obtained results were consistent. It will let the transfer of this model to the fluidic devices to study the effects of cisplatin under a more physiological environment (discussed in chapter 4).

3.6 BIBLIOGRAPHY

- [1] T. Ludwig, C. Riethmuller, M. Gekle, G. Schwerdt, H. Oberleithner, Nephrotoxicity of platinum complexes is related to basolateral organic cation transport, *Kidney Int* 66(1) (2004) 196-202.
- [2] V. Cepeda, M.A. Fuertes, J. Castilla, C. Alonso, C. Quevedo, J.M. Perez, Biochemical mechanisms of cisplatin cytotoxicity, *Anticancer Agents Med Chem* 7(1) (2007) 3-18.
- [3] R.P. Miller, R.K. Tadagavadi, G. Ramesh, W.B. Reeves, Mechanisms of Cisplatin nephrotoxicity, *Toxins (Basel)* 2(11) (2010) 2490-518.
- [4] B. Rosenberg, L. Vancamp, T. Krigas, Inhibition of Cell Division in *Escherichia Coli* by Electrolysis Products from a Platinum Electrode, *Nature* 205 (1965) 698-9.
- [5] J.M. Hill, R.J. Speer, Organo-platinum complexes as antitumor agents (review), *Anticancer Res* 2(3) (1982) 173-86.
- [6] J.M. Hill, E. Loeb, A. MacLellan, N.O. Hill, A. Khan, J.J. King, Clinical studies of Platinum Coordination compounds in the treatment of various malignant diseases, *Cancer Chemother Rep* 59(3) (1975) 647-59.
- [7] D. Wang, S.J. Lippard, Cellular processing of platinum anticancer drugs, *Nat Rev Drug Discov* 4(4) (2005) 307-20.
- [8] C.M. Sorenson, A. Eastman, Mechanism of cis-diamminedichloroplatinum(II)-induced cytotoxicity: role of G2 arrest and DNA double-strand breaks, *Cancer Res* 48(16) (1988) 4484-8.
- [9] R.S. Go, A.A. Adjei, Review of the comparative pharmacology and clinical activity of cisplatin and carboplatin, *J Clin Oncol* 17(1) (1999) 409-22.

- [10] T.L. Cornelison, E. Reed, Nephrotoxicity and hydration management for cisplatin, carboplatin, and ormaplatin, *Gynecol Oncol* 50(2) (1993) 147-58.
- [11] X. Yao, K. Panichpisal, N. Kurtzman, K. Nugent, Cisplatin nephrotoxicity: a review, *Am J Med Sci* 334(2) (2007) 115-24.
- [12] S.M. Sancho-Martinez, L. Prieto-Garcia, M. Prieto, J.M. Lopez-Novoa, F.J. Lopez-Hernandez, Subcellular targets of cisplatin cytotoxicity: an integrated view, *Pharmacol Ther* 136(1) (2012) 35-55.
- [13] M.K. Kuhlmann, G. Burkhardt, H. Kohler, Insights into potential cellular mechanisms of cisplatin nephrotoxicity and their clinical application, *Nephrol Dial Transplant* 12(12) (1997) 2478-80.
- [14] J.B. Hook, J.H. Smith, Biochemical mechanisms of nephrotoxicity, *Transplant Proc* 17(4 Suppl 1) (1985) 41-50.
- [15] G.F. Rush, J.H. Smith, J.F. Newton, J.B. Hook, Chemically induced nephrotoxicity: role of metabolic activation, *Crit Rev Toxicol* 13(2) (1984) 99-160.
- [16] A. Wilmes, C. Bielow, C. Ranninger, P. Bellwon, L. Aschauer, A. Limonciel, H. Chassaing, T. Kristl, S. Aiche, C.G. Huber, C. Guillou, P. Hewitt, M.O. Leonard, W. Dekant, F. Bois, P. Jennings, Mechanism of cisplatin proximal tubule toxicity revealed by integrating transcriptomics, proteomics, metabolomics and biokinetics, *Toxicol In Vitro* 30(1 Pt A) (2015) 117-27.
- [17] D.M. Townsend, M. Deng, L. Zhang, M.G. Lopus, M.H. Hanigan, Metabolism of Cisplatin to a nephrotoxin in proximal tubule cells, *J Am Soc Nephrol* 14(1) (2003) 1-10.
- [18] G. Ciarimboli, T. Ludwig, D. Lang, H. Pavenstadt, H. Koepsell, H.J. Piechota, J. Haier, U. Jaehde, J. Zisowsky, E. Schlatter, Cisplatin

nephrotoxicity is critically mediated via the human organic cation transporter 2, *Am J Pathol* 167(6) (2005) 1477-84.

[19] S. Ishida, J. Lee, D.J. Thiele, I. Herskowitz, Uptake of the anticancer drug cisplatin mediated by the copper transporter Ctr1 in yeast and mammals, *Proc Natl Acad Sci U S A* 99(22) (2002) 14298-302.

[20] N. Pabla, R.F. Murphy, K. Liu, Z. Dong, The copper transporter Ctr1 contributes to cisplatin uptake by renal tubular cells during cisplatin nephrotoxicity, *Am J Physiol Renal Physiol* 296(3) (2009) F505-11.

[21] A. Bernareggi, L. Torti, R.M. Facino, M. Carini, G. Depta, B. Casetta, N. Farrell, S. Spadacini, R. Ceserani, S. Tognella, Characterization of cisplatin-glutathione adducts by liquid chromatography-mass spectrometry. Evidence for their formation in vitro but not in vivo after concomitant administration of cisplatin and glutathione to rats and cancer patients, *J Chromatogr B Biomed Appl* 669(2) (1995) 247-63.

[22] T. Ishikawa, F. Ali-Osman, Glutathione-associated cis-diamminedichloroplatinum(II) metabolism and ATP-dependent efflux from leukemia cells. Molecular characterization of glutathione-platinum complex and its biological significance, *J Biol Chem* 268(27) (1993) 20116-25.

[23] D.M. Townsend, K.D. Tew, L. He, J.B. King, M.H. Hanigan, Role of glutathione S-transferase Pi in cisplatin-induced nephrotoxicity, *Biomed Pharmacother* 63(2) (2009) 79-85.

[24] Y. Sadzuka, Y. Shimizu, Y. Takino, S. Hirota, Protection against cisplatin-induced nephrotoxicity in the rat by inducers and an inhibitor of glutathione S-transferase, *Biochem Pharmacol* 48(3) (1994) 453-9.

[25] T. Nakamura, A. Yonezawa, S. Hashimoto, T. Katsura, K. Inui, Disruption of multidrug and toxin extrusion MATE1 potentiates

cisplatin-induced nephrotoxicity, *Biochem Pharmacol* 80(11) (2010) 1762-7.

[26] X. Wen, B. Buckley, E. McCandlish, M.J. Goedken, S. Syed, R. Pelis, J.E. Manautou, L.M. Aleksunes, Transgenic expression of the human MRP2 transporter reduces cisplatin accumulation and nephrotoxicity in Mrp2-null mice, *Am J Pathol* 184(5) (2014) 1299-308.

[27] D.M. Townsend, M.H. Hanigan, Inhibition of gamma-glutamyl transpeptidase or cysteine S-conjugate beta-lyase activity blocks the nephrotoxicity of cisplatin in mice, *J Pharmacol Exp Ther* 300(1) (2002) 142-8.

[28] K. Yamauchi, H. Sakurai, T. Kimura, P. Wiriyasermkul, S. Nagamori, Y. Kanai, N. Kohno, System L amino acid transporter inhibitor enhances anti-tumor activity of cisplatin in a head and neck squamous cell carcinoma cell line, *Cancer Lett* 276(1) (2009) 95-101.

[29] N.A. dos Santos, M.A. Carvalho Rodrigues, N.M. Martins, A.C. dos Santos, Cisplatin-induced nephrotoxicity and targets of nephroprotection: an update, *Arch Toxicol* 86(8) (2012) 1233-50.

[30] S.A. Alhasan, H. Pietrasczkiewicz, M.D. Alonso, J. Ensley, F.H. Sarkar, Genistein-induced cell cycle arrest and apoptosis in a head and neck squamous cell carcinoma cell line, *Nutr Cancer* 34(1) (1999) 12-9.

[31] D.V. Ratnam, D.D. Ankola, V. Bhardwaj, D.K. Sahana, M.N. Kumar, Role of antioxidants in prophylaxis and therapy: A pharmaceutical perspective, *J Control Release* 113(3) (2006) 189-207.

[32] K. Hasegawa, S. Wakino, K. Yoshioka, S. Tatematsu, Y. Hara, H. Minakuchi, K. Sueyasu, N. Washida, H. Tokuyama, M. Tzukerman, K. Skorecki, K. Hayashi, H. Itoh, Kidney-specific overexpression of Sirt1 protects against acute kidney injury by retaining peroxisome function, *J Biol Chem* 285(17) (2010) 13045-56.

- [33] P. Wlodek, M. Sokolowska, O. Smolenski, L. Wlodek, The gamma-glutamyltransferase activity and non-protein sulfhydryl compounds levels in rat kidney of different age groups, *Acta Biochim Pol* 49(2) (2002) 501-7.
- [34] K. Saotome, H. Morita, M. Umeda, Cytotoxicity test with simplified crystal violet staining method using microtitre plates and its application to injection drugs, *Toxicol In Vitro* 3(4) (1989) 317-21.
- [35] A.M. Rutenburg, H. Kim, J.W. Fischbein, J.S. Hanker, H.L. Wasserkrug, A.M. Seligman, Histochemical and ultrastructural demonstration of gamma-glutamyl transpeptidase activity, *J Histochem Cytochem* 17(8) (1969) 517-26.
- [36] Q. Huang, R.T. Dunn, 2nd, S. Jayadev, O. DiSorbo, F.D. Pack, S.B. Farr, R.E. Stoll, K.T. Blanchard, Assessment of cisplatin-induced nephrotoxicity by microarray technology, *Toxicol Sci* 63(2) (2001) 196-207.
- [37] Y.K. Kim, H.J. Kim, C.H. Kwon, J.H. Kim, J.S. Woo, J.S. Jung, J.M. Kim, Role of ERK activation in cisplatin-induced apoptosis in OK renal epithelial cells, *J Appl Toxicol* 25(5) (2005) 374-82.
- [38] M. Takano, N. Nakanishi, Y. Kitahara, Y. Sasaki, T. Murakami, J. Nagai, Cisplatin-induced inhibition of receptor-mediated endocytosis of protein in the kidney, *Kidney Int* 62(5) (2002) 1707-17.
- [39] Y. Yuan, H. Wang, Y. Wu, B. Zhang, N. Wang, H. Mao, C. Xing, P53 Contributes to Cisplatin Induced Renal Oxidative Damage via Regulating P66shc and MnSOD, *Cell Physiol Biochem* 37(4) (2015) 1240-56.
- [40] M.E. Rodriguez-Garcia, A.G. Quiroga, J. Castro, A. Ortiz, P. Aller, F. Mata, Inhibition of p38-MAPK potentiates cisplatin-induced apoptosis via GSH depletion and increases intracellular drug accumulation in growth-arrested kidney tubular epithelial cells, *Toxicol Sci* 111(2) (2009) 413-23.

- [41] R. Mandic, C.J. Rodgarkia-Dara, V. Krohn, S. Wiegand, R. Grenman, J.A. Werner, Cisplatin resistance of the HNSCC cell line UT-SCC-26A can be overcome by stimulation of the EGF-receptor, *Anticancer Res* 29(4) (2009) 1181-7.
- [42] M.P. Barr, S.G. Gray, A.C. Hoffmann, R.A. Hilger, J. Thomale, J.D. O'Flaherty, D.A. Fennell, D. Richard, J.J. O'Leary, K.J. O'Byrne, Generation and characterisation of cisplatin-resistant non-small cell lung cancer cell lines displaying a stem-like signature, *PLoS One* 8(1) (2013) e54193.
- [43] C. Sourbier, V. Valera-Romero, A. Giubellino, Y. Yang, S. Sudarshan, L. Neckers, W.M. Linehan, Increasing reactive oxygen species as a therapeutic approach to treat hereditary leiomyomatosis and renal cell carcinoma, *Cell Cycle* 9(20) (2010) 4183-9.
- [44] L. Gao, W.F. Wu, L. Dong, G.L. Ren, H.D. Li, Q. Yang, X.F. Li, T. Xu, Z. Li, B.M. Wu, T.T. Ma, C. Huang, Y. Huang, L. Zhang, X. Lv, J. Li, X.M. Meng, Protocatechuic Aldehyde Attenuates Cisplatin-Induced Acute Kidney Injury by Suppressing Nox-Mediated Oxidative Stress and Renal Inflammation, *Front Pharmacol* 7 (2016) 479.
- [45] E.H. Bae, H.S. Choi, S.Y. Joo, I.J. Kim, C.S. Kim, J.S. Choi, S.K. Ma, J. Lee, S.W. Kim, Farnesoid X receptor ligand prevents cisplatin-induced kidney injury by enhancing small heterodimer partner, *PLoS One* 9(1) (2014) e86553.
- [46] X. Ye, C. Zhang, Y. Chen, T. Zhou, Upregulation of Acetylcholinesterase Mediated by p53 Contributes to Cisplatin-Induced Apoptosis in Human Breast Cancer Cell, *J Cancer* 6(1) (2015) 48-53.
- [47] F. Farma, Ficha técnica Cisplatino Ferrer Farma. <https://www.aemps.gob.es/cima/pdfs/es/ft/62187/62187_ft.pdf>, Abril 2013).

- [48] S.M. Sancho-Martinez, F.J. Piedrafita, J.B. Cannata-Andia, J.M. Lopez-Novoa, F.J. Lopez-Hernandez, Necrotic concentrations of cisplatin activate the apoptotic machinery but inhibit effector caspases and interfere with the execution of apoptosis, *Toxicol Sci* 122(1) (2011) 73-85.
- [49] J.X. Huang, G. Kaeslin, M.V. Ranall, M.A. Blaskovich, B. Becker, M.S. Butler, M.H. Little, L.H. Lash, M.A. Cooper, Evaluation of biomarkers for in vitro prediction of drug-induced nephrotoxicity: comparison of HK-2, immortalized human proximal tubule epithelial, and primary cultures of human proximal tubular cells, *Pharmacol Res Perspect* 3(3) (2015) e00148.
- [50] N. Ferrell, R.R. Desai, A.J. Fleischman, S. Roy, H.D. Humes, W.H. Fissell, A microfluidic bioreactor with integrated transepithelial electrical resistance (TEER) measurement electrodes for evaluation of renal epithelial cells, *Biotechnol Bioeng* 107(4) (2010) 707-16.
- [51] K.J. Jang, A.P. Mehr, G.A. Hamilton, L.A. McPartlin, S. Chung, K.Y. Suh, D.E. Ingber, Human kidney proximal tubule-on-a-chip for drug transport and nephrotoxicity assessment, *Integr Biol (Camb)* 5(9) (2013) 1119-29.
- [52] M.J. Bissell, D.C. Radisky, A. Rizki, V.M. Weaver, O.W. Petersen, The organizing principle: microenvironmental influences in the normal and malignant breast, *Differentiation* 70(9-10) (2002) 537-46.
- [53] Q. Guo, B. Xia, S. Moshiach, C. Xu, Y. Jiang, Y. Chen, Y. Sun, J.M. Lahti, X.A. Zhang, The microenvironmental determinants for kidney epithelial cyst morphogenesis, *Eur J Cell Biol* 87(4) (2008) 251-66.
- [54] M. El Mouedden, G. Laurent, M.P. Mingeot-Leclercq, P.M. Tulkens, Gentamicin-induced apoptosis in renal cell lines and embryonic rat fibroblasts, *Toxicol Sci* 56(1) (2000) 229-39.
- [55] L. Fliedl, M. Wieser, G. Manhart, M.P. Gerstl, A. Khan, J. Grillari, R. Grillari-Voglauer, Controversial role of gamma-glutamyl

transferase activity in cisplatin nephrotoxicity, *ALTEX* 31(3) (2014) 269-78.

[56] A.K. Godwin, A. Meister, P.J. O'Dwyer, C.S. Huang, T.C. Hamilton, M.E. Anderson, High resistance to cisplatin in human ovarian cancer cell lines is associated with marked increase of glutathione synthesis, *Proc Natl Acad Sci U S A* 89(7) (1992) 3070-4.

[57] S. Daubeuf, D. Balin, P. Leroy, A. Visvikis, Different mechanisms for gamma-glutamyltransferase-dependent resistance to carboplatin and cisplatin, *Biochem Pharmacol* 66(4) (2003) 595-604.

[58] A. Paolicchi, M. Sotiropoulou, P. Perego, S. Daubeuf, A. Visvikis, E. Lorenzini, M. Franzini, N. Romiti, E. Chieli, R. Leone, P. Apostoli, D. Colangelo, F. Zunino, A. Pompella, gamma-Glutamyl transpeptidase catalyses the extracellular detoxification of cisplatin in a human cell line derived from the proximal convoluted tubule of the kidney, *Eur J Cancer* 39(7) (2003) 996-1003.

[59] D. Ding, J. He, B.L. Allman, D. Yu, H. Jiang, G.M. Seigel, R.J. Salvi, Cisplatin ototoxicity in rat cochlear organotypic cultures, *Hear Res* 282(1-2) (2011) 196-203.

[60] S. Khoshyomn, G.C. Manske, S.M. Lew, S.L. Wald, P.L. Penar, Synergistic action of genistein and cisplatin on growth inhibition and cytotoxicity of human medulloblastoma cells, *Pediatr Neurosurg* 33(3) (2000) 123-31.



CHAPTER

4

Transfer of the
generated
nephrotoxicity
model to fluidic
devices that mimic
the cellular
physiological
microenvironment

4.1 INTRODUCTION

Renal tubular cells are continuously exposed to a plasma ultrafiltrate flowing along the luminal compartment. Luminal flow generates a shear stress (SS) force over the cells apical surface. Cells can sense SS magnitudes through mechanical bending of the primary cilium or brush-border microvilli in PT cells, so thus, the intracellular signaling triggered by luminal SS is a key physiological stimulus for renal tubular cells [1, 2].

The conventional 2D culture conditions eliminate the possibility to reproduce real tubular function, which consists in concentrating or diluting solutes in the luminal fluid. It is thus evident that conventional 2D culture techniques fail to reproduce the actual environment of renal tubule cells, which may explain the difficulty in translating *in vitro* results to *in vivo* applications [3-7]. Regarding this loss of reproducibility, there is a current surge of intense cooperation between technical engineering and biological laboratories interested in developing fluidic devices for their use in studies of the renal epithelium. These new technologies mimic in a more reliable way, the physiological environment found *in vivo*.

The fluidic devices technology applied in the cell culture field is defined as a cell culture model in a system with a micrometer scale that incorporates important features like dimensional and morphological relevance, flow shear stress, mechanical strain, and co-culture capabilities, among others [8]. The fluidic technology represents some advantages compared to the traditional cell culture models: 1) Saving money in the use of expensive reagents due to the small volumes running through the micro-scaled chambers, 2) enabling prolonged culture of cells without the need for subpassaging or repeated media changes, 3) incorporating mechanical stimulation that can be interesting for those cells or tissues

that endure such stimulation *in vivo* and respond to it by acquiring specific phenotypes. All these advantages make this new technology very useful to be applied in biomedical research, being highly valuable for studying renal physiology and pathology. In the particular case of the nephron, the size of a microfluidic channel is very well suited to recreate the flow inside a renal tubule lumen, which usually ranges in the 20–60 μm diameter.

The most employed material to generate microchannels for tissue culture is polydimethylsiloxane (PDMS) by using soft photolithography technique [4, 9-11]. Alternatives to PDMS are thermoplastics such as PMMA (polymethylmethacrylate) [12], PS (polystyrene), PC (polycarbonate), COP (cyclic olefin copolymer) [13] and Teflon.

The simplest microfluidic pattern design includes a single cell culture chamber with inlet and outlet fluidic channels connected for culture medium delivery and removal, but the goal of this technology is the creation of flexible microfluidic patterning for a myriad of complex designs aimed to provide useful characteristics such as exposure to solute gradients, migration tests [14], hydrogel confinement, and to include actuators imitating specialized organ structure and function [15, 16]. Probably the most ambitious goal for microfluidic-based cell culture devices is to achieve long-term culture under automatized maintenance and experimentation interventions.

These new technologies that mimic the cellular environment in a more realistic way are going to approach us to different areas of study, unknown so far, providing us relevant results, similar to physiological environments found *in vivo* and it will let us transfer these results to the clinic in a more reliable way than the conventional 2D cell models used today. This chapter presents the efforts in the integration of cells, fluidic and assays as a new

technological model. Such a model will allow a leap forward in understanding critical parameters of a renal epithelial function that will subsequently provide better drug and nephrotoxicity screening assays.

4.2 OBJECTIVES

The Specific Aims worked out in this chapter were:

1. Development of methods and procedures for the isolation and cell culture of human primary proximal tubular cells (hPTPC).
2. Phenotypic characterization of cells obtained from the primary culture at the level of gene expression, protein markers, enzymatic activity in living cells and transporters.
3. Development and validation of a new nephrotoxicity model using cisplatin for the study of cell viability and expression of specific markers implied in the bioactivation of this molecule.
4. Screening of molecules potentially repaired of the damage produced by the cisplatin.
- 5. Development of the protocol for differentiated proximal tubular cell cultures in a device that allows us the application of Shear Stress (SS).**
- 6. Determination of the SS effect in the sensibility to cisplatin in hPTPC.**

4.3 MATERIAL AND METHODS

4.3.1 Cell culture

At the beginning of the project, hPTPC cells seeded inside microfluidic devices came from cell suspensions obtained after trypsinization. Once the freezing of amplified cultures was implemented, most experiments were performed with thawed cells, which were directly seeded inside microfluidic channels. Seeding was typically performed by pipetting the cell solution directly into the channel inlet. Cell concentrations varied depending on the particular device. Specific cell densities that allowed for adequate attachment and growing were characterized for each device employed during the project. hPTPC cells growing inside channels were cultured in MCR medium and maintained in an incubator at 37 °C, in a 5% CO₂ atmosphere.

hPTPC cultures in fluidic channels were followed by microscopy to evaluate cell attachment, survival, and proliferation.

The continuous cell line NRK-52E, a proximal tubular cell line from rat, was used to compare the results obtained with hPTPC in Ibidi fluidic devices. NRK-52E was seeded at 7.500 cells/cm² in DMEM (Lonza, BE12-604F), + 5% FBS (Sigma, F7524), + 1% penicillin – streptomycin (Sigma, P433).

4.3.2 Coating protocol

Cell culture fluidic device was coated with Collagen I from calf skin (Sigma, C8919), Matrigel (BD, 354234) and GelTrex (Thermo Fis., A1413201).

The stock solution of Collagen I was diluted 10 times in cold MiliQ H₂O, and the resulting solution was pipetted into channel inlet using between

10-12 $\mu\text{g}/\text{cm}^2$. The coated fluidic devices were kept at RT during 4 hours, in order to get a correct polymerization and after that, they were washed 2 times with MiliQ H_2O .

A working solution of Matrigel (1:4) was prepared using cold culture medium without serum and then, the resulting solution was pipetted into channel inlet. The coated fluidic devices were kept in an incubator at 37 °C, in a 5% CO_2 atmosphere during one hour. After the incubation, the coating was washed twice with culture medium without serum.

GelTrex was used at 0.4 mg/mL and prepared in serum free medium. The coated fluidic devices were kept in an incubator at 37 °C, in a 5% CO_2 atmosphere during one hour. After the incubation, the coating was washed twice with PBS buffer.

4.3.3 Fluidic devices

This PhD thesis was part of a coordinated research project, carried out in collaboration with a bioengineering group, aiming to develop an innovative solution for cell culture and assessment in microfluidic devices. In such model, cells would be grown inside a longitudinal channel to allow for their exposure to physiological shear stress. The system was initially conceived as two-part: a flat microfluidic chip that is encapsulated in a larger holder to provide fluidic connections.

Several prototypes (with their iterations) were tested during the project:

- SU-8 gradient chips
- SU-8 longitudinal channel
- Polystyrene (PS) longitudinal channel.

- Polystyrene (PS) longitudinal channel, which incorporated the fluidic connections and makes unnecessary the encapsulate.

Culture protocols were successfully developed in most cases, as detailed below. However, limitations came from material biocompatibility, perfusion ability, and fabrication. Thus, a commercial solution (Ibidi μ Slide VI 0.4, (Ibidi, AI-80606)) was eventually used to complete the aims of this chapter.

4.3.4 Fluidic perfusion system

Culture medium flow was provided by pumping MCR medium from a reservoir through the microfluidic devices, by using a peristaltic pump (Ismatec Reglo ICC). The reservoir was connected to the microfluidic device in a close circuit comprising 0.5 mm ID (Internal diameter) Tygon tubing. Flow (mL/min) was set to a value calculated to provide physiological shear stress (0.2 dyne/h/cm^2) [4] according to the formula:

$$\tau = 6mQ/bh^2$$

where m is medium viscosity ($\text{g cm}^{-1} \text{ s}^{-1}$), Q is the volumetric flow rate ($\text{cm}^3 \text{ s}^{-1}$), b is channel width (cm), and h is channel height (cm). To set up the perfusion with Ibidi μ Slides, the tubing of the pump and the bottle of the system were primed with the peristaltic pump. Three hours before the fluidic connection, I placed the tube adapter sets and the bottle containing the MCR medium into the incubator for equilibration. This will prevent the liquid inside the tubes or connectors from emerging air bubbles over the incubation time. After the equilibration time, the Ibidi device was connected to the system. Flow passed continuously through the device

during 48 h at a flow of 0.17 mL/min (providing a shear stress of 0.2 dyne/h/cm²).

4.3.5 Phenotyping of cells cultured in microfluidic devices by Multiplex PCR and GGT1 cytochemical staining

4.3.5.1 Analysis of phenotypic markers expression by Reverse transcriptase-polymerase chain reaction (RT-PCR)

RNA isolation

RNA isolation was performed with all the seeded cells in each channel of the fluidic devices with the commercial kit Total RNA Purification (Norgen Biotek, 37500) according to manufacturer's instructions. A sample of human kidney tissue was used as a control. The RNA isolation for the control was performed using TriZol reagent (Invitrogen, 15596-026) according to manufacturer's instructions. Isolated RNA was quantified using a Nanodrop spectrophotometer (ThermoSci., Nanodrop 2000) and its integrity was tested using a 2% agarose gel with TBE buffer (FisherSci. 15881-044). The isolated RNA was kept at -80°C to avoid degradation.

cDNA synthesis

The isolated RNA was retrotranscribed into cDNA through the commercial kit High-Capacity cDNA Reverse Transcription Kit (Applied Biosystems, 4387406) according to manufacturer's instructions.

RT-PCR

Twelve pairs of primers were combined in a multiplex PCR (Table 4.1).

Table 4.1: Multiplex primers

Mix	Primer	Sequence	Amplicon	Location
1	Megalyn	PF: CATCCCAAGCGAATGGATCTG PR: CAGTACAATCCACATCGCCATC	185 bp	TP
	KSP	PR: TCCCATGCCTACCTCACCTT PF: TTGCAGCGACACACGATCA	125 bp	Kidney-specific cadherin
	DPPIV	PF: TACTACTGGCTGGGTTGGAAG PR: TGTCTGTAACCTTCTTCATTGCT	102 bp	TP
2	APN	PF: GAACGATCTCTTCAGCACATCAG PR: GAAGAGGGTGTGTTTCAGCG	232 bp	TP
	GADPH	PF: TTGACGCTGGGGCTGGCATT PR: GTGCTCTTGCTGGGGCTGGT	157 bp	Endogenous control
	GGT1	PF: TGAGCCCAGAAGTGAGAGCAGT PR: ATGTCCACCAGCTCAGAGAGGG	185 bp	TP
3	THP	PF: GAGTGTCACCTGGCGTACTG PR: CATGGGTTTCATTCTCGTCAAC	358 bp	TAL
	α SMA	PF: CAGGCATGGATGGCATCAATCA PR: ACTCTAGCTGTGAAGTCAGTGTC	172 bp	Myofibroblast
	SGLT-2	PF: ACGCCTGATTCCCGAGTTCT PR: AGAACAGCACAATGGCGAAGT	110 bp	TP

4	AQP-2	PF: ATCACGCCAGCAGACATCC PR: AGCACGTAGTTGTAGAGGAGG	350 bp	CD
	NKCC2	PF: GGGGAGTCATGCTCTTCATTCGC PR: CCACGAACAAACCCGTTAGTTG	149 bp	TAL
	NCC	PF: CACCAAGAGGTTTGAGGACATG PR: GACAGTGGCCTCATGCCTGAA	70 bp	DT

RT-PCR was set up using the commercial kit DSF-Taq (Bioron, 101005). The final volume of the reaction mixture was 20 μ L and 1 μ L of cDNA was added (Table 4.2).

Table 4.2: Reagents and working concentration for mixes of PCR

Reagent (concentration)	Working concentration
H ₂ O	
Buffer incomplete 10x	1x
Mg ²⁺ 4 mM	0.16 Mm
dNTP 10 mM	200 μ M
Primers 4 mM	0.5 μ M
Taq polymerase	5*10 ⁻⁴ U

RT-PCR cycles were as follows (Table 4.3):

Table 4.3: PCR procedure

Cycle repetitions	Temperature	Time	Process
1x	94°C	2'	Initialization step
40x	94°C	45''	Denaturation step
40x	62°C	30''	Annealing step
40x	72°C	1.30'	Elongation step
1x	74°C	5'	Final elongation
1x	4°C	∞	Final hold

The PCR products were separated on a 2% agarose gel with TBE buffer (FisherSci., 15881-044) and stained with ethidium bromide (Sigma, E7637). The gels were visualized using a camera GBOX (Sygene) with an ultraviolet light integrated.

4.3.5.2 Gamma Glutamyl Transpeptidase (GGT1) cytochemical staining

This assay let us visualize the GGT activity obtained through the reaction between a diazonium salt and the naphthylamine releases by hydrolysis of a synthetic GGT substrate, γ -glutamyl-4-methoxy-2-naphthylamide (GMNA).

Cells were fixed for 10 min with ice-cold methanol (Fisher Sci. M/3950/21) and ice-cold acetone (Sigma, 90872) (1:1) and washed with 0.85% NaCl (Saline solution). Then, cells were incubated with the working solution (Table 4.4) for 20 minutes in the dark and again, they were washed with saline solution. To stop the reaction, cells were incubated with a 0.1 M solution of cupric sulfate (Sigma, C1297) for 2 min and then,

washed with a saline solution [17]. The pictures were taken using an inverted microscope (Olympus IX81).

Table 4.4: Working substrate solution for a volume of 5 mL

Substrate solutions*	Working concentration	Volume
GMNA solution 2.5 mg/mL (SC, 215216)	0,25 mM	0,25 mL
Tris buffer, pH 7.4	0.1 M	1,25 mL
NaCl (Saline solution)	0.85%	3,5 mL
Glycylglycine (Sigma, G3915)	3,78 mM	2,5 mg
Fast blue salt hemi zin chloride (Sigma, F3378)	1,20 mM	2,5 mg

**The substrate solution was filtered through a Whatman No. 1 filter paper just prior to use to remove any insoluble aggregates of the substrate.*

4.3.5.3 Analysis by Immunofluorescence

Cells were seeded at the adequate concentration of the fluidic device. Confluent monolayers were fixed with 4% paraformaldehyde for 10 minutes and then washed with PBS [18]. The fixed cells were permeabilized with 0.2% Triton-X 100 (Sigma, X100), incubated for 10 minutes and washed with PBS. Afterward, cells were incubated for 10 minutes in a quenching solution, using 50 mM NH₄Cl, and then washed again. The blocking solution, PBS, 0.1% Tween 20 (Sigma, P5927), 0.1 % BSA and 10 % Goat Serum (Sigma, G6767), was incubated for 30 minutes at room temperature (RT) and finally, cells were incubated with primary

antibodies in blocking solution overnight at 4°C. The primary antibodies used were ZO-1 (1:40; Santa Cruz Biotechnology, SC-10804) and acetylated tubulin (1:100, Sigma T6793). Cells were incubated with secondary anti-mouse Alexa 555 (1:1000; Invitrogen, A31621) and anti-rabbit antibodies, Alexa 488 (1:1000; Invitrogen, A-11008) for 1 hour in blocking solution buffer at room temperature. Ibidi were mounted in Vectashield Hard Set™ Mounting Medium (VectorLabs, H-1400) with DAPI (1:1000). Ibidi were examined under a fluorescence microscope (Olympus IX81).

4.3.5.4 Analysis of phenotypic markers by Immunocytochemistry

Cells were seeded at the adequate concentration of the fluidic device. Confluent monolayers were fixed with 4% paraformaldehyde for 10 minutes at RT and permeabilized with 0.1% Triton X100 for 10 minutes [19]. After the permeabilization step, cells were washed with PBS and incubated with 3% H₂O₂ (quenching solution for endogenous peroxidase activity) for 5 minutes. Non-specific binding sites were blocked by incubation with Vectastain Elite ABC kit (VectorLabs, PK-6100) according to manufacturer's instructions and finally, cells were incubated overnight at 4°C with α-SMA (1:50, Sigma A5228) primary antibodies. Afterward, cells were washed and then exposed to their corresponding biotinylated secondary antibodies (1:200) for 1 hour at RT. The protocol continued with the incubation of the reagents from Vectastain Elite ABC kit (VectorLabs, PK6100) to create the Avidin/Biotinylated Complex, followed by the incubation with Sigmafast DAB kit (Sigma, D0246), the precipitated substrate system to peroxidase, till the cells changed the color. Cells were counterstained with hematoxylin-eosin (Vector, H3404), mounted in Vectashield Hard Set™ Mounting Medium and examined in an inverted microscopy (Olympus IX81). Unspecific binding and residual background

peroxidase activity could be detected in control cells processed without the primary antibody.

4.3.6 Modifications of Cisplatin cytotoxicity assay for use in microfluidic devices

The same cytotoxicity assay described in Chapter 3 was used on cells growing in microfluidic devices (Ibidi μ Slide) with the following adaptations.

4.3.6.1 Cisplatin treatment

The static Ibidi device was maintained 7 days post-seeding under this condition, and the fluidic Ibidi device was maintained 5 days post-seeding in static and 48 h under flow conditions. Next, cells were exposed to cisplatin, 7 days after the seeding for both devices. A stock solution of 3.33 mM of cisplatin (Sigma, P4394) dissolved in a NaCl solution 140 mM was prepared. The working concentrations were 300, 100, 50, 30, and 5 μ M. The higher concentration of cisplatin, 300 μ M, was prepared from the stock solution, and the other concentrations were serially diluted from the higher concentration. All the working concentrations were prepared with MCR medium, to reach the final volume

Each channel from an Ibidi device was exposed to 150 μ L of a different cisplatin concentration during 8 hours in the incubator. One channel was not exposed to cisplatin, to be used as a control. After the treatment time, MCR medium containing cisplatin was replaced by fresh MCR medium and the Ibidi were kept in the incubator for 40 h, before to start with the assays to evaluate the effects of cisplatin. The cisplatin exposure with the

continuous cell line NRK-52E is the same described here, but using the growth medium for these cells.

4.3.6.2 Cell viability and GGT1 functional assay

After the incubation time and before to determine the cisplatin effects, it was performed PrestoBlue cell viability assay and GGT1 enzymatic activity at the same time. Cells were washed with HBSS buffer (Lonza, BE10-527F) to remove the cell culture medium. The assay solution was prepared containing: 1/10 PrestoBlue reagent (TermoFisher Scientific, A13262) + 2 mM γ -glutamyl-p-nitroanilide (Sigma, G133) + 50 mM glycylglycine (Sigma, G3915) in 1 mL DMEM (Lonza, BE12-917F) and 40 μ L of this solution was added per channel. Cells were incubated at 37°C for 21 minutes, taking measures every 7 minutes and after the incubation, results were read in a plate reader using fluorescence for PrestoBlue quantification (ex.530 nm / em.590 nm) and absorbance for GGT1 quantification (410 nm). 3 channels of an Ibidi without cells were used as blank to subtract the background in each assay. The dose response was plotted using the normalized relative absorbance for GGT1 enzymatic activity and the normalized relative fluorescence for cell viability vs. drug concentration. GGT1 enzymatic activity was also expressed as mmol p-nitroaniline/hour/cm².

4.3.6.3 Quantification of cell number

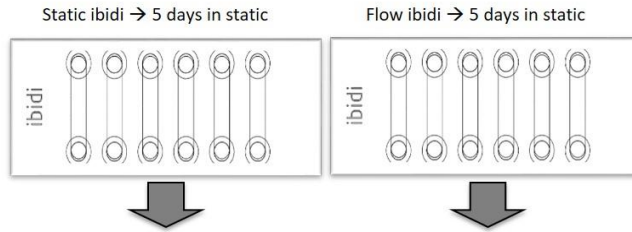
The Crystal Violet assay was based on the method of *Saotome et al.* [20] and it determined the total number of cells in each. This quantification let to normalize the enzymatic activity and the cell viability per channel in a more exactly way. After the determination of cell viability and GGT1 enzymatic activity, the quantification of cell number with crystal violet was performed. Cells were washed with PBS buffer, fixed with 4 % of

Paraformaldehyde during 15 minutes, and washed again with PBS buffer to eliminate the rest of the fixer. Then cells were stained with 0.1% of crystal violet solution (Sigma, C0775) in PBS buffer for 30 minutes. After the incubation, the excess of dye was removed by extensive washing with tap water. Pictures were taken under the microscope and then, the formed crystal were dissolved by using 10% acetic acid. The crystal violet was measured using a plate reader at 590 nm absorbance.

It is important to mention that all the experiments performed to evaluate the cytotoxicity produced by cisplatin were based in colorimetric assays. This kind of assays enables the direct quantification of the results without the need to work with the limited number out of the device. The Figure 4.1 shows the experimental design for the Shear Stress experiments carried out with Ibidi μ Slides.

Nephrotoxicity model in fluidic devices

a) Seeding



b) Flow Exposure

+ 48 hours in static conditions

+ 48 hours under flow conditions

c) Cisplatin treatment during 8 hours (static and flow)

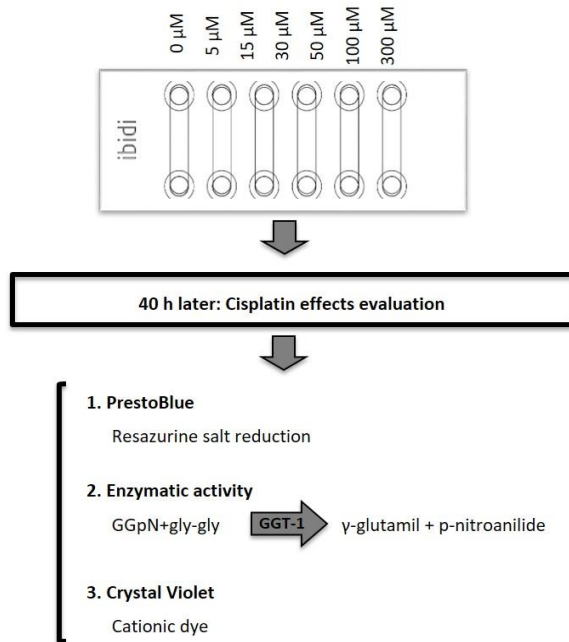


Figure 4.1: Schematic representation of the methods. a) Cells were seeded in Ibidi devices. b) 5 days after the seeding, one of the Ibidi was connected to flow during 48 hours. c) 7 days after the seeding, both devices were exposed to different cisplatin concentration during 8h. d) 48 h after cisplatin treatment was evaluated the effects of this nephrotoxic by using different assays.

4.3.7 Statistic

Differences between groups were considered to be statistically significant when $p < 0.05$ using two-tailed Student's t-test in Excel.

4.4 RESULTS

4.4.1 Culture of hPTPC cells in custom-made Fluidic devices

4.4.1.1 Cellular seeding

Each custom-made fluidic device had defined properties. For example, the volume used in each channel limited the supply of oxygen and nutrients and maximized accumulation of waste. The different plastic materials used in the fabrication of the device had different gas permeability. All these properties were different in each custom-made fluidic device, and it affected cell survival directly and consequently, the success of the experiment. So, cell concentrations, as well as the media change were optimized for attachment and proliferation of either device used to grow hPTPC (Table 4.5).

Table 4.5: . Data for cell seeding optimization

Custom-made fluidic device	Cells per channel	Volume	Height	Media change
Su-8 gradient chip	25.000	10 μ L	300 μ m	1 st day: 3/5/7 h a.s.* Then: Twice/day
SU-8 longitudinal channel	25.000	10 μ L	300 μ m	1 st day: 3 hours a.s. Then: Once /day
PS longitudinal	25.000	10 μ L	200 μ m	1 st day: 4 hours a.s. Then: Once /day
PS longitudinal with incorporated fluidic connections	200.000	80 μ L	200 μ m	1 st day: 4 hours a.s. Then: Once/day

**after seeding (a.s.)*

4.4.1.2 Prototypes made of SU-8

SU-8 is an epoxy resin with eight epoxy groups in a typical molecule. It offers high fabrication resolution, transparency for optical inspection, enough mechanical stability for easy handling, fabrication of the structures in a short time and with a wide range of thickness, biocompatibility, and compared with other materials, SU-8 is cheap [21, 22]. All these properties converted SU-8 in a good material to be used for rapid prototyping of the microfluidic device.

The first prototype was designed to be used as a gradient chip, showing a central culture chamber and two lateral microchannels, and it was fabricated by photolithography and bonding techniques. So, it was designed to seed cells in the central chamber, and in the lateral microchannels, one could test different conditions to create a gradient chip (Figure 4.2).



Figure 4.2: SU-8 gradient chip used as a prototype.

I started to use this first prototype to test SU-8 compatibility and establish cell culture conditions and flow protocols. Because of the delay in the fabrication process of the fluidic device designed for my project, cells in gradient chips used as a prototype were seeded in the central channel and also, in lateral microchannels.

The seeded hPTPC were able to survive only in the central chamber and in inlets/outlets of all channels (Figure 4.3), and cell confluency was not reached in all the experiments.

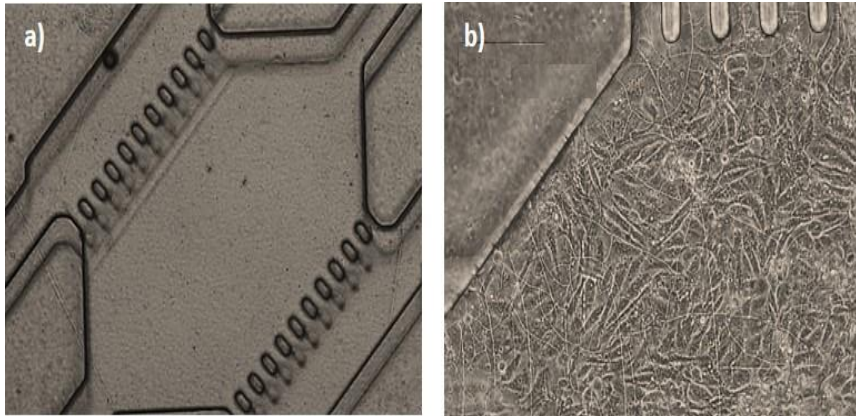


Figure 4.3: Cell survival in SU-8 prototype. a) SU-8 design. b) hPTPC growing in the central channel.

We tried to improve cell survival and cell confluency by using Collagen I and Matrigel coatings to compare with cell survival obtained when cells were seeded on the SU-8 surface (Figure 4.4). Matrigel worsened cell survival, and cell confluency and Collagen improved both parameters. Coatings were compared with the SU-8 surface.

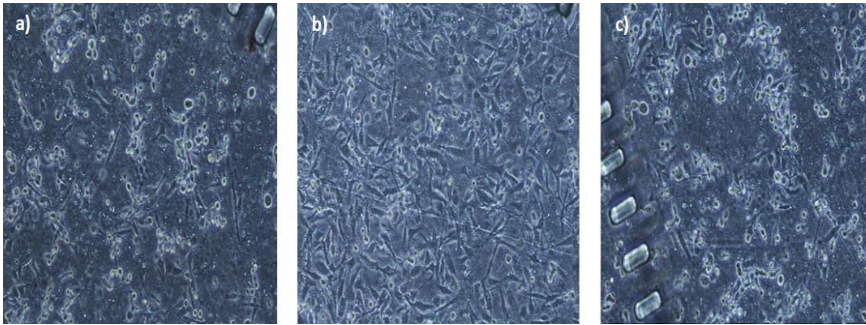


Figure 4.4: Strategy to improve hPTPC cell viability. 5 days after the seeding the cell viability was compared between the different conditions: a) SU-8 surface. b) Collagen I. c) Matrigel.

A total number of 34 SU-8 gradient fluidic devices were tested in our lab. hPTPC reached cell confluence in a 50% of the seeded devices, but only a 15% of these confluent devices survived in culture for 5 days. The efficiency of cell confluency and cell survival was significantly limited.

The geometry of these devices changed to three longitudinal channels with a central chamber to grow cells (Figure 4.5). Each channel could be operated independently, and cells were injected and seeded on the bottom of the channel. At this point, a prototype version of an encapsulate was also tested (see below), that allows for easy manipulation and reduced bubble formation once connected to a fluidic system.

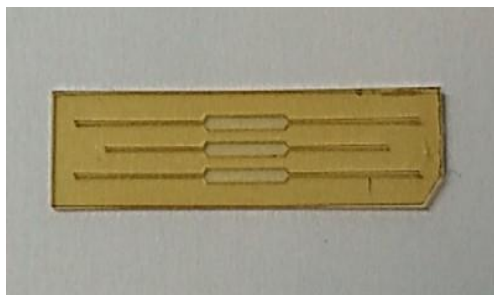


Figure 4.5: SU-8 longitudinal fluidic device

A total of 16 SU-8 longitudinal fluidic devices were used in the lab. Only 40% of the seeded cells reached confluence in the central channel of the device or in inlets/outlets, even when cells were seeded on coated surfaces with Matrigel or Collagen I to improve cell attachment and cell viability.

The longitudinal fluidic devices presented additional problems: the different layers of the device were separated easily, and it produced leaks and also, the continuous formation of bubbles diffculted the work with the devices. These problems hindered the connection of the fluidic devices to flow.

At the beginning, we thought that maybe some toxic waste coming from the sterilization process with isopropanol was the responsible of the reduced efficiency in cell survival. For this reason, the sterilization process was modified, including more washes with H₂O to eliminate possible toxic wastes and also, leaving the microchips with cell medium in the incubator O/N the day before to be used. The modification in the sterilization process did not improve cell survival.

4.4.1.3 Prototypes made of PS

The next devices tested in the lab were fabricated with culture grade polystyrene (PS). PS is the material most cell culture plastics are made of. Once fabricated, culture surfaces were treated with O₂ plasma to improve their hydrophilicity, otherwise, cells were not able to attach on the device surface.

The geometry of prototypes made of PS was the same that was used for SU-8 longitudinal fluidic devices: three longitudinal independent channels with a central chamber (Figure 4.6).

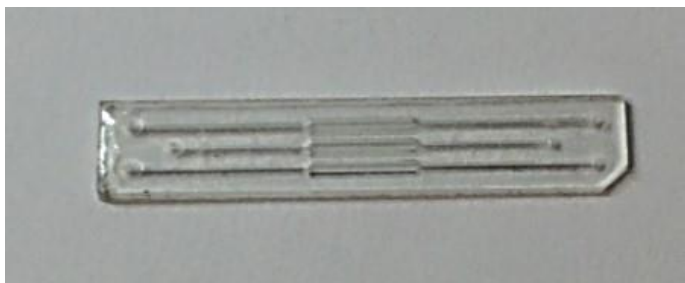


Figure 4.6: Representative image of the prototype made of PS.

The process of fabrication with this type of material was different: channels were laser-cut to generate different layers and then, layers were glued. As a consequence of the fabrication process, a large majority of the generated layers were not perfectly fixed, losing the geometry from a device to other, and obviously from batch to batch. It also implicated the appearance of cell/medium leaks. Another problem from these devices was the decontrolled generation of bubbles, so the cells only survive for a maximum time of 72 h. If bubbles were not generated or leaks did not appear, cells were able to reach the confluence, and the survival of the cells in this device can be maintained for more than 7 days in culture. A total number of 49 PS fluidic devices were used. More than 60% presented geometry problems, for example, inlets or outlets were obstructed, avoiding the access of cells or media to the central channel (Figure 4.7a). Of the 40% of the PS fluidic devices used, 25% was filled with bubbles preventing cell growth or culture media (Figure 4.7b). Finally, only 15% of the seeded devices with hPTPC survived in the central chamber at confluence for 7 days (Figure 4.7c).

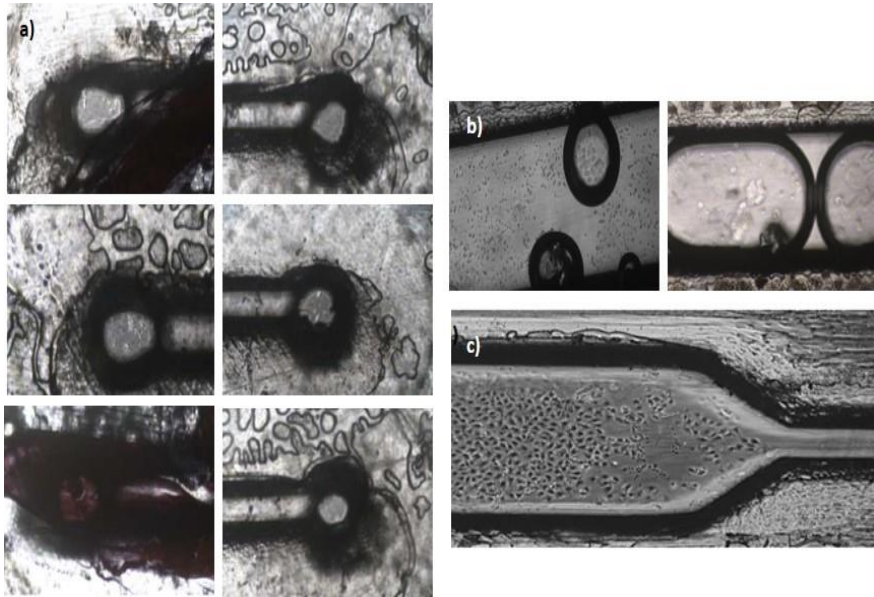


Figure 4.7: Efficiency in fluidic device fabrication and cell seeding. a) Inlets/outlets representation of three different channels in the same fluidic device. b) 4 hours after hPTPC seeding, in the central chamber appeared 3 bubbles, but 24 hours after the seeding, the bubbles occupied all the space in the central chamber. c) In the absence of the problems mentioned before, cells were able to grow, reach the confluence and survive in the device at least, 7 days.

4.4.1.4 The problem of fluidic connections: encapsulates

The fabricated fluidic devices were flat. This characteristic prevented the direct connection of the device to a pump, to induce flow. To enable the connection to flow system, devices were encapsulated in a holder which, in addition, constituted the interface between the micro and the macro scales. The encapsulated design removed most of the difficulties posed by the tiny size of the fluidic devices for cell culture: The idea for the fabrication of the holder was a piece with a channel that had same dimensions that fluidic devices and its **design allowed direct connection between tubes from flow system and fluid devices through the use of standard connectors.**

The first fabricated holder was a prototype, and the fluidic device was located between two screwed pieces (Figure 4.8).



Figure 4.8: First holder prototype with two screwed pieces

The final design of the encapsulated was made up of three different pieces, and the material used for the fabrication of the holders was methacrylate. The pieces were coupled to the fluidic devices through a flange system (Figure 4.9).



Figure 4.9: Methacrylate encapsulates. On the left is situated the piece where the fluidic device was fit. The piece in the middle of the picture closed the piece explained before. The encapsulated is completely hermetic when the piece on the right closes the other two pieces.

A total of 7 PS longitudinal fluidic devices with encapsulated were seeded with hPTPC. The seeding protocol is the same used without encapsulation: 200.000 cells resuspended in 80 μL MCR medium were seeded using the inlets of the encapsulated that directly connected to the fluidic device (Figure 4.10).



Figure 4.10: Seeding process in encapsulated fluidic devices.

Once the cells were seeded, the encapsulated was closed with the third piece and 4 hours after the seeding, connected to a peristaltic pump to be exposed to flow. The efficiency of this process was not successful, basically because pieces did not close well, producing medium leaks. The experiments were stopped 48-72 hours after the fluidic connection, without cells in the devices.

4.4.1.5 Flow chip of PS with self-connections

The last design of fluidic device tested in the lab was a fluidic device of injected PS. It had three longitudinal and independent channels. Once the cast of the fluidic device was fabricated, a layer of PS was glued to the

bottom. This device was not flat, and it let the direct connections to the tubes and adapters for the fluidic system. The fluidic device was treated with O_2 plasma to modify the hydrophobicity of the surface and improve cell attachment (Figure 4.11).

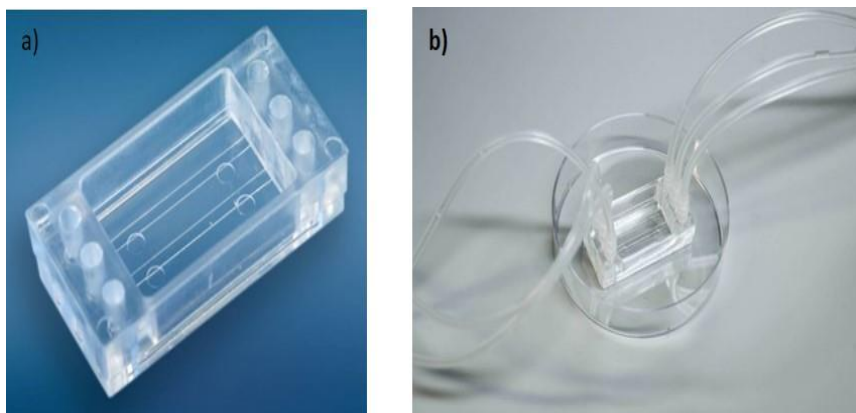


Figure 4.11: PS fluidic device. a) PS longitudinal 3 channels fluidic device. b) Representative image of the PS microfluidic devices with direct connections to flow.

25 devices were seeded in this type of fluidic device: 19 devices were discarded around 24-48 hours after seeding because they presented some of the problems explained below and only some channels of 6 devices were used to characterize cells and also to perfuse luminal flow (Figure 4.12).

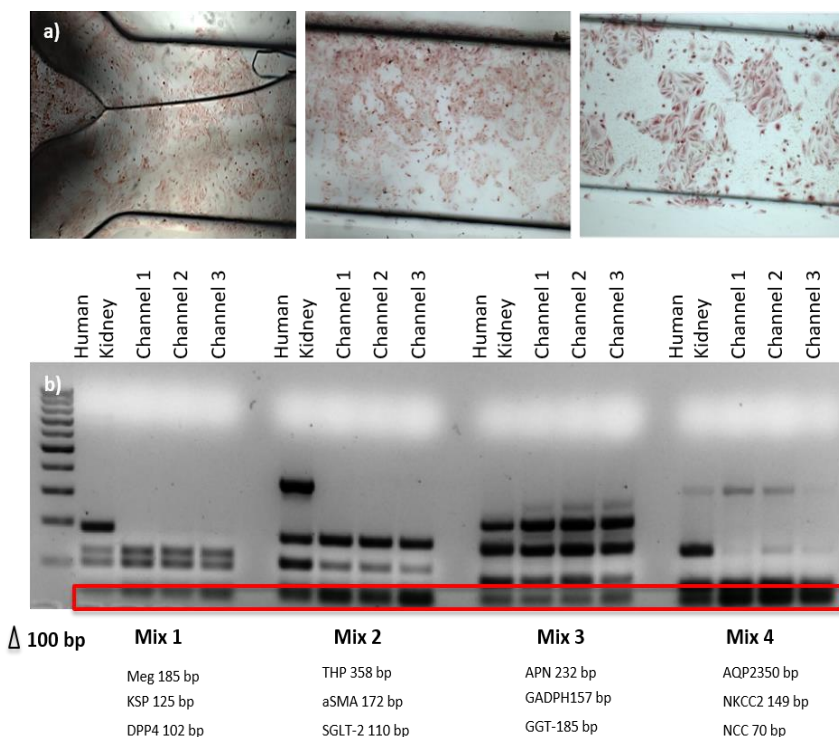


Figure 4.12: Characterization of hPTPC growing in PS longitudinal fluidic devices. a) GGT1 cytochemical staining in areas of different channels. b) Multiplex PCR. The red box showed primer dimers.

The problem presented in this type of fluidic device was associated with the glued PS layer, because it was not fixed correctly, so cells sometimes grew up outside of the seeding area (Figure 4.13a) and also, because the used glue invaded the seeding area, and it limited the cell attachment and proliferation (Figure 4.13b). Bubbles formation was another important problem (Figure 4.13 c) and also, the material fragility when connectors for adapting pump tubes were used (Figure 4.13 d). Again, the seeding protocol was not a problem, because when the seeding

area did not present any problems, cells were able to grow, reach confluence and survive for more than 7 days in culture (Figure 4.13 e).

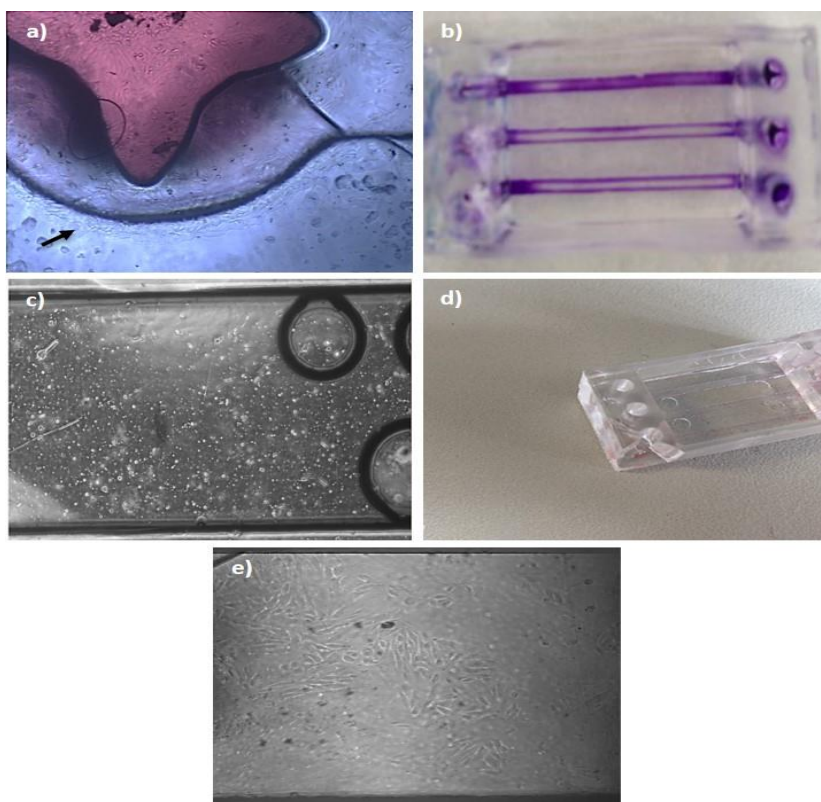


Figure 4.13: PS device with incorporated fluidic connections. a) Arrows showed cells growing outside of the channel. b) Channels were stained with a dye to show how the glue invaded the seeding area and also, closed this area c) Bubbles formation along the channel. d) One of the direct connections to flow system was broken after fixing the connector. e) Confluent cells after 7 days in culture

Undoubtedly, it was the best fabricated fluidic device, compared with the previous one, because we performed some characterization assays, not possible so far.

4.4.2 Culture of hPTPC cells in Ibidi μ -Slide VI 0.4

All the problems coming from the custom-made microchips impelled us to search another type of devices to achieve the central goal of the Thesis. Commercially available solutions are very young in the market and have not been widely adopted yet. However, different companies provide solutions to perform assays based on microfluidic plates (see Annex). We started to work with the devices supplied by IBIDI, specifically with Ibidi μ -Slide VI 0.4 because of the geometry of the device, the number of channels and also for the number of papers published using the devices from this company.

Each Ibidi μ -Slide VI 0.4 device has 6 independent channels made up of a plastic with a very high optical quality and the surface of the device is treated with biopolymers, which mediate cell adhesion and growth (Fig 4.14). The dimensions of the channels were: length 17 mm, width 3.8 mm, height 0.4 mm. The growth area of each channel was 0.6 cm² and the volume of each channel was 30 μ L. Each channel had 2 reservoirs, and the volumen per reservoir was 60 μ L. The company provided tube adapter sets for the fluidic connection. The tube adapter sets contained tubes and adapters for the connection between the Ibidi μ -Slide (female Luer) and the tubing of the pump in use.



Figure 4.14: Ibidi μ -Slide VI 0.4 design

4.4.2.1 Cell density, refreshing medium, coating

The seeding process with these devices required the optimization of the number of seeded cells. The formation of a homogenous cell monolayer around the fifth day after cell seeding and before to connect the Ibidi with the flow was the goal. Different cell concentrations were tested. The use of GelTrex on the surface of the channels was also tested (Figure 4.15). Our results indicated that using the small cell concentration, we did not reach a homogenous confluence 5 days after the seeding. The largest cell concentration reached the confluence before the established 5 days after the seeding, but we spent too many primary human proximal tubular cells. The use of GelTrex did not improve the cell growth, and sometimes the coating blocked the correct seeding in the channels. Based on these results, the best cell concentration was 42.000 cells per cm^2 without coating. Cell media was refreshed every 24 hours.

hPTPC proliferated and reached cell confluence easily. Cell survival in this device was not a problem and cells were able to be in culture for more than 14 days if the medium was refreshed every day.

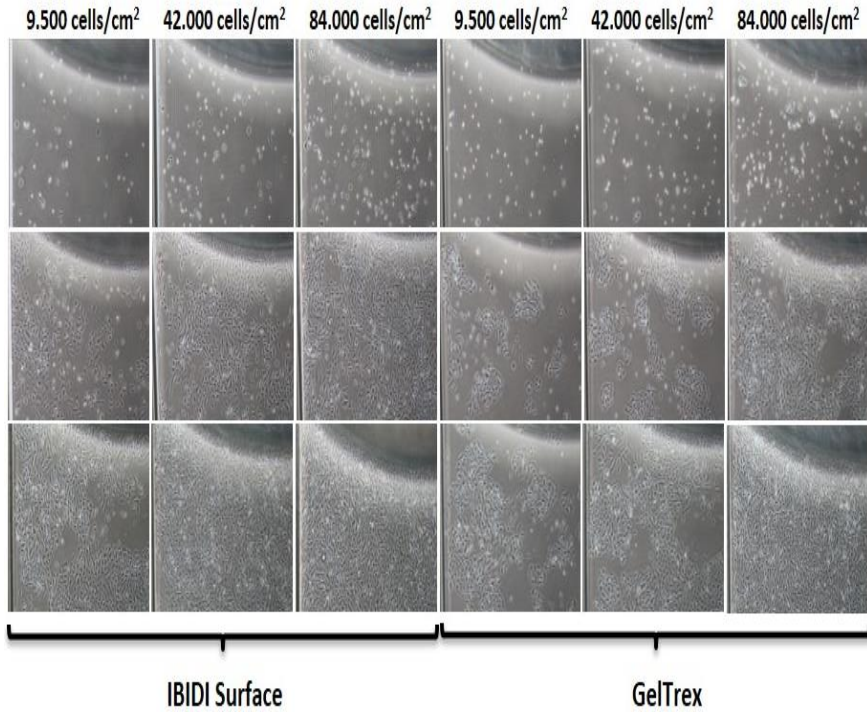


Figure 4.15: Evolution of the cellular confluence-dependent on cell concentration and the used coating. The first row of pictures corresponded to 24 hours after seeding, the second to 72 hours after seeding and the last to 5 days after seeding.

Cells growing on Ibidi surface were analyzed through GMNA immunocytochemical staining. This test helped us to be sure that hPTPC continued to express the GGT1 enzymatic activity, a specific marker for PT cells (Figure 4.16). The intensity of the staining was variable, with areas of intense reddish-brown staining by the side of other areas of less intensity and it can be explained as a consequence of cell aging. This expression's profile was the same for hPTPC growing in 96 wells/plate.

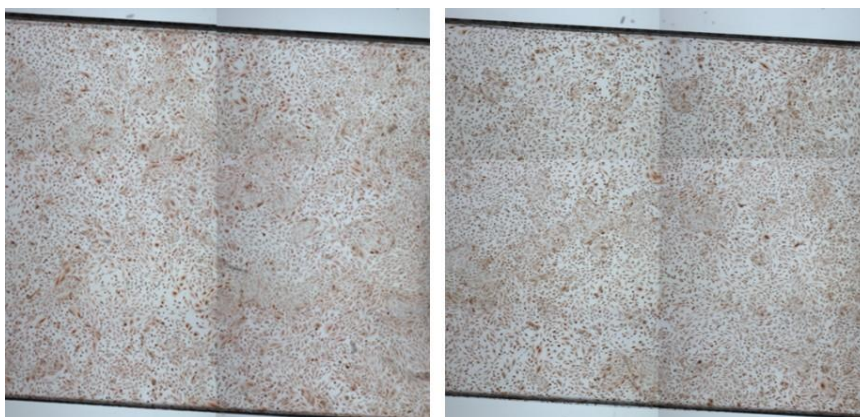


Figure 4.16: GGT1 enzymatic activity in hPTPC cells growing on Ibidi surface. The picture showed two channels of Ibidi where cells are positive for this marker.

4.4.2.2 Developing a Perfusion protocol

5 days after the seeding and once the cells reached the confluence, one of the seeded Ibidi was connected to a peristaltic pump to be exposed to luminal flow. The first experiments performed under flow presented many problems related with the optimization of the fluidic system, as well as the cellular stress produced by the luminal flow. The different problems that we had to overcome were (Figure 4.17):

- Optimization of the material (tubes, adapters, connectors) used to achieve the maintaining of flow in medium/long term in IBIDI devices using a peristaltic pump. The principal limitation found was related to material sterilization and duration.
- Bubbles reduction. The presence of bubbles is the principal limiting factor in the fluidic area because it can damage cells or stop the perfusion. All these problems were improved with the incorporation of an intravenous therapy filter of 5 microns. This element improved cell survival in the fluidic device significantly.

- Flow pulsatility reduction. Peristaltic pumps are the ideal solution to achieve the necessary flow rates during the time required for the test. In the experiments described in this Thesis, an 8-roller head pump with a very small pulse was employed. However, we detected that flow pulsatility in the perfused channels was a different channel to channel. This problem was tried to be resolved through the use of a custom-made pulse dampener. The pulse dampener, like the in-line filter, would also help to eliminate bubbles coming from upstream the Ibidi. However, the benefit obtained was not significant, since the generation of bubbles inside the device itself remained the most deleterious factor.

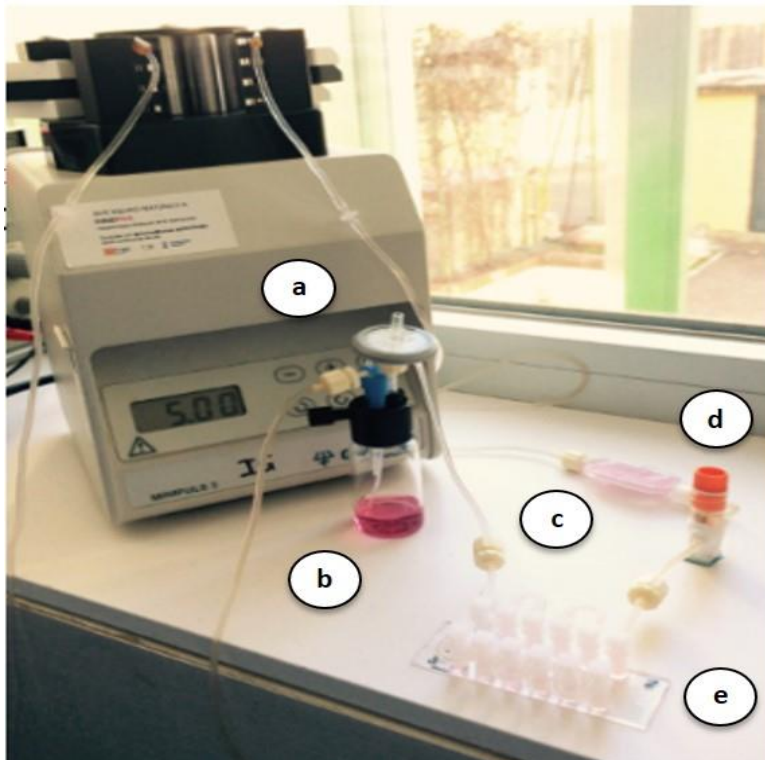


Figure 4.17: Perfusion system. a) Peristaltic pump. b) Medium bottle. c) Intravenous therapy filter d) Pulse dampener and e) IBIDI μ -Slide VI 0.4

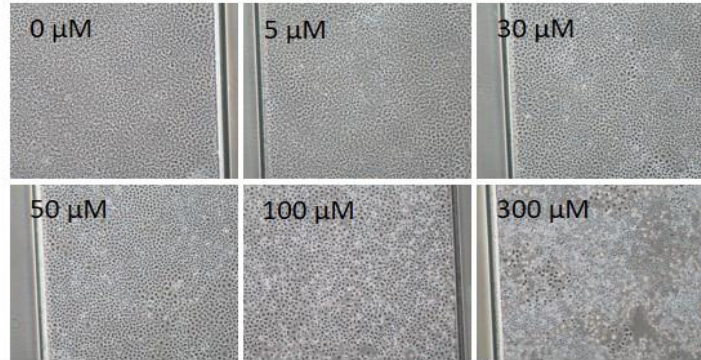
4.4.3 Nephrotoxicity model based in cisplatin employed in hPTPC growing in Ibidi μ Slides

The nephrotoxicity model to study the SS effect on cisplatin cytotoxicity was explained in materials and methods section, and it was represented in Figure 4.1. Additionally, all the experiments in this section were also performed with the continuous cell line NRK. The work performed with hPTPC and NRK allowed us to compare the results between these cells and check the robustness of our model for its validation.

4.4.3.1 Nephrotoxicity assays in Ibidi under static conditions

hPTPC and NRK cells growing inside fluidic channels were exposed to different concentrations of cisplatin during 8 hours and the effects produced by cisplatin were analyzed 40 hours later. The first parameter evaluated was cell morphology (Figure 4.18) and pictures showed a decrease in the number of NRK and hPTPC cells from 100 μ M of cisplatin.

a) NRK



b) hPTPC

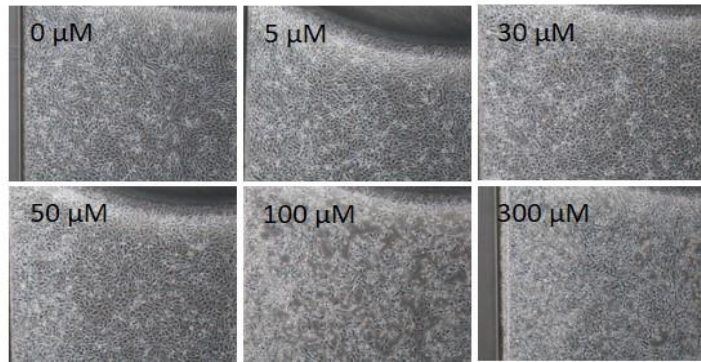


Figure 4.18: Cisplatin effects on cells growing in IBIDI device. a) NRK continuous cell line. b) hPTPC isolated and characterized along this Thesis.

After morphological evaluation, hPTPC and NRK cells were analyzed by optical assays explained in the section of methods and the results obtained with static ibidi were compared with the results obtained when cells were seeded in 96 wells plate (Fig 4.19).

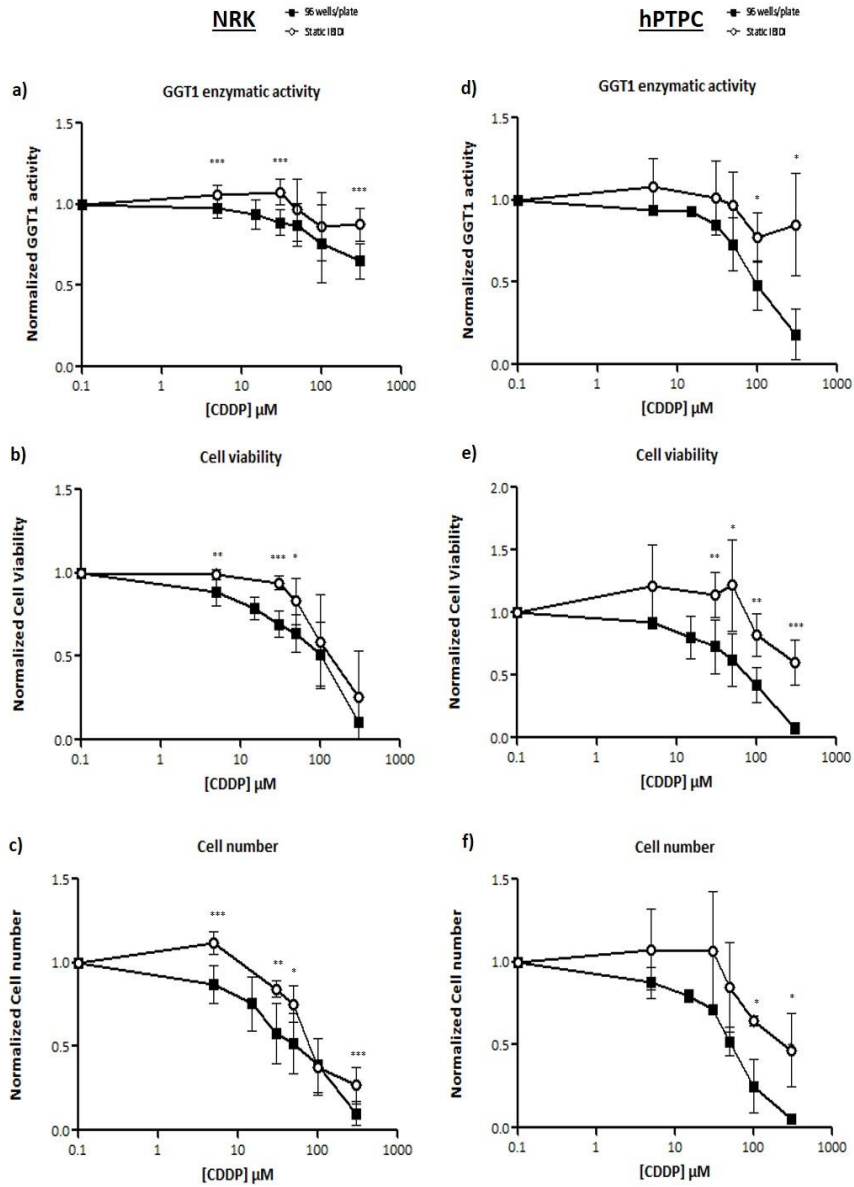


Figure 4.19: Growing on Ibdid μ -slide effects on NRK and hPTPC sensitivity to cisplatin (96w vs. Ibdidi). a, d) GGT1 activity; b, e) Cell viability; c, f) cell numbers. NRK data were expressed as mean \pm SD (n=5), and hPTPC data were expressed as mean \pm SD (n=3). *p< 0.05; **p<0.01; ***p<0.001.

EC50 was calculated for NRK and hPTPC growing in 96 wells/plate and static Ibidi after cisplatin exposure (Table 4.6). The analyzed data showed that hPTPC cells growing in Ibidi devices were more resistant to cisplatin exposure than the same cells and under the same concentrations of cisplatin in 96 wells plate.

Table 4.6: EC50 of NRK and hPTPC after cisplatin exposure in 96 wells/plate and static Ibidi. Data were represented as mean \pm SD of three independent experiments

	96 w/p	Static Ibidi
EC 50 \pm SD(μ M) NRK	103.53 \pm 43.92	118.964 \pm 48.43
EC 50 \pm SD(μ M) hPTPC	65.2 \pm 35.07	103.31 \pm 53.65

We also compared the results obtained with the optical assays between NRK and hPTPC (Figure 4.20).

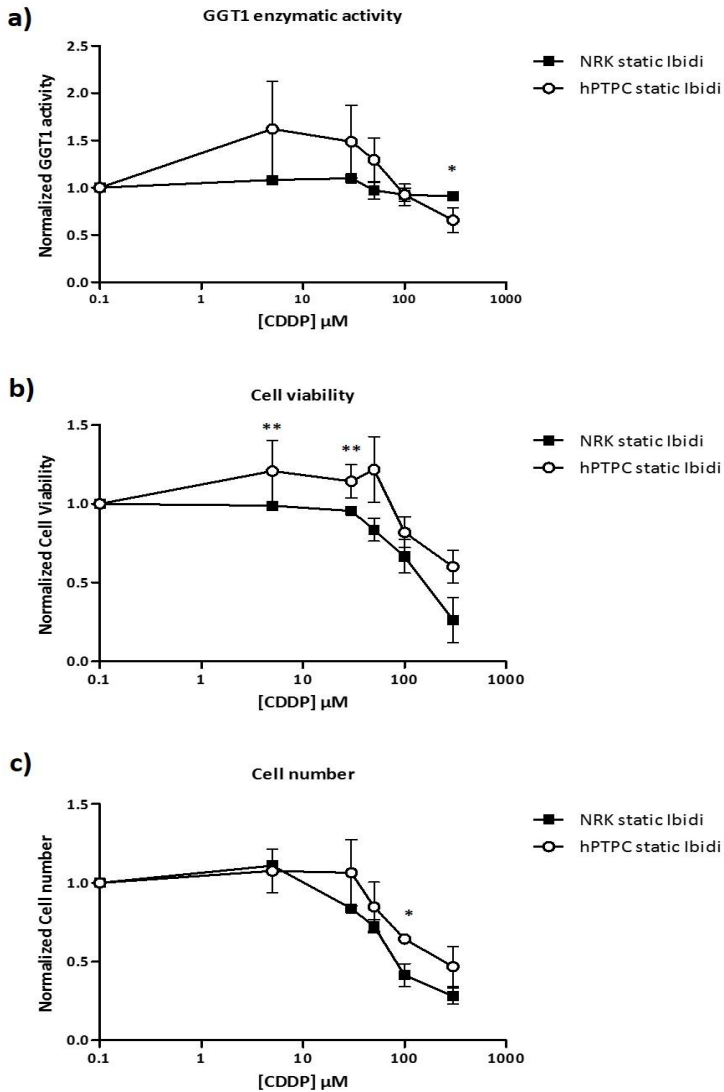


Figure 4.20: Comparison between NRK and hPTPC in static Ibidi after cisplatin exposure. a) GGT1 enzymatic activity; b) Cell viability; c) Cell number. * < 0.05; ** < 0.01; *** < 0.001

4.4.3.2 Shear stress effects on viability and phenotypical characterization

Different techniques were performed with the aim to analyze the differences between cells growing in Ibidi in static conditions and cells growing in Ibidi and exposed to flow for 48 hours.

First, we evaluated cell viability with PrestoBlue reagent, and we did not find any difference between both conditions (Figure 4.21).

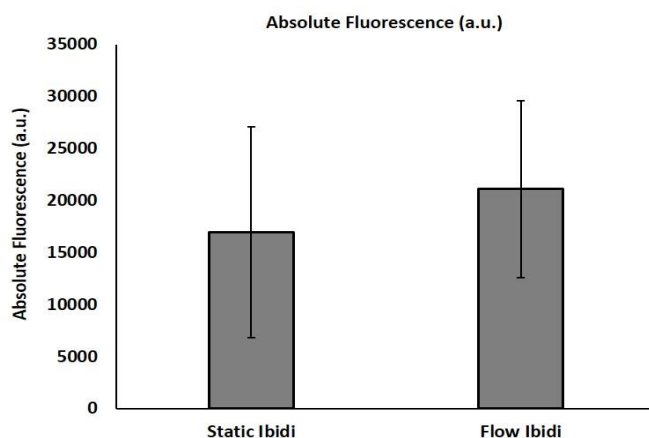


Figure 4.21: Cell viability comparing ibidi in static and under flow. Data were represented as mean \pm SD of two independent experiments.

GGT1 enzymatic activity was also determined and also here, we did not observe any significant difference (Figure 4.22).

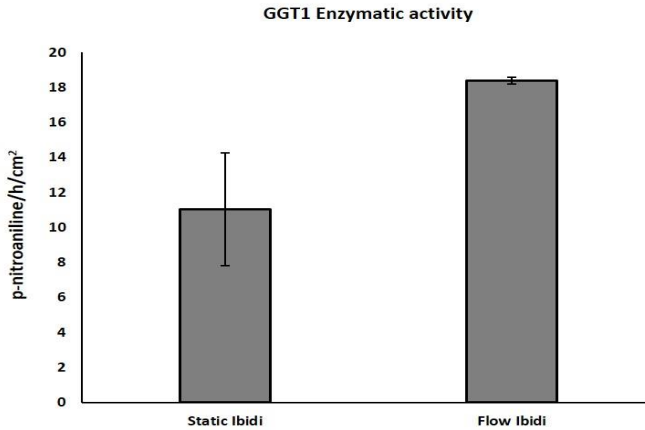


Figure 4.22: GGT1 enzymatic activity comparing Ibidi in static and under flow. Data were represented as mean \pm SD of two independent experiments.

Then, we analyzed morphological changes, and we detected some differences between cells growing in static condition versus cells exposed to luminal flow: cells presented an organized monolayer made up of epithelial cells under luminal flow. In contrast, cells in the static conditions showed a heterogeneous monolayer made up of different cell types. Other detected difference was that cells under flow showed granules in the cytoplasm, compared with cells in static condition (Figure 4.23).

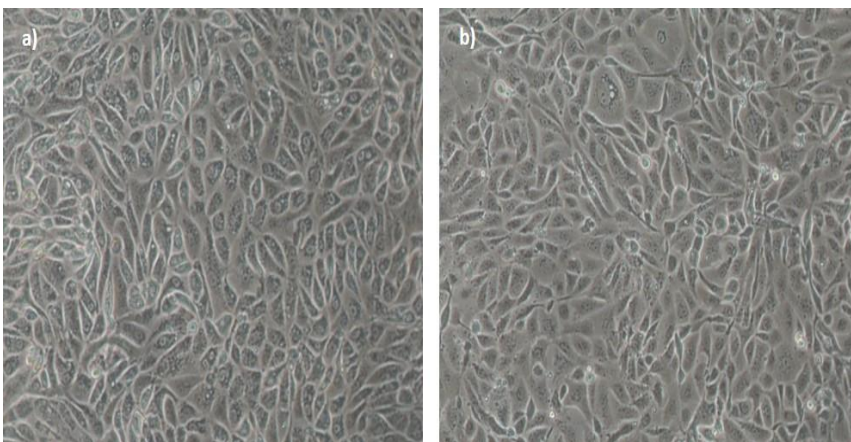


Figure 4.23: Morphological differences between both conditions. a) Cells exposed to 48 hours of luminal flow. b) Cells grown in static conditions.

We also performed immunostainings to determine the expression of the epithelial marker ZO1 and acetylated alpha-tubulin for primary cilia (Figure 4.24), and α SMA for EMT (Figure 4.25). None of these markers presented any difference between both conditions.

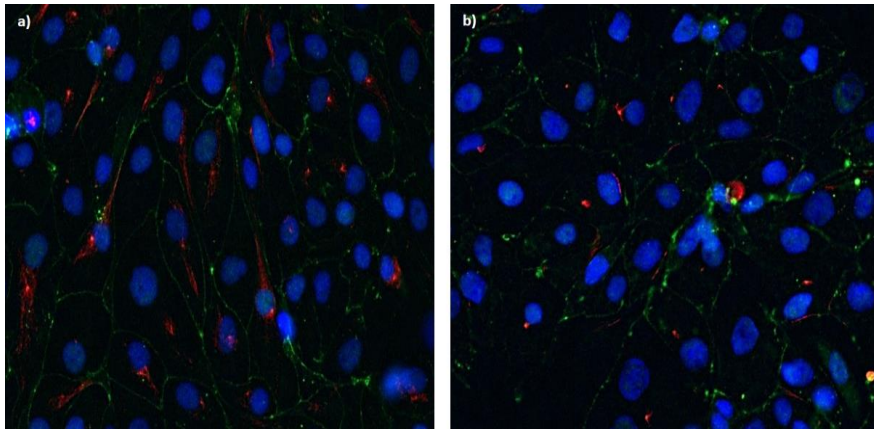


Figure 4.24: Proximal tubular epithelial origin of hPTPC in Ibidi fluidic devices. a) Cells in static ibidi and b) cells in Ibidi under flow (48 h) were analyzed by IF. Expression of epithelial marker ZO-1 confirmed the formation of tight junctions (green). The analysis of acetylated tubulin showed the expression of primary cilia (brighter dots in red).

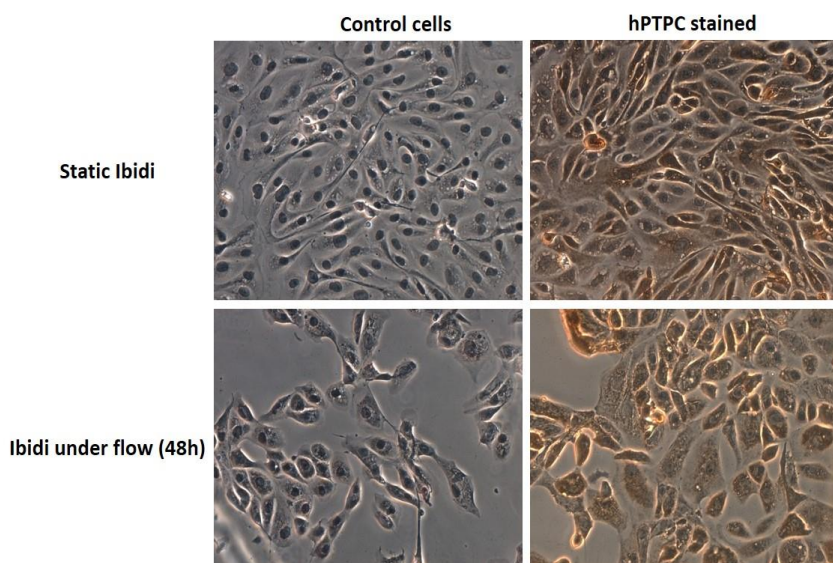


Figure 4.25: Immunocytochemistry of α SMA in cells growing in Ibidi fluid devices. The marker α SMA is a specific marker of Myofibroblast. Its positive expression in hPTPC confirmed a possible EMT

4.4.3.3 Shear stress effects on hPTPC sensitivity to cisplatin

Cells were exposed to luminal flow for 48 hours, and after that, static and fluidic conditions were treated with cisplatin for 8 hours. 40 hours after cisplatin exposure, shear stress effects on hPTPC sensitivity to cisplatin were evaluated. Firstly, morphological observations were performed to detect differences between channels in static condition or exposed to luminal flow in the presence of cisplatin (Figure 4.26).

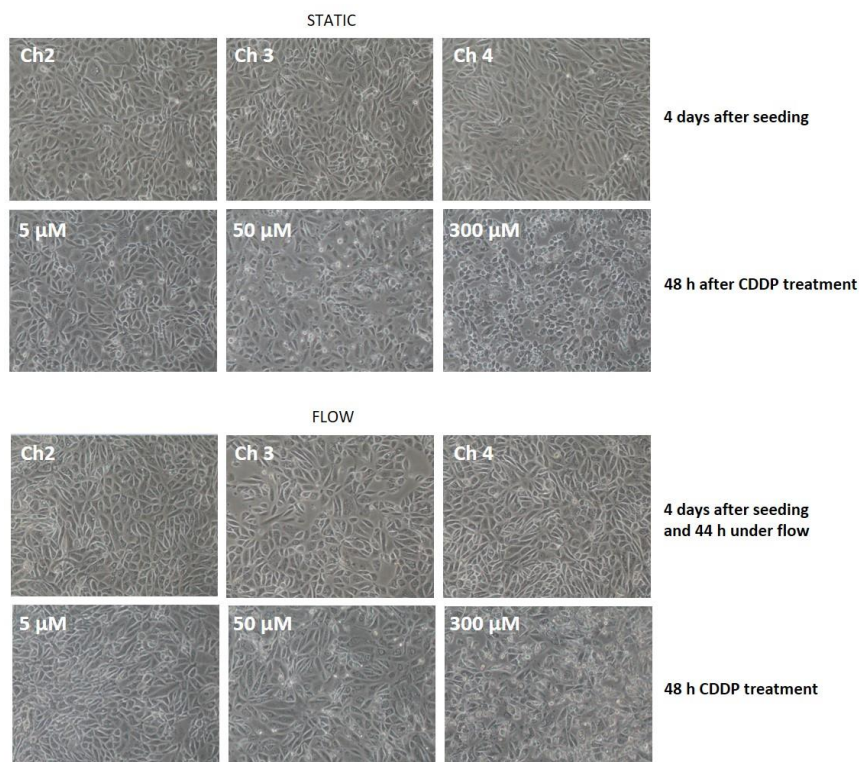


Figure 4.26: Shear Stress effects on hPTPC.

Eventually, the optical assay allowed us to determine numerically the experiments tested after cisplatin treatment, under static and fluidic conditions in hPTPC (Figure 4.27). When results were compared, hPTPC exposed to 0.2 dyne/h/cm^2 did not show any difference in cisplatin sensitivity compared with cells in static conditions. EC_{50} for cells under flow conditions was $143.48 \mu\text{M} \pm 96.61 \mu\text{M}$ and for cells in static conditions was $103.31 \mu\text{M} \pm 53.65 \mu\text{M}$.

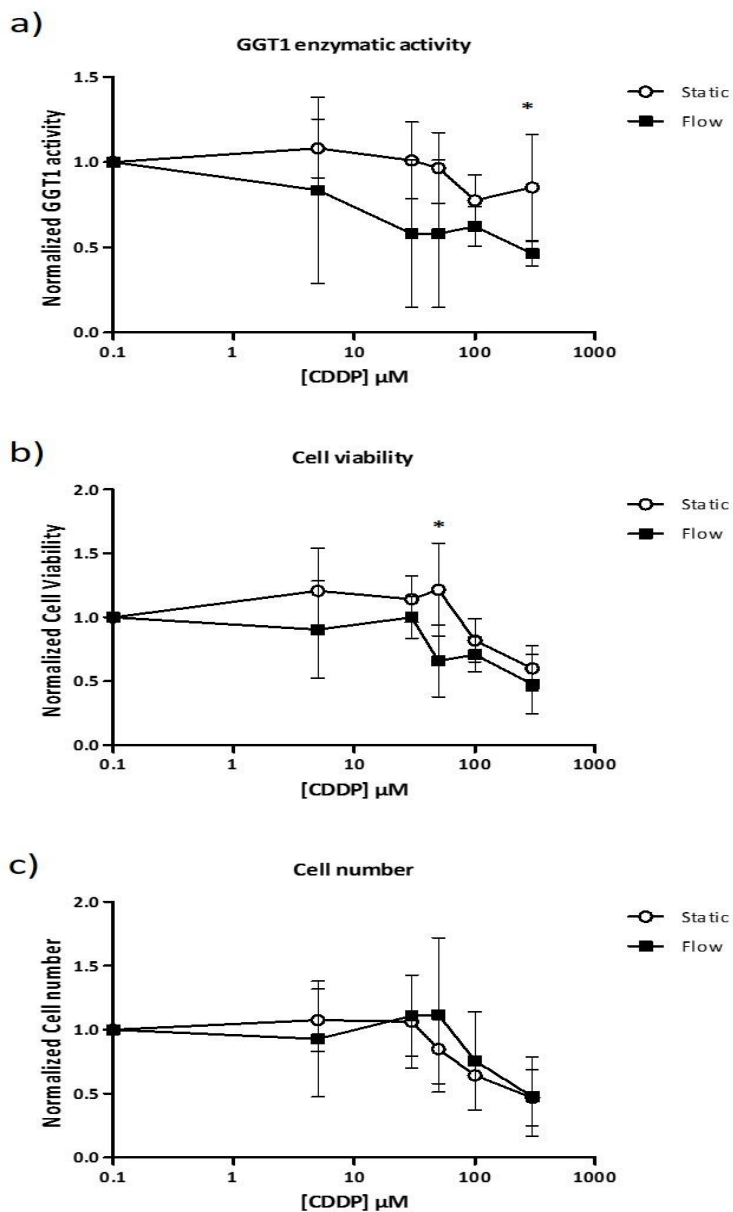


Figure 4.27: Cisplatin effects evaluated through optical assays in hPTPC in static and under fluidic condition. a) GGT1 enzymatic activity; b) Cell viability; c) Crystal violet. The results were expressed as mean \pm SD of three separate experiments.

GGT1 enzymatic activity and PrestoBlue cell viability were normalized with the total number of cells using Crystal Violet (Figure 4.28). These assays revealed that GGT1 presented greater enzymatic activity at the highest cisplatin concentrations: 50, 100 and 300 μM . This increase can be explained as a resistance mechanism to the oxidative stress. As the cisplatin concentration increases, the oxidative stress does too, and it could suppose the increase of the enzymatic activity, but at the same time, this increase activates and enhances cisplatin nephrotoxicity producing a fall in cellular viability. Normalization for PrestoBlue cell viability showed approximately the same number of cells per channel in each condition, except in ibidi under flow. Usually the differences in cell viability of these ibidis were found mainly due to the appearance of bubbles in the channels.

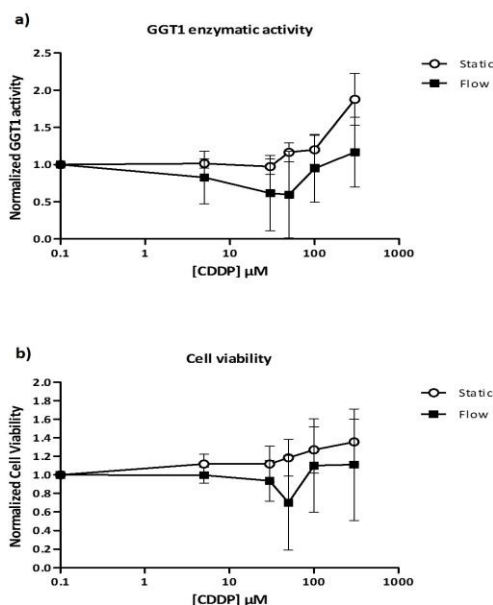


Figure 4.28: GGT1 enzymatic activity and PrestoBlue cell viability normalized with the total number of cells (CV). a) Normalized GGT1 enzymatic activity. b) Normalized PrestoBlue. The results were expressed as mean \pm SD of three separate experiments.

4.5 DISCUSSION

The use of fluidic devices promises to bring about significant advances in the development of *in vitro* physiological systems able to reproduce *in vivo* function. Focused on this purpose, we started to work with fluidic devices with the goal to establish cultures of human proximal tubule cells grown under luminal flow, providing physiological mechanical stimulus (shear stress). To validate the utility of such model, we sought to determine the effects of shear stress on the hPTPC sensitivity to a well-known nephrotoxic.

This project was associated with a bioengineering effort to develop microfluidic devices tailored to our specific needs. Several prototypes were tested for cell attachment and proliferation. In most cases, a successful protocol for hPTPC culture was accomplished, and even a few experiments were performed under flow conditions. However, we realized that prototypic devices are not the best suited to perform systematic biological studies. Materials like SU-8 are ideal for rapid prototyping and SU-8 based microfluidic devices have been successfully employed in proof of concept reports for several cell culture devices [21, 22]. However, the biocompatibility of SU-8 has been recently put into question [23], and our results clearly demonstrated it is not a suitable material for long-term culture of renal cells. Microfabrication techniques at the prototyping level are optimal for the validation of the materials and the designs. Indeed, our results demonstrate the feasibility of generating PS based microchannels devices, where hPTPC cells could be successfully seeded and grown. However, these devices presented too many problems for continuous use, and they were not available in high numbers.

The experience with the custom-made devices and the shortage of time to complete the aims of this Thesis prompted us to use a commercially available device. Ibidi μ -Slide VI 0.4 was the selected commercial solution because of its design. This standard slide-sized device contained 6 channels and allowed us to transfer the nephrotoxicity model generated in P96 wells easily. The connection to a fluidic system is simplified by the presence of female Luer connectors attached to each channel inlet. An optimized perfusion system was designed to provide flow-mediated shear stress under physiological range. The generation of bubbles inside of the device is a general issue in the microfluidic world that we could not completely overcome. This has limited the length of exposure to the flow. Also, the geometry of the Ibidi is not ideal, since its height (0.4 mm, compared to the 0.1-0.2 mm of the custom-made microfluidic devices) makes necessary to pass a higher flow than desired.

The use of NRK cell line was essential to perform the experiments because it allowed a comparison with the results obtained from hPTPC and more importantly, it helped to determine the sensibility of a primary cell culture versus a continuous cell line.

The experiments performed with NRK and hPTPC growing in static Ibidi and 96 wells plate confirmed that cells growing in static Ibidi were more resistant to cisplatin exposure than cells in 96 wells plate. Among the possible explanations, there is a dosing factor that was not taken into account while designing the experiment. In a well of a 96 wells plate, the volume of cisplatin solution was 100 μ L/well. Taking into account that 0.335 cm^2 is the area of a well, the total overall dose of cisplatin here was 298.5 $\mu\text{L}/\text{cm}^2$ for any given concentration. In the Ibidi, the volume of cisplatin solution was 30 μ L/channel. Taking into account that 0.6 cm^2 is

the area of a channel, the total overall dose of cisplatin here was 50 $\mu\text{L}/\text{cm}^2$. Thus, the overall dose of the drug between 96 wells plate and ibidi in static condition presented a ratio of 5.97. Depending on the relative amount of cisplatin uptake during the 8 hours of incubation, the reduced dose in the Ibidi might have been limiting its toxicity. Other explanations would imply phenotypic changes of the hPTPC by the fact of being grown in a different environment, resulting in modified sensitivity to cisplatin.

The nephrotoxicity model was tested in hPTPC growing in Ibidi fluidic devices, and all the experiments were performed in static and under flow conditions. The generated results showed that hPTPC exposed to flow did not present any difference compared with cells in static conditions. Kyung-Jin Jang *et al.* [4], worked with human proximal tubular primary cells exposed to cisplatin at 100 μM in static and under flow and in their work, cells under flow were more resistant to cisplatin than cells kept under static conditions. The publication mentioned above was reported by D.E. Ingber's group. Although they used a fluidic device, human primary PT cells and a nephrotoxic like cisplatin, the differences with our model were quite significant: The design of the chip had two compartments: A top channel mimicked the urinary lumen and had fluid flow, whereas the bottom chamber mimicked interstitial space and was filled with media. Cisplatin was introduced into the bottom space, and cisplatin-induced cellular damage was monitored for 24 hours. During the following 72 hours, shear stress was helpful facilitating recovery of the injured cells and associated biomarkers. Since 2013, this is the only report in the literature on this subject. This fact makes us think that probably working under fluidic conditions is not that easy to adopt as a cell culture model, substituting the conventional cell culture plates.

The work done during this Thesis adds to previous studies of proof of concept demonstrating the approach feasibility, and further supports the idea that this technology will provide a stronger model for the study of renal function and disease in a short future. Fundamental questions applied to significant clinical problems like renal toxicology [4, 24-26], EMT and proper cell differentiation [27], albumin handling [28], stone formation [29] and metabolomics [30] have already been addressed by using such devices.

4.6 BIBLIOGRAPHY

- [1] S. Weinbaum, Y. Duan, L.M. Satlin, T. Wang, A.M. Weinstein, Mechanotransduction in the renal tubule, *Am J Physiol Renal Physiol* 299(6) (2010) F1220-36.
- [2] Y. Duan, N. Gotoh, Q. Yan, Z. Du, A.M. Weinstein, T. Wang, S. Weinbaum, Shear-induced reorganization of renal proximal tubule cell actin cytoskeleton and apical junctional complexes, *Proc Natl Acad Sci U S A* 105(32) (2008) 11418-23.
- [3] N. Ferrell, R.R. Desai, A.J. Fleischman, S. Roy, H.D. Humes, W.H. Fissell, A microfluidic bioreactor with integrated transepithelial electrical resistance (TEER) measurement electrodes for evaluation of renal epithelial cells, *Biotechnol Bioeng* 107(4) (2010) 707-16.
- [4] K.J. Jang, A.P. Mehr, G.A. Hamilton, L.A. McPartlin, S. Chung, K.Y. Suh, D.E. Ingber, Human kidney proximal tubule-on-a-chip for drug transport and nephrotoxicity assessment, *Integr Biol (Camb)* 5(9) (2013) 1119-29.
- [5] M.J. Bissell, D.C. Radisky, A. Rizki, V.M. Weaver, O.W. Petersen, The organizing principle: microenvironmental influences in the normal and malignant breast, *Differentiation* 70(9-10) (2002) 537-46.
- [6] Q. Guo, B. Xia, S. Moshiah, C. Xu, Y. Jiang, Y. Chen, Y. Sun, J.M. Lahti, X.A. Zhang, The microenvironmental determinants for kidney epithelial cyst morphogenesis, *Eur J Cell Biol* 87(4) (2008) 251-66.
- [7] M. El Mouedden, G. Laurent, M.P. Mingeot-Leclercq, P.M. Tulkens, Gentamicin-induced apoptosis in renal cell lines and embryonic rat fibroblasts, *Toxicol Sci* 56(1) (2000) 229-39.
- [8] M.J. Wilmer, C.P. Ng, H.L. Lanz, P. Vulto, L. Suter-Dick, R. Masereeuw, Kidney-on-a-Chip Technology for Drug-Induced Nephrotoxicity Screening, *Trends Biotechnol* 34(2) (2016) 156-70.

- [9] H.C. Huang, Y.J. Chang, W.C. Chen, H.I. Harn, M.J. Tang, C.C. Wu, Enhancement of renal epithelial cell functions through microfluidic-based coculture with adipose-derived stem cells, *Tissue Eng Part A* 19(17-18) (2013) 2024-34.
- [10] D. Huh, H.J. Kim, J.P. Fraser, D.E. Shea, M. Khan, A. Bahinski, G.A. Hamilton, D.E. Ingber, Microfabrication of human organs-on-chips, *Nat Protoc* 8(11) (2013) 2135-57.
- [11] R. Baudoin, L. Griscom, M. Monge, C. Legallais, E. Leclerc, Development of a renal microchip for in vitro distal tubule models, *Biotechnol Prog* 23(5) (2007) 1245-53.
- [12] S. Rydholm, T. Frisk, J.M. Kowalewski, H. Andersson Svahn, G. Stemme, H. Brismar, Microfluidic devices for studies of primary cilium mediated cellular response to dynamic flow conditions, *Biomed Microdevices* 10(4) (2008) 555-60.
- [13] P.M. van Midwoud, A. Janse, M.T. Merema, G.M. Groothuis, E. Verpoorte, Comparison of biocompatibility and adsorption properties of different plastics for advanced microfluidic cell and tissue culture models, *Anal Chem* 84(9) (2012) 3938-44.
- [14] M.H. Wu, S.B. Huang, G.B. Lee, Microfluidic cell culture systems for drug research, *Lab Chip* 10(8) (2010) 939-56.
- [15] D. Huh, G.A. Hamilton, D.E. Ingber, From 3D cell culture to organs-on-chips, *Trends Cell Biol* 21(12) (2011) 745-54.
- [16] D. Huh, Y.S. Torisawa, G.A. Hamilton, H.J. Kim, D.E. Ingber, Microengineered physiological biomimicry: organs-on-chips, *Lab Chip* 12(12) (2012) 2156-64.
- [17] A.M. Rutenburg, H. Kim, J.W. Fischbein, J.S. Hanker, H.L. Wasserkrug, A.M. Seligman, Histochemical and ultrastructural demonstration of gamma-glutamyl transpeptidase activity, *J Histochem Cytochem* 17(8) (1969) 517-26.

[18] C.J. Gottardi, M. Arpin, A.S. Fanning, D. Louvard, The junction-associated protein, zonula occludens-1, localizes to the nucleus before the maturation and during the remodeling of cell-cell contacts, *Proc Natl Acad Sci U S A* 93(20) (1996) 10779-84.

[19] I.L.S.P. Services).

[20] K. Saotome, H. Morita, M. Umeda, Cytotoxicity test with simplified crystal violet staining method using microtitre plates and its application to injection drugs, *Toxicol In Vitro* 3(4) (1989) 317-21.

[21] V. Esteve, J. Berganzo, R. Monge, M.C. Martinez-Bisbal, R. Villa, B. Celda, L. Fernandez, Development of a three-dimensional cell culture system based on microfluidics for nuclear magnetic resonance and optical monitoring, *Biomicrofluidics* 8(6) (2014) 064105.

[22] K.V. Nemani, K.L. Moodie, J.B. Brennick, A. Su, B. Gimi, In vitro and in vivo evaluation of SU-8 biocompatibility, *Mater Sci Eng C Mater Biol Appl* 33(7) (2013) 4453-9.

[23] V.N. Vernekar, D.K. Cullen, N. Fogleman, Y. Choi, A.J. Garcia, M.G. Allen, G.J. Brewer, M.C. LaPlaca, SU-8 2000 rendered cytocompatible for neuronal bioMEMS applications, *J Biomed Mater Res A* 89(1) (2009) 138-51.

[24] L. Choucha-Snouber, C. Aninat, L. Grsicom, G. Madalinski, C. Brochot, P.E. Poleni, F. Razan, C.G. Guillouzo, C. Legallais, A. Corlu, E. Leclerc, Investigation of ifosfamide nephrotoxicity induced in a liver-kidney co-culture biochip, *Biotechnol Bioeng* 110(2) (2013) 597-608.

[25] L. Choucha Snouber, S. Jacques, M. Monge, C. Legallais, E. Leclerc, Transcriptomic analysis of the effect of ifosfamide on MDCK cells cultivated in microfluidic biochips, *Genomics* 100(1) (2012) 27-34.

[26] L.C. Snouber, F. Letourneur, P. Chafey, C. Broussard, M. Monge, C. Legallais, E. Leclerc, Analysis of transcriptomic and proteomic profiles demonstrates improved Madin-Darby canine kidney cell

function in a renal microfluidic biochip, *Biotechnol Prog* 28(2) (2012) 474-84.

[27] M. Zhou, H. Ma, H. Lin, J. Qin, Induction of epithelial-to-mesenchymal transition in proximal tubular epithelial cells on microfluidic devices, *Biomaterials* 35(5) (2014) 1390-401.

[28] N. Ferrell, K.B. Ricci, J. Groszek, J.T. Marmorstein, W.H. Fissell, Albumin handling by renal tubular epithelial cells in a microfluidic bioreactor, *Biotechnol Bioeng* 109(3) (2012) 797-803.

[29] Z. Wei, P.K. Amponsah, M. Al-Shatti, Z. Nie, B.C. Bandyopadhyay, Engineering of polarized tubular structures in a microfluidic device to study calcium phosphate stone formation, *Lab Chip* 12(20) (2012) 4037-40.

[30] L. Shintu, R. Baudoin, V. Navratil, J.M. Prot, C. Pontoizeau, M. Defernez, B.J. Blaise, C. Domange, A.R. Pery, P. Toulhoat, C. Legallais, C. Brochot, E. Leclerc, M.E. Dumas, Metabolomics-on-a-chip and predictive systems toxicology in microfluidic bioartificial organs, *Anal Chem* 84(4) (2012) 1840-8.

[31] E.R. Shamir, A.J. Ewald, Three-dimensional organotypic culture: experimental models of mammalian biology and disease, *Nat Rev Mol Cell Biol* 15(10) (2014) 647-64.

[32] L. Fliedl, G. Manhart, F. Kast, H. Katinger, R. Kunert, J. Grillari, M. Wieser, R. Grillari-Voglauer, Novel human renal proximal tubular cell line for the production of complex proteins, *J Biotechnol* 176 (2014) 29-39.

[33] W.W. Minuth, L. Denk, A. Glashauser, Cell and drug delivery therapeutics for controlled renal parenchyma regeneration, *Adv Drug Deliv Rev* 62(7-8) (2010) 841-54.

[34] E.J. Kelly, Z. Wang, J.L. Voellinger, C.K. Yeung, D.D. Shen, K.E. Thummel, Y. Zheng, G. Ligresti, D.L. Eaton, K.A. Muczynski, J.S. Duffield, T. Neumann, A. Tourovskaja, M. Fauver, G. Kramer, E. Asp,

J. Himmelfarb, Innovations in preclinical biology: ex vivo engineering of a human kidney tissue microperfusion system, *Stem Cell Res Ther* 4 Suppl 1 (2013) S17.

[35] H.D. Humes, D. Buffington, A.J. Westover, S. Roy, W.H. Fissell, The bioartificial kidney: current status and future promise, *Pediatr Nephrol* 29(3) (2014) 343-51.

[36] N. Sanchez-Romero, Meade, P. , Giménez, I., *Microfluidic-Based 3D Models of Renal Function for Clinically Oriented Research*, Elsevier 2016.

4.7 ANNEX

During the developing of this Thesis several products have been made available from different commercial sources that could serve for the aims of this study. Table Annex summarizes their main features.

Table 4.7: Commercial Devices Providing Microfluidic Solutions for Cell Culture.

Company	Applications	a	Impulsion solutions	Geometries	Publications
Cellix Ltd	Cell rolling, adhesion, migration, chemotaxis, shear stress	8	Syringe pump, peristaltic pump	Parallel longitudinal channels	Endothelium, blood cells, cancer cells
Cytoo	Renal PT model (closed lumen)	100s	N/A	Micropatterned chips and wells plate	Cell biology, polarization, mechano transduction
Ebers	Chemical gradients, shear stress, cell polarization	3	Incubators integrate peristaltic pumps	Parallel channels	Cell biology, epithelial biology, cancer research

Fluxion BioSc.	Aggregation, adhesion, cell rolling, shear stress.	24	Electropneumatic pump	Well plates	Microbiology Cell biology
Gradien-tech	Migration, chemotaxis, morphogenesis	1	Syringe pump	2D and 3D chemical gradients	Cancer biology, immunology
IBIDI	Cell migration, chemotaxis, angiogenesis, shear stress	6	Air pressure pump, syringe pump	Parallel channels	[15, 31, 32]
Kirkstall	Organ models (skin, cornea, respiratory epithelium)	1	Peristaltic pump	Individual chambers	Cancer, stem cell, drug discovery
Merck Millipore	Chemotaxis/migration, Drug screening, Hypoxia, Shear stress	4	Pneumatic pump	Parallel chambers	Cell Biology, microbiology, cancer
Micronit Microfluidics	Organ on a chip	1	Pneumatic (on chip)	Customized	Cell Biology
Minucells	Gradient culture for a single tissue carrier	1-6	Peristaltic pump	Single channel	[33, 34]

Nortis	Organ on a chip/vascular biology	12	Pneumatic pump	3D hydrogels	[35]
--------	----------------------------------	----	----------------	--------------	------

^aHigh throughput screening, number of samples per chip/device. *Source: N. Sánchez-Romero, P. Meade and I. Giménez, Microfluidic-Based 3D Models of Renal Function for Clinically Oriented Research, 2016 [36].*

5 CONCLUSIONS

1. hPTPC showed the main PT markers, although the culture included cells expressing markers from other renal segments.
2. Combined use of GGT1 activity assay and cell viability assay allowed us to distinguish different cisplatin effects and were validated as useful assays to monitor cell function and viability.
3. The cisplatin nephrotoxicity model was consistent and amenable to use on cells grown in fluidic devices.
4. In our model, cimetidine, genistein or β -lapachone did not exhibit protection against cisplatin-mediated cytotoxicity.
5. hPTPC were able to adapt to growing conditions inside microfluidic channels.
6. Cells growing in static ibidi were more resistant to cisplatin exposure than cells growing in 96 wells plate, as a consequence of cisplatin availability.
7. hPTPC didn't present any difference in the sensitivity to cisplatin under flow compared with cells growing in static Ibidi.
8. The generation of bubbles, the main technical challenge of these type of platforms, was the key limitation in the use of this technology. So, optimization efforts are needed and should continue.

5 CONCLUSIONES

1. Las hPTPC expresaron los principales marcadores típicos de TP, aunque el cultivo poseía células que expresaban marcadores procedentes de otros segmentos renales.
2. El uso combinado del ensayo de actividad enzimática GGT1 y del ensayo de viabilidad celular, nos permitió distinguir diferentes efectos del cisplatino. El uso combinado de ambos ensayos fue validado como un ensayo práctico para monitorizar la función y viabilidad celular.
3. El modelo de nefrotoxicidad basado en cisplatino era consistente y permitió su uso en células que crecían en dispositivos fluidicos.
4. En nuestro modelo, ni cimetidina, ni genisteína, ni β -lapachone mostraron protección frente a la citotoxicidad medida por el cisplatino.
5. Las hPTPC se adaptaron a las condiciones de crecimiento dentro de los canales microfluídicos.
6. Las células que crecieron en ibidi en estático fueron más resistentes a la exposición al cisplatino que las células que crecieron en placas de 96 pocillos, como consecuencia de la disponibilidad del nefrotóxico.
7. Las hPTPC no mostraron ninguna diferencia en la sensibilidad al cisplatino en presencia de flujo, en comparación con las células que crecieron en los ibidi en estático.
8. La generación de burbujas, el principal desafío técnico de este tipo de plataformas, fue la principal limitación en el uso de esta tecnología. Los esfuerzos en la optimización para evitar la

generación de burbujas en este tipo de tecnología son imprescindibles actualmente.

